Journal of
Nonlinear
Science

Check for
updates

Adaptive Dynamics of a Stoichiometric Phosphorus–Algae–Zooplankton Model with Environmental Fluctuations

Shengnan Zhao[1] · Sanling Yuan[1] (iD) **· Hao Wang[2]**

Abstract

We present a stochastic evolutionary phosphorus–algae–zooplankton model with phosphorus recycling and originally investigate the patterns and outcomes of adaptive changes in algal cell size, under the influence of environmental fluctuations. The threshold that determines whether the stochastic model will ecologically persist or not is first obtained. We then introduce fitness functions with stochastic fluctuations and obtain the evolutionary conditions for continuously stable strategy (CSS) and evolutionary branching, confirmed by numerical simulation. Our results predict that environmental fluctuation could drive algal evolution toward smaller cell size. Algal cell size varies significantly with phosphorus input in the presence of zooplankton, but has no response to the changing phosphorus inflow without zooplankton, and evolutionary branching will never occur without zooplankton. With the existence of zooplankton that has a fixed trait, evolutionary branching occurs with small environmental fluctuation and moderate phosphorus inflow, and the existence of environmental fluctuation could narrow the cell size difference between the newly emerging algal species, while large fluctuation or extreme phosphorus inflow will result in CSS. Moreover, environmental fluctuation potentially benefits algal biodiversity in eutrophic environments, and oligotrophication inhibits algal diversity. For the coevolution of algae and zooplankton, evolutionary cycling could appear, i.e., algal cell size and zooplankton body size can coevolve to a stable limit cycle (the Red Queen dynamics) in an eutrophic environment. In oligotrophic or moderate phosphorus environments, the influence of

---

Communicated by Paul Newton.

✉ Sanling Yuan
    sanling@usst.edu.cn

   Hao Wang
    hao8@ualberta.ca

[1] University of Shanghai for Science and Technology, Shanghai 200093, China

[2] Department of Mathematical and Statistical Sciences, University of Alberta, Edmonton, Alberta T6G 2G1, Canada

    © Springer

environmental fluctuation on algal evolution in the coevolution process is similar to the scenario that algae evolves only.

Keywords Stochastic EPAZ model · Adaptive dynamics · Evolutionary branching · Continuously stable strategy · Evolutionary cycling

Mathematics Subject Classification 37H99

1 Introduction

Algal size structure determines its own metabolic rates and biomass (Tang and Peters 1995; Peters 1983); meanwhile, as the primary productivity and the basis of aquatic food webs, algal size structure also significantly affects community structure and global carbon cycle through size-dependent species interactions and sinking (Falkowski et al. 1998; Jiang et al. 2005; Cohen et al. 2003). With no doubt, it is one of the most important indicators for an aquatic ecosystem. The sizes of single-celled algae span several orders of magnitude, ranging from $\sim 0.6\,\mu m$ to >1 mm equivalent spherical diameter (Sheldon et al. 1972). Litchman et al. (2009, 2010) suggested that the cell size diversity is a result of diverse selective pressures, such as different patterns of nutrient limitation, physical mixing and grazing pressure, and under certain environmental conditions, only certain algal species could exist, i.e., there is no universal best size for algae. Many observed phenomena also support this viewpoint (Moczydłowska 2010; Servais et al. 2010; Finkel et al. 2005; Mclaughlin 1977; Butterfield 1997; Falkowski et al. 2004; Murphy and Hart 1945). For example, the mean area of marine diatom frustules has decreased by more than twofold in response to the changes in upwelling zones over the last half of the Cenozoic (Finkel et al. 2005). The increased nutrient abundance due to orogenic and volcanic activity may have led to the dramatic increase of the biodiversity of marine plankton (phytoplankton and zooplankton) during the Cambrian and the Ordovician (Servais et al. 2010). Moreover, the changes of diversity and abundance between phytoplankton and its consumers in the Cambrian were synchronous in time and tightly coupled (Moczydłowska 2010). All the above observations suggest that environmental factors, such as nutrient abundance, mixing and grazing pressure, can directly or indirectly cause evolutionary changes in algal species.

Much progress has been made in understanding the mechanisms that drive algae to evolve and maintaining species diversity (Falkowski et al. 2004; Pu et al. 2017; Litchman et al. 2009; Stomp et al. 2004; Jiang et al. 2005), and the development of adaptive dynamics (Dieckmann et al. 1995; Geritz et al. 1998) has no doubt significantly contributed to this. Stomp et al. (2004) proposed one of the first adaptive planktonic systems and studied the adaptive dynamics of the pigment composition in *Tolypothrix*, revealing that the divergence in pigment composition favors species coexistence and contributes to algal diversity as a result. Litchman et al. (2009) utilized a periodically forced system to model the growth and competition of algae, by taking $\log_{10}$ cell volume as the trait and using techniques from evolutionary game theory (Geritz et al. 1998). They derived the evolutionarily stable cell sizes of marine and freshwater diatoms under different scenarios of nutrient limitation. Jiang et al. (2005) presented

and investigated an evolutionary nutrient–phytoplankton–zooplankton model, predicting that phytoplankton have a tendency to evolve to small cell size and increasing nutrient flux tends to increase phytoplankton cell size. Recently, Pu et al. (2017) analyzed the relations between species richness and environmental productivity, by using the evolutionary nutrient–phytoplankton–zooplankton model, and their results showed that the coevolution of plankton can lead to the unimodal and positive relationships of productivity–richness.

Marine populations are inevitably disturbed by a variety of unpredictable factors, such as light, water temperature, acidity, wind and many other physical factors (Yu et al. 2018), and these factors also play important roles in the evolution of phenotypic traits by affecting the natural selection process (Dieckmann and Law 1996). Hence, the influence of environmental stochasticity in marine ecosystem cannot be ignored, and instead of the deterministic models with constant environment, stochastic models are more realistic in describing the population dynamics as well as the adaptive dynamics of a marine ecosystem. Many stochastic models have been built to reveal the significance of environmental stochasticity (Zhao et al. 2016; Melbourne and Hastings 2008; White et al. 2014; Zhao et al. 2017; Bandyopadhyay et al. 2008; Zhao et al. 2020; Ripa and Dieckmann 2013; Carpenter et al. 2011). For example, Bandyopadhyay et al. (2008) considered a two-dimensional phytoplankton competitive model, where one of the phytoplankton species is toxic and the other species is nontoxic, revealing that environmental fluctuation controls the phytoplankton dynamics in competition. Zhao et al. (2020) proposed a stochastic nutrient–phytoplankton–zooplankton model with phytoplankton cell size and investigated the interactions between the internal mechanism of population and the external environmental factors, suggesting that white noises and phytoplankton cell sizes could determine the plankton survival and the model stability. Ripa and Dieckmann (2013) extended the previous classic canonical adaptive dynamics equation, predicting the change rate of evolutionary heritable trait on long evolutionary time scales, by calculating the invasion probability of a beneficial, mutant allele in a monomorphic, large population under the influence of environmental fluctuations. To achieve a deeper understanding for the population and adaptive dynamics of plankton species, it is meaningful to further incorporate the environmental stochasticity into the marine ecosystems.

To sum up, nutrient abundance, grazing and environmental stochasticity could all significantly affect algal evolution process. Moreover, phosphorus is often a limiting nutrient for algal production in lakes (Wang et al. 2007). Motivated by these considerations, we devote to investigating whether and how environmental fluctuations, grazing and phosphorus inflow affect algal cell size and species diversity. The rest of the paper is organized as follows: In Sect. 2, we model a stoichiometry of phosphorus–algae–zooplankton (PAZ) interactions with environmental fluctuations and phosphorus recycling in the epilimnion, obtain the threshold that determines whether the stochastic model will ecologically persist as well as the explicit estimation of the long-term mean persistent level. When only algal species evolve, we investigate the evolutionary conditions for CSS and evolutionary branching in the presence/absence of zooplankton in Sects. 3 and 4. In Sect. 5, the adaptive dynamics of algae–zooplankton coevolution are investigated. Finally, a brief discussion in Sect. 6 concludes the paper.
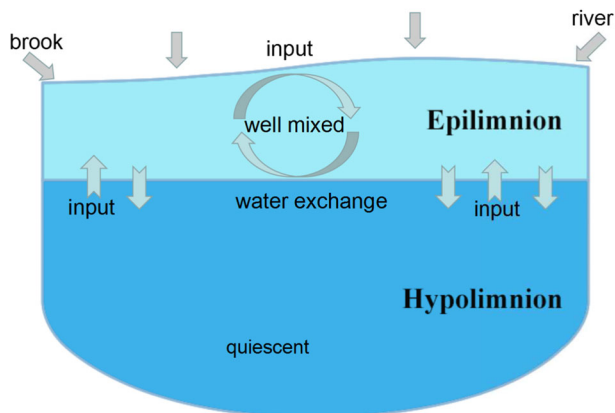
Fig. 1 The stratified lake ecosystem for our mathematical modelling. Adapted from Wang et al. (2007)

2 The Stochastic EPAZ Model and Some Fundamental Results

2.1 Model Formulation

Our theoretical model in terms of limiting dissolved mineral phosphorus concentration P (mgP/m^3), algal carbon density A (mgC/m^3) and zooplankton carbon density Z (mgC/m^3) in temperate lakes, which are seasonally separated by a thermocline into two zones, namely epilimnion (the upper well mixed warmer layer) and hypolimnion (the bottom quiescent colder layer), respectively, see Fig. 1.

We assume that phosphorus in all dead organisms, including algae and zooplankton, could be recycled immediately and zooplankton could return the excess phosphorus taken from algae to the nutrient pool. In addition, plankton sinking and water exchange take place at the interface between epilimnion and hypolimnion. The interactions between dissolved mineral phosphorus, algae and zooplankton can be described as follows:

$$
\begin{cases}
\dfrac{dP(t)}{dt} = \underbrace{e(P_{in} - P)}_{\text{P input and exchange}} + \underbrace{d_1 Q(x) A}_{\text{P recycling from algal natural loss}} + \underbrace{\big(Q(x) - \delta q(y)\big)c(x,y)AZ}_{\text{P recycling from zooplankton wastes}} \\
\qquad + \underbrace{d_2 q(y) Z}_{\text{P recycling from zooplankton natural loss}} - \underbrace{\mu(x) f(P) A Q(x)}_{\text{P consumption by algae}}, \\
\dfrac{dA(t)}{dt} = \underbrace{\mu(x) f(P) A}_{\text{algal growth}} - \underbrace{c(x,y)AZ}_{\text{grazing by zooplankton}} - \underbrace{s_1(x)A}_{\text{sinking}} - \underbrace{d_1 A}_{\substack{\text{mortality and respiration} \\ \text{nature loss}}}, \\
\dfrac{dZ(t)}{dt} = \underbrace{\delta c(x,y)AZ}_{\text{zooplankton growth}} - \underbrace{s_2(y)Z}_{\text{sinking loss}} - \underbrace{d_2 Z}_{\text{mortality and respiration}}.
\end{cases}
\tag{1}
$$

The text below each term of the model explains its biological meaning, and a more intuitive schematic diagram can be seen in Fig. 2. Parameters with biologically meaningful values/ranges and units are provided in Table 1.
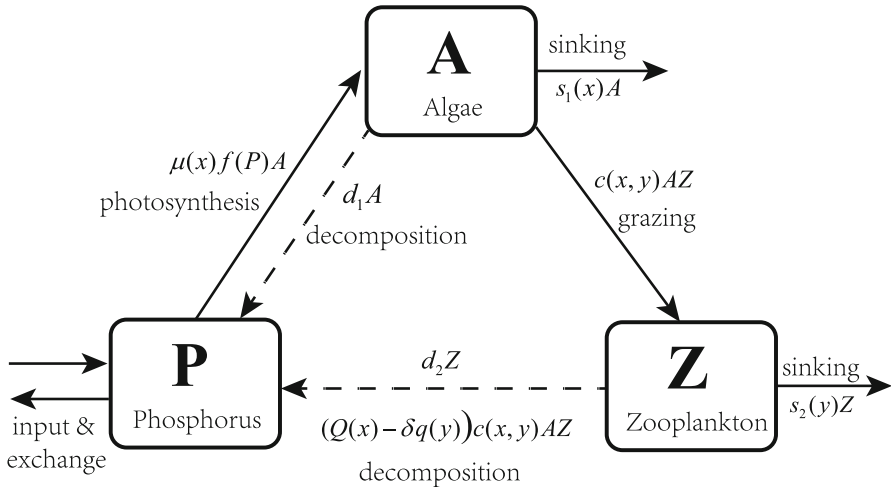
Fig. 2 Schematic diagram for the dissolved mineral phosphorus–algae–zooplankton interactions. The solid lines represent direct interactions and the dashed lines represent indirect interactions

Despite the fact that the above model takes similar form as the model in Jiang et al. (2005), the modeling principle of these two models is different. Jiang et al. (2005) utilized the *energy flow* principle (Loladze et al. 2000), focusing on the energy flow through trophic levels. We aim to track the amount of two essential elements, carbon (C) and phosphorus (P), in each trophic level, based on the *element cycling* principle (Loladze et al. 2000). Due to the second law of thermodynamics, the energy recycled back to the nutrient pool must be dissipated during the heterotrophic bacterial decomposition process, while chemical elements are conserved. This explains why only a fraction of nutrient in dead organisms (algae and zooplankton) and zooplankton wastes could be recycled in Jiang et al. (2005)'s model, while in our model phosphorus from these two components can be completely recycled. Moreover, Jiang et al. (2005) assumed a calm, relatively stratified system without considering the physical processes in water column. We further take the wind-temperature-caused water mixing (overnight mixing and eddy flow) across the interface between epilimnion and hypolimnion into account; as a result, the exchange of phosphorus and the sinking of zooplankton are further incorporated in our model. In the rest of this paper, we will perform a complete analysis on plankton adaptive evolution processes under the influence of environmental stochasticity, including how environmental stochasticity affects the evolutionary trends and outcomes of plankton traits (algal cell size and zooplankton body size), and the analysis on the stable coexistence of two algal species plus one zooplankton species and the possibilities of further evolutionary branching.

The wind-temperature-caused water mixing could strongly influence the water flow exchange rate. Theoretically, we set up this environmental stochasticity as $-e \rightarrow -e + \sigma_1 \dot{B}_1(t)$, $-s_1(x) \rightarrow -s_1(x) + \sigma_2(x, \rho_1) \dot{B}_2(t)$, $-s_2(y) \rightarrow -s_2(y, \rho_2) + \sigma_3(y, \rho_2) \dot{B}_3(t)$, we then obtain the stochastic PAZ model, corresponding to the deterministic model (1):

Table 1 Parameters and functions with biological descriptions, ranges and units

Parameter/function	Description	Range	Unit
x	Algal cell size (spherical diameter (SD))	0.6–1000 (Raven 1998; Polovina and Woodworth 2012)	μm
y	Zooplankton body size (SD)	2–2000 (Figueiredo et al. 2020)	μm
P_{in}	Phosphorus input	0–150 (Wang et al. 2007)	mgP m^{-3} day^{-1}
d_1	Natural loss of algae	0.04–0.13 (Wang et al. 2007)	day^{-1}
δ	Conversion efficiency of zooplankton	0.6 (Wang et al. 2009)	No unit
d_2	Natural loss of zooplankton	0.15 (Loladze et al. 2000)	day^{-1}
e	Water exchange rate	0.05 (Wang et al. 2007; JaGer et al. 2010)	day^{-1}
α	Per unit P uptake efficiency of algae	0.2 (Wang et al. 2008)	m^3 mg P^{-1}
c_m	Maximum ingestion rate of zooplankton	0.81 (Loladze et al. 2000)	day^{-1}
$\mu(x) = \dfrac{x}{a_1 x^2 + a_2 x + a_3}$	Maximum algal production rate	0–5 (Ichimi et al. 2012)	day^{-1}
$Q(x) = b + \beta_1 x^3$	$P:C$ ratio of algae	0.0038–2 (Peace et al. 2014)	mg P mg C^{-1}
$s_1(x) = k_1 x^2$	Algal sinking loss	0.05–0.25 (Wang et al. 2007)	day^{-1}
$q(y) = \beta_2 y^3$	$P:C$ ratio of zooplankton	0.004–0.04 (Sterner and Elser 2002; Wang et al. 2008)	mg P/mg C
$c(x,y) = c_m \exp(-v(x - \theta y)^2)$	Ingestion rate of zooplankton on algae	0–0.81 (Loladze et al. 2000)	m^3 mg C^{-1} day^{-1}
$f(P) = \alpha P$	P-uptake function (follows mass action law)	$f(0) = 0,\ f(P) > 0$	no unit
$s_2(y) = \dfrac{1}{\beta_3} \exp(k_2 y)$	Sinking loss of zooplankton	0–0.15 (Edwards and Andrew 2000)	day^{-1}

1. The natural losses of algae and zooplankton are mainly the mortality and respiration.

2. The functions $\mu(x)$, $s_1(x)$, $q(y)$ and $c(x, y)$ are from Jiang et al. (2005), Pu et al. (2017)

3. We add a positive constant b to $Q(x)$ in (Jiang et al. 2005) to guarantee its value will not fall below the minimum algal phosphorus cell quota (0.0038 mg P/mg C) (Peace et al. 2014)

4. Normally we should have $Q(x) \geq \delta q(y)$

$$\begin{cases} dP(t) = \big[e(P_{\mathrm{in}} - P) + d_1 Q(x) A + \big(Q(x) - \delta q(y)\big) c(x, y) A Z + d_2 q(y) Z \\ \qquad\quad - \alpha \mu(x) P A Q(x)\big] dt + \sigma_1 P d B_1(t), \\ dA(t) = \big[\alpha \mu(x) P A - c(x, y) A Z - s_1(x) A - d_1 A\big] dt + \sigma_2(x, \rho_1) A d B_2(t), \\ dZ(t) = \big[\delta c(x, y) A Z - s_2(y) Z - d_2 Z\big] dt + \sigma_3(y, \rho_2) Z d B_3(t), \end{cases} \quad (2)$$

where $B_1(t)$, $B_2(t)$, $B_3(t)$ are independent standard Brownian motions defined in a complete probability space $(\Omega, \{\mathscr{F}_t\}_{t\geq 0}, \mathcal{P})$ with a filtration $\{\mathscr{F}_t\}$ satisfying the usual normal conditions, which is right continuous and increasing, while $\mathscr{F}_0$ contains all $\mathcal{P}$-null sets. The quantities $\sigma_1, \sigma_2(x, \rho_1), \sigma_3(y, \rho_2)$ denote the intensities of environmental noise. Taking into account some biological factors, we assume that the stochastic fluctuations $\sigma_2(x, \rho_1)$ and $\sigma_3(y, \rho_2)$ for algae and herbivores, respectively, depending on both plankton traits x, y and the intensity parameters ρ_i, $i = 1, 2$, should satisfy the following properties:

1. The environmental fluctuation experienced by algae $\sigma_2(x, \rho_1)$ is a continuous, monotone increasing function with respect to x, due to the fact that algae with a smaller cell have lower sinking rate and are better able to acquire and effectively use limiting resources than a larger cell (Raven 1998);
2. The environmental fluctuation experienced by zooplankton $\sigma_3(y, \rho_2)$ is a continuous, monotone decreasing function with respect to y, due to the fact that zooplankton with a larger body size are more competitive in a resource limiting environment and could take a more extensive range of algal species, in the absence of predation from higher trophic levels (Hanazato 1998; Mitchell 1975).
3. $\sigma_2(x, \rho_1)$ and $\sigma_3(y, \rho_2)$ are monotone increasing functions with respect to their respective intensity parameters ρ_1 and ρ_2 (Zhang et al. 2020). This indicates that larger intensity parameters result in greater environmental fluctuations, and consequently, in the absence of environmental fluctuations experienced by algae and zooplankton, we have $\sigma_2(x, 0) = 0$, $\sigma_3(y, 0) = 0$, respectively.

Based on the above assumptions, we choose the functions $\sigma_2(x, \rho_1)$ and $\sigma_3(y, \rho_2)$ as:

$$\sigma_2(x, \rho_1) = \frac{k_3 \rho_1}{k_4 + \rho_1} x^2, \quad \sigma_3(y, \rho_2) = \frac{k_5 \rho_2}{k_6 + \rho_2} \exp(-k_7 y), \quad (3)$$

where k_3, k_4, k_5, k_6, c_1, k_7 are positive constants. Other parameters have the same meanings as in the corresponding deterministic model (1). Throughout this paper, we always choose the following parameters for numerical simulation: $a_1 = 0.042$; $a_2 = 0.055$; $a_3 = 0.121$; $k_1 = 0.1085$; $d_1 = 0.054$; $b = 0.0038$; $\beta_1 = 0.03$; $\beta_2 = 0.00256$; $k_3 = 0.88$; $k_4 = 15$; $k_2 = 0.03815$; $\beta_3 = 11$; $v = 0.92$; $\theta = 0.4$; $k_5 = 6$; $k_6 = 1$; $k_7 = 0.5$.

2.2 Fundamental Results on Population Dynamics

In this subsection, we provide notations, definitions and basic properties about model (2), including the global existence, uniqueness, boundedness of positive solutions, the extinction and persistence as well as the existence of a unique stationary distribution.

For the convenience of discussion, we introduce the following notations and definitions:

$$\hat{\phi} = \min\{\phi(x_1), \phi(x_2)\}, \quad \check{\phi} = \max\{\phi(x_1), \phi(x_2)\}.$$

For any integrable function $f(t)$,

$$\langle f \rangle = \lim_{t \to \infty} \frac{1}{t} \int_0^t f(s)\mathrm{d}s, \quad \overline{\langle f \rangle} = \limsup_{t \to \infty} \frac{1}{t} \int_0^t f(s)\mathrm{d}s, \quad \underline{\langle f \rangle} = \liminf_{t \to \infty} \frac{1}{t} \int_0^t f(s)\mathrm{d}s,$$

If in addition f is parametrized by x or x_1, x_2, respectively, we let

$$\langle f(x) \rangle' = \frac{\mathrm{d}\langle f(x) \rangle}{\mathrm{d}x}, \quad \langle f(x_1, x_2) \rangle'_{x_i} = \frac{\partial \langle f(x_1, x_2) \rangle}{\partial x_i}, \quad i = 1, 2.$$

Moreover, we denote

$$\lambda(x, y) = e P_{\mathrm{in}} - \frac{e\eta(x, \rho_1)}{\alpha\mu(x)} - \frac{s_1(x)Q(x)\kappa(y, \rho_2)}{\delta c(x, y)}, \tag{4}$$

where

$$\eta(x, \rho_1) = s_1(x) + d_1 + \frac{\sigma_2^2(x, \rho_1)}{2}, \quad \kappa(y, \rho_2) = s_2(y) + d_2 + \frac{\sigma_3^2(y, \rho_2)}{2} \tag{5}$$

are the loss functions of algae and zooplankton, respectively, characterizing their total loss caused by sinking, mortality and respiration as well as environmental fluctuations. We now present our main results about the asymptotic dynamics of the stochastic model (2), and the detailed proofs are presented in appendices.

Theorem 1 *For any given initial value $(P(0), A(0), Z(0)) \in R_+^3$, the stochastic model (2) has a unique positive solution $(P(t), A(t), Z(t))$ for all $t > 0$ almost surely (a.s.). Moreover, $(P(t), A(t), Z(t))$ satisfies*

$$\limsup_{t \to \infty} [P(t) + Q(x)A(t) + q(y)Z(t)] < \infty, \ a.s.$$

Theorem 1 can be regarded a corollary from Theorem 7, and the detailed proof of Theorem 7 can be seen in "Appendix D". Based on Theorem 1, we have the following lemma.

Lemma 1 *For any given positive initial value $(P(0), A(0), Z(0)) \in R_+^3$, the solution of model (2) has the properties that*

$$\limsup_{t \to \infty} \frac{\ln P(t)}{t} \leq 0, \quad \limsup_{t \to \infty} \frac{\ln A(t)}{t} \leq 0, \quad \limsup_{t \to \infty} \frac{\ln Z(t)}{t} \leq 0, \ a.s. \tag{6}$$

We then perform the analysis on the persistence and extinction as well as the existence of a unique ergodic stationary distribution for model (2), which will be used in the following analysis for adaptive dynamics.

Theorem 2 *Assume $\Phi(t) = (P(t), A(t), Z(t))$ is the solution of model (2) with any given initial value $\Phi(0) \in R_+^3$. Then, the following conclusions hold.*

(1) *If $P_{in} < \frac{\eta(x,\rho_1)}{\alpha\mu(x)}$, then both algal and zooplankton populations (measured in carbon content) will go to extinction, a.s. Furthermore, $\langle P \rangle = P_{in}$, a.s.*

(2) *If $\frac{\eta(x,\rho_1)}{\alpha\mu(x)} < P_{in} < \frac{\eta(x,\rho_1)}{\alpha\mu(x)} + \frac{s_1(x)Q(x)\kappa(y,\rho_2)}{e\delta c(x,y)}$, then zooplankton population will go to extinction a.s., the population of algae and the concentration of phosphorus will be stable in mean a.s., and*

$$\langle P(x) \rangle = \frac{\eta(x, \rho_1)}{\alpha\mu(x)}, \quad \langle A(x) \rangle = \frac{1}{s_1(x)Q(x)} \left(eP_{in} - \frac{e\eta(x, \rho_1)}{\alpha\mu(x)} \right), \quad a.s. \quad (7)$$

(3) *If $P_{in} > \frac{\eta(x,\rho_1)}{\alpha\mu(x)} + \frac{s_1(x)Q(x)\kappa(y,\rho_2)}{e\delta c(x,y)}$, then model (2) will be persistent in mean a.s., namely*

$$\langle P(x, y) \rangle > 0, \quad \langle A(x, y) \rangle > 0, \quad \langle Z(x, y) \rangle > 0, \quad a.s.$$

The proof of Theorem 2 can be found in "Appendix A". From Theorem 2, adequate phosphorus in the environment could support the survival of both algal and zooplankton populations. Less abundant phosphorus may only allow the algal population to survive and the extreme lack of phosphorus would wipe out both algal and zooplankton populations. Note that the condition in Theorem 2 (1) can be converted into $\frac{\sigma_2^2(x,\rho_1)}{2} > \alpha\mu(x)P_{in} - s_1(x) - d$. This indicates that large noises are devastating to both algal and zooplankton populations; in other words, the ability for either algal or zooplankton population to adapt to the external environmental fluctuations is limited. Theorems 2 (2) and (3) introduce the situations when the noises are not too large. Also, the condition in Theorem 2 (3) can be converted into $\lambda(x, y) > 0$. Then, $\lambda(x, y)$ is the threshold that determines the persistence and extinction of zooplankton: when $\lambda(x, y) > 0$, the zooplankton population will be persistent in mean, while when $\lambda(x, y) < 0$, zooplankton population will eventually die out.

Theorem 2 is verified in Fig. 3. Let $\rho_1 = 75$, by calculation $P_{in} - \frac{\eta(x,\rho_1)}{\alpha\mu(x)} = -0.0023 < 0$, then both algae and zooplankton go extinct a.s., see Fig. 3b. When $\rho_1 = 0.5$, $\rho_2 = 12$, by calculation we have $0.217 = \frac{\eta(x,\rho_1)}{\alpha\mu(x)} < P_{in} = 0.74 < \frac{\eta(x,\rho_1)}{\alpha\mu(x)} + \frac{s_1(x)Q(x)\kappa(y,\rho_2)}{e\delta c(x,y)} = 0.7697$, then as shown in Fig. 3c the zooplankton population goes extinct a.s., the algae population and the phosphorus concentration are stable in mean a.s. Moreover, we choose $\rho_1 = 0.1$, $\rho_2 = 0.002$, then $\lambda(x, y) = 0.0262 > 0$. In this situation, the stochastic model (2) will be persistent in mean, see Fig. 3d. Fixing the value of ρ_1 and ρ_2 in Fig. 3d, respectively, and increasing the other intensity parameter to 0.3 and 8, it is easy to check out that for these two cases, $\lambda(x, y) > 0$ always holds. Also, it is clear to see that for both $i \in \{1, 2\}$, the increasing of ρ_i will lead to a smaller persistent level for zooplankton and phosphorus, while the persistent level of algal population will increase, see Fig. 3e, f. Biologically, these observations
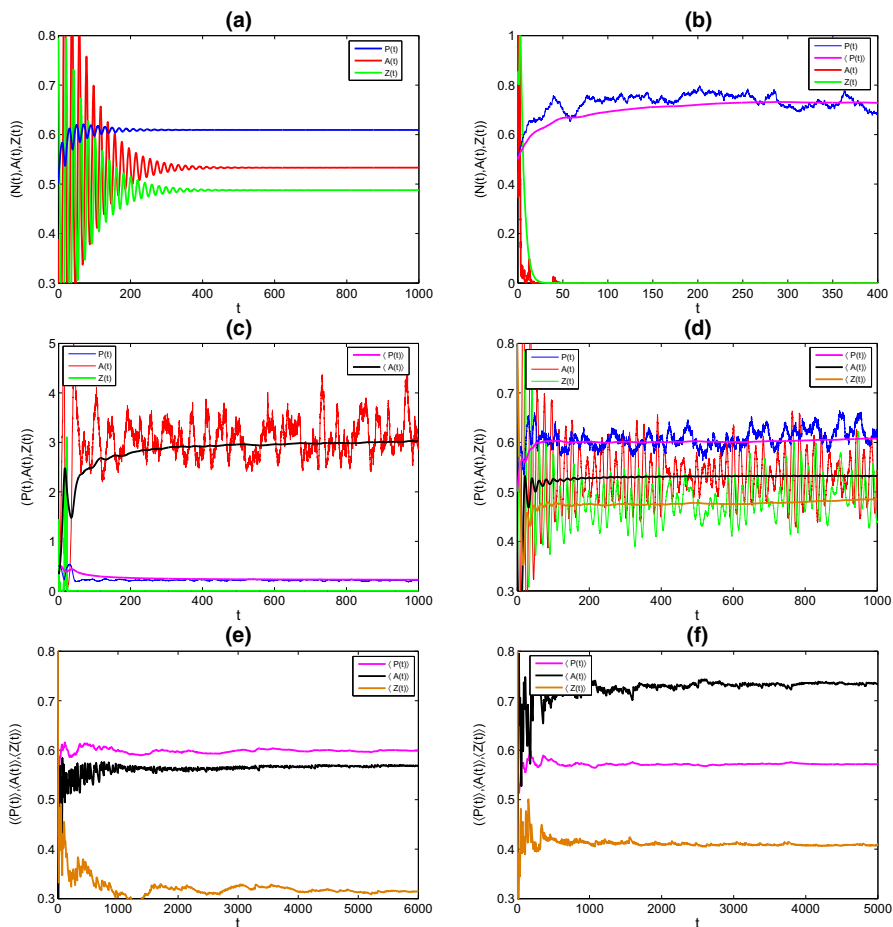
Fig. 3 **a** Time series for the deterministic model (1); **b** time series for the corresponding stochastic model (2) when $\rho_1 = 75$, $\rho_2 = 0.002$; **c** time series for the stochastic model (2) when $\rho_1 = 0.5$, $\rho_2 = 12$; **d** time series for the stochastic model (2) when $\rho_1 = 0.1$, $\rho_2 = 0.002$; **e** the persistent level for the stochastic model (2) when $\rho_1 = 8$, $\rho_2 = 0.002$; **f** the persistent level for the stochastic model (2) when $\rho_1 = 0.1$, $\rho_2 = 0.3$. Here $(P(0), A(0), Z(0)) = (0.5, 0.4, 0.8)$, $\sigma_1 = 0.01$, $x = 1.197$, $y = 2.5$, $P_{\text{in}} = 0.74$ in all panels. Other parameter values can be found in Table 1

suggest that the presence of environmental fluctuations is adverse to the persistence of zooplankton, and as a result, algal population could benefit from the decrease of grazing pressure from zooplankton; meanwhile, the growth of algae population requires more consumption of dissolved phosphorus.

Theorem 2 gives the sufficient and necessary criteria for the persistence of model (2), but this could not guarantee that model (2) is stable in mean. To address this issue, we obtain the following theorem.
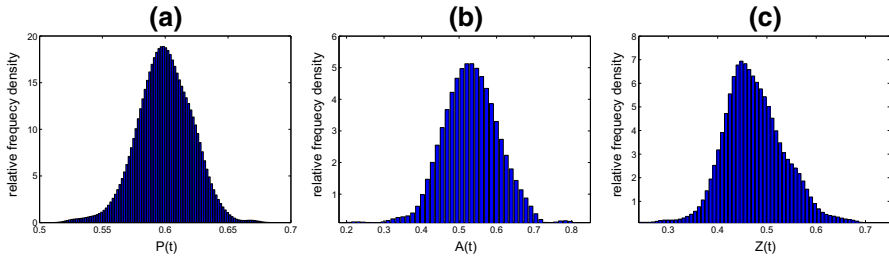
Fig. 4 **a** Histogram of probability density function for dissolved phosphorus; **b** histogram of probability density function for algae; **c** Histogram of probability density function for zooplankton. Parameters are same as in Fig. 3d

Theorem 3 *Assume that model* (2) *is persistent in mean a.s., and then, it admits a unique ergodic stationary distribution $\pi(\cdot)$, provided that*

$$\frac{1}{2} \max \left\{ \sigma_1^2, \sigma_2^2(x, \rho_1), \sigma_3^2(y, \rho_2) \right\} < \min\{e, s_1(x), s_2(y)\}. \tag{8}$$

Moreover, its solution $\Phi(t)$ has the following property:

$$
\begin{aligned}
\langle P(x, y) \rangle &= \int_{R_+^3} \phi_1 \pi(\mathrm{d}\phi_1, \mathrm{d}\phi_2, \mathrm{d}\phi_3) = \frac{c(x, y)\langle Z(x, y)\rangle + \eta(x, \rho_1)}{\alpha \mu(x)}, \ a.s., \\
\langle A(x, y) \rangle &= \int_{R_+^3} \phi_2 \pi(\mathrm{d}\phi_1, \mathrm{d}\phi_2, \mathrm{d}\phi_3) = \frac{\kappa(y, \rho_2)}{\delta c(x, y)}, \ a.s., \\
\langle Z(x, y) \rangle &= \int_{R_+^3} \phi_3 \pi(\mathrm{d}\phi_1, \mathrm{d}\phi_2, \mathrm{d}\phi_3) = \frac{\lambda(x, y)}{s_2(y)q(y) + ec(x, y)/\alpha\mu(x)}, \ a.s.
\end{aligned}
\tag{9}
$$

The proof of Theorem 3 can be found in "Appendix B", and the predicted dynamics are verified in Fig. 4.

Remark 1 In our analysis for the stochastic asymptotic behaviors of model (2), the traits of plankton are considered as a set of certain parameters. This is reasonable based on the basic assumptions of adaptive dynamics (Geritz et al. 1998).

Remark 2 Theorem 3 shows that model (2) is stable in mean almost surely. Moreover, the long-term mean persistent level of model (2) estimated in (9) could be approximately treated as the positive stable "stochastic ecological equilibrium" of model (2).

We then investigate how environmental fluctuations, the concentration of dissolved phosphorus and zooplankton grazing affect algal evolution, and whether one algal species with an ancestral trait can gradually evolve to two species with different traits (Meng et al. 2015; Pu et al. 2017), by deriving and analyzing the invasion fitness of a rare mutant algal species. We start our investigation with a special case in the absence of zooplankton grazing.

3 Adaptive Dynamics in Stochastic EPA Model

In the absence of zooplankton grazing, the stochastic phosphorus–algae interaction dynamics can be described as follows:

$$
\begin{cases}
\mathrm{d}P(t) = \big[e(P_{\mathrm{in}} - P) + d_1 Q(x)A - \alpha\mu(x)PAQ(x)\big]\mathrm{d}t + \sigma_1 P\mathrm{d}B_1(t), \\
\mathrm{d}A(t) = \big[\alpha\mu(x)PA - s_1(x)A - d_1 A\big]\mathrm{d}t + \sigma_2(x,\rho_1)A\mathrm{d}B_2(t),
\end{cases}
\tag{10}
$$

where the parameters have the same meanings as in model (2). From the analysis of Theorems 2 and 3, when $P_{\mathrm{in}} > \frac{\eta(x,\rho_1)}{\alpha\mu(x)}$ and inequality (8) holds, model (10) is stable in mean, and the value of the stochastic ecological equilibrium is given in (7).

We assume that the mutation is of small effect, such that when mutant algal species A_{mut} appear in the resident stochastic model (10), their trait x_{mut} is ecologically close to the resident trait x, and the per capita growth rate of mutant algae is also similar to that of residents (Ripa and Dieckmann 2013). That is

$$
\mathrm{d}A_{\mathrm{mut}}(t) = \big[\alpha\mu(x_{\mathrm{mut}})PA_{\mathrm{mut}} - s_1(x_{\mathrm{mut}})A_{\mathrm{mut}} - d_1 A_{\mathrm{mut}}\big]\mathrm{d}t + \sigma_2(x_{\mathrm{mut}},\rho_1)A_{\mathrm{mut}}\mathrm{d}B_2(t).
\tag{11}
$$

In order to investigate the evolution of algal cell size, we first define the fitness function. Throughout this paper, we choose the fitness to be the long-term mean fitness, i.e., the long-term mean exponential growth rate of the mutant. Applying the Itô formula (Mao 2006) to (11), integrating from 0 to t and dividing by t on both sides leads to

$$
\frac{1}{t}\ln\frac{A_{\mathrm{mut}}(t)}{A_{\mathrm{mut}}(0)} = \alpha\mu(x_{\mathrm{mut}})\frac{1}{t}\int_0^t P(s)\mathrm{d}s - \eta(x_{\mathrm{mut}},\rho_1) + \frac{1}{t}\int_0^t \sigma_2(x_{\mathrm{mut}},\rho_1)\mathrm{d}B_2(s).
$$

We also assume the mutants appear at a low density, such that it does not perturb the concentration of phosphorus at the stochastic ecological equilibrium. Then, by using the strong law of large numbers for martingales (Mao et al. 2002), the invasion fitness of the mutant algae can be described as follows:

$$
F_1(x, x_{\mathrm{mut}}) := \lim_{t\to\infty}\frac{\ln A_{\mathrm{mut}}(t)}{t} = \alpha\mu(x_{\mathrm{mut}})\langle P(x)\rangle - \eta(x_{\mathrm{mut}},\rho_1),
\tag{12}
$$

where $F_1(x, x) = 0$, $\langle P(x)\rangle$ is the stochastic ecological equilibrium concentration of dissolved phosphorus, which is given in (7). Note that the value of $F_1(x, x_{\mathrm{mut}})$ is determined by the maximum production rate of mutants, the mean persistent level of the phosphorus concentration in model (10), as well as the total loss rate of mutants. The sign of $F_1(x, x_{\mathrm{mut}})$ determines the fate of mutant algae: if $F_1(x, x_{\mathrm{mut}}) > 0$, then the population density of the mutants will initially increase, i.e., mutant algae can invade; otherwise, they cannot invade and are doomed to go extinct. When successive invasions and replacements can occur, algae evolve to larger cell sizes if the fitness gradient

$$
D_1(x) = \frac{\partial F_1(x, x_{\mathrm{mut}})}{\partial x_{\mathrm{mut}}}\bigg|_{x_{\mathrm{mut}}=x} = \alpha\mu'(x)\langle P(x)\rangle - \eta'(x,\rho_1)
\tag{13}
$$

is positive, where $\eta'(x, \rho_1) = \left.\dfrac{\mathrm{d}\eta(x_{\mathrm{mut}}, \rho_1)}{\mathrm{d}x_{\mathrm{mut}}}\right|_{x_{\mathrm{mut}}=x}$. On the contrary, when $D_1(x)$ is negative, algae will evolve to smaller cell sizes.

Particularly, according to Dieckmann and Law's work in (Dieckmann and Law 1996), if mutations are rare and sufficiently small, then the step-by-step evolution can be approximately described by the canonical equation as follows:

$$\frac{\mathrm{d}x}{\mathrm{d}\tau} = \frac{1}{2}\nu_x \xi_x^2 \langle A(x)\rangle D_1(x), \tag{14}$$

where time τ spans the longer evolutionary timescale. The parameter ν_x is the probability of individual mutation, which is born in resident algal population and ξ_x^2 is the variance of mutation distribution of phenotypic effect of mutations, both of which are assumed to be trait-irrespective. The quantity $\langle A(x)\rangle$ is the algal population density at the stochastic ecological equilibrium. The quantity $\frac{1}{2}\nu_x \xi_x^2 \langle A(x)\rangle$ is the evolutionary rate of the population and $\frac{1}{2}$ means that half of the population are disadvantageous and are doomed to extinction (Dieckmann et al. 1995). Model (10) together with (14) is called the stochastic evolutionary–phosphorus–algae (EPA) model.

Repeated invasions and substitutions result in directional evolution until the population reaches an evolutionary singularity x^*, where directional evolution vanishes, i.e.,

$$D_1(x^*) = \alpha\mu'(x^*)\langle P(x^*)\rangle - \eta'(x^*, \rho_1) = 0. \tag{15}$$

There are two evolutionary possibilities at x^*: the population of resident algae can allow for evolutionary branching or the evolution would come to a halt. Whether the resident algae can undergo an evolutionary branching depends on its convergence stability and evolutionary stability at x^*. Before the analysis of these two stabilities, we first determine the range of x^*. Combining Eqs. (15) and (7) leads to

$$\langle P(x^*)\rangle = \frac{\eta(x^*, \rho_1)}{\alpha\mu(x^*)} = \frac{\eta'(x^*, \rho_1)}{\alpha\mu'(x^*)}. \tag{16}$$

Moreover, from the expression of $\langle P(x)\rangle$ in (7) we have

$$\langle P(x^*)\rangle' = \left.\frac{\partial\langle P(x)\rangle}{\partial x}\right|_{x=x^*} = \frac{\mu(x^*)\eta'(x^*, \rho_1) - \mu'(x^*)\eta(x^*, \rho_1)}{\alpha\mu^2(x^*)} = 0. \tag{17}$$

According to the expression of $\eta(x, \rho_1)$ in (5), $\sigma_2(x, \rho_1)$ in (3), as well as $s_1(x)$ in Table 1, $\eta(x, \rho_1)$ is polynomial in x with $\eta'(x, \rho_1) > 0$ and $\eta''(x, \rho_1) = \dfrac{\mathrm{d}^2\eta(x, \rho_1)}{\mathrm{d}x^2} > 0$, which together with (16) leads to $\mu'(x^*) > 0$. Then, by the expression of $\mu(x)$ in Table 1, we can compute that $x^* \in (0, \sqrt{a_3/a_1})$.

The evolutionary stability can be estimated by calculating the second partial derivative of the invasion fitness with respect to mutant trait x_{mut} and evaluating at x^*, and the convergence stability can be determined by the first derivative of the fitness gradient at

x^* (Geritz et al. 1998; Rossa et al. 2015; Dercole et al. 2016). Since $x^* \in (0, \sqrt{a_3/a_1})$, then by simple calculation $\mu''(x^*) < 0$ and the following inequality holds,

$$\left.\frac{\partial^2 F_1(x, x_{\text{mut}})}{\partial x_{\text{mut}}^2}\right|_{x_{\text{mut}}=x^*} = \left.\frac{\partial D_1(x)}{\partial x}\right|_{x=x^*} = \mu''(x^*)\frac{\eta(x^*, \rho_1)}{\mu(x^*)} - \eta''(x^*, \rho_1) < 0.$$

(18)

This implies that once the evolutionary singularity x^* exists, it is both convergence stable and evolutionary stable, i.e., x^* is a CSS (Christiansen 1991; Eshel 1983), and the evolution would cease there. According to (15), (17) and (18), we can conclude that, in the absence of zooplankton, algae always evolve toward their fitness maximum, and the long-time mean persistent level of phosphorus concentration approaches its minimum as algal cell size approaches x^*. Furthermore, since $x^* < \sqrt{a_3/a_1}$ (where $\mu'(x^*) > 0$), this raises an interesting question why algal evolution does not cease at the optimal size $\sqrt{a_3/a_1}$ (where $\mu'(\sqrt{a_3/a_1}) = 0$), but instead decreases further, under the influence of environmental fluctuations. One reasonable explanation is that the fitness advantage brought by a high growth rate and a small noise intensity is not enough to offset the fitness disadvantage afforded by a relatively high sinking rate at the optimal size. The deterministic model also shows a similar phenomenon (Jiang et al. 2005).

We then prove the evolutionary singular strategy x^* is unique. From the above analysis, we only need to prove $\langle P(x)\rangle' = 0$ has only one solution in $(0, \sqrt{a_3/a_1})$. From (7),

$$\langle P(x)\rangle' = \frac{\mu(x)\eta'(x, \rho_1) - \mu'(x)\eta(x, \rho)}{\alpha\mu^2(x)} = \frac{f_4(x)}{\alpha\mu^2(x)},$$

(19)

where $f_4(x) = \mu(x)\eta'(x, \rho_1) - \mu'(x)\eta(x, \rho)$ and $f_4'(x) = \mu(x)\eta''(x, \rho_1) - \mu''(x)\eta(x, \rho)$. Since $\eta''(x, \rho_1) > 0$ and when $x < \sqrt{a_3/a_1}$, $\mu''(x) < 0$, then $f_4'(x) > 0$. It has at most one $x^* \in (0, \sqrt{a_3/a_1})$ such that $f_4(x^*) = 0$, i.e., $\langle P(x^*)\rangle' = 0$. Thus, once the evolutionary singularity x^* exists, it is unique.

We then investigate the effect of environmental fluctuation on algal cell size. Considering x^* as a function of ρ_1, by the implicit function theorem, we have

$$\frac{\mathrm{d}x^*}{\mathrm{d}\rho_1} = \frac{\frac{\partial D_1(x^*)}{\partial \rho_1}}{-\frac{\partial D_1(x^*)}{\partial x^*}}.$$

By (18), $-\frac{\partial D_1(x^*)}{\partial x^*} > 0$. Therefore, the sign of $\frac{\mathrm{d}x^*}{\mathrm{d}\rho_1}$ is completely determined by the sign of $\frac{\partial D_1(x^*)}{\partial \rho_1}$. By simple calculation,

$$\begin{aligned}
\frac{\partial D_1(x^*)}{\partial \rho_1} &= k_3^2 x^{*3}\left(\frac{a_3 - a_1 x^2}{2(a_1 x^{*2} + a_2 x^* + a_3)} - 2\right)\frac{\partial}{\partial \rho_1}\left(\frac{\rho_1}{k_4 + \rho_1}\right)^2 \\
&= k_3^2 x^{*3}\left(\frac{a_3 - a_1 x^{*2}}{2(a_1 x^{*2} + a_2 x^* + a_3)} - 2\right)\frac{k_4 \rho_1}{(k_4 + \rho_1)^3} \\
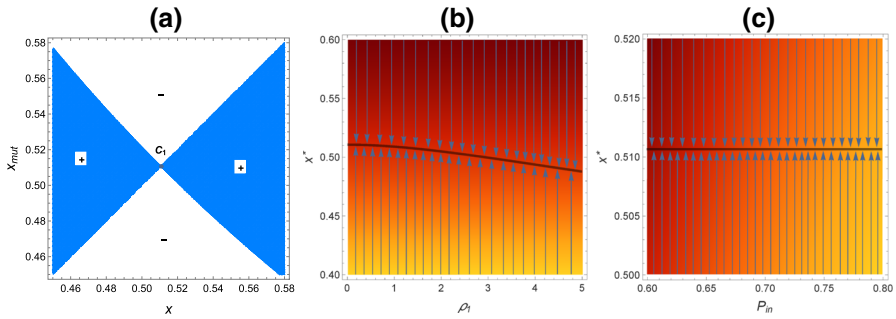&< 0.
\end{aligned}$$

Fig. 5 **a** Pairwise invasibility plots (PIP) when $P_{in} = 0.74$, $\rho_1 = 0.01$; **b** bifurcation diagrams for stochastic fluctuation experienced by algae when $P_{in} = 0.74$; **c** Bifurcation diagrams for dissolved phosphorus input when $\rho = 0.01$. In **a**, the fitness of the mutant is negative in the white regions, while in the blue shaded regions, the fitness of the mutant is positive. Point C_1 is a CSS. In **b** and **c**, the black solid lines indicate the CSS, the arrows indicate directions of the evolutionary changes of algal cell size, the orange shaded area represents the DensityPlot of algal carbon density in the feasible region, where the stochastic model (10) is persistent in mean for different algal sizes, and the lighter the area, the higher the algal density. Here $\sigma_1 = 0.01$ in all panels. Other parameter values are listed in Table 1 (Colour figure online)

Then, $\frac{dx^*}{d\rho} < 0$. Moreover, from (13), it is obvious that the phosphorus input rate P_{in} does not influence the value of $D_1(x)$, i.e., $\frac{\partial D_1(x^*)}{\partial P_{in}} = 0$, then $\frac{dx^*}{dP_{in}} = 0$. As a summary, we have the following theorem.

Theorem 4 *Once the evolutionary singularity x^* exists, it is unique and must be a CSS. Moreover, $x^* \in (0, \sqrt{a_3/a_1})$ and the value of x^* always decreases with respect to ρ_1, but has no response to the changing phosphorus input P_{in}.*

Theorem 4 is illustrated in Fig. 5. Figure 5a is the 'pairwise invasibility plot' (PIP), which is a graph of the sign of the fitness $F_1(x, x_{mut})$. The fitness of mutant is positive in the blue regions marked by '+', and negative in the white regions. In Fig. 5a, the vertical line through the singularity x^* lies completely in the region in which the fitness of mutant is negative; this implies that point C_1 is an ESS (evolutionary stable strategy). There is a '+' above the diagonal on the left, and below the diagonal on the right of point C_1, then point C_1 is also convergence stable. Hence, point C_1 is a CSS. Figure 5b, c are bifurcation diagrams for stochastic fluctuation and nutrient input in model (10). Fixing $P_{in} = 0.74$, it is obvious that there is a decreasing trend of x^* with the increase of ρ_1, see Fig. 5b. Fixing $\rho_1 = 0.01$, the increasing nutrient input has no influence on algal cell size in the absent of zooplankton, see Fig. 5c. Moreover, all lines in Fig. 5b, c are black, which implies that all evolutionary singularities are CSSs, i.e., evolutionary branching will never occur when zooplankton are absent, no matter how large the noise intensity and phosphorus input are. This confirms the competitive exclusion principle (Hardin and G. 1960) in both deterministic ($\rho_1 = 0$) and stochastic models, from the perspective of adaptive dynamics.

From the above analysis, we observe that without zooplankton, when mutate algal population is small, they either cannot invade and go extinct, or out-compete the resident algae and become the new residents after successful invasion (Geritz 2005; Diekmann et al. 2005; Dercole and Rinaldi 2008; Dercole and Geritz 2015). There must

be a winner and a loser in this repeated competitive game between the resident and the mutant algal species, i.e., the coexistence of two algal species with different cell sizes would be impossible, though environmental fluctuations will lead to different values of fitness and drive algal evolution toward smaller cell sizes. In other words, without the existence of zooplankton, environmental stochasticity may not have significant influence on the outcomes of algal evolution.

4 Adaptive Dynamics of the Stochastic EPAZ Model with Fixed Zooplankton Body Size

From the analysis in Sect. 3, we know that, in the absence of zooplankton, environmental stochasticity will drive algal evolution toward smaller cell, but it does not have significant influence on the outcomes of algal evolution. In this section, we investigate whether environmental stochasticity can cause different evolutionary trends and consequences in algal cell size, in the presence of zooplankton. Assume that zooplankton have a fixed body size h and $h < \frac{2}{\theta\sqrt{v}}$, where θ and v are the parameters in the function of zooplankton ingestion rate in Table 1, and θ is a constant that defines zooplankton selectivity, v is a constant depicting how rapidly the ingestion rate deviates from its preferred algal size θh (Pu et al. 2017). Then, the stochastic PAZ model (2) becomes

$$
\begin{cases}
\mathrm{d}P(t) = \big[e(P_{\text{in}} - P) + d_1 Q(x)A + \big(Q(x) - \delta q(h)\big)c(x,h)AZ + d_2 q(h)Z \\
\qquad - \alpha\mu(x)PAQ(x)\big]\mathrm{d}t + \sigma_1 P\mathrm{d}B_1(t), \\
\mathrm{d}A(t) = \big[\alpha\mu(x)PA - c(x,h)AZ - s_1(x)A - d_1 A\big]\mathrm{d}t + \sigma_2(x,\rho_1)A\mathrm{d}B_2(t), \\
\mathrm{d}Z(t) = \big[\delta c(x,h)AZ - s_2(h)Z - d_2 Z\big]\mathrm{d}t + \sigma_3(h,\rho_2)Z\mathrm{d}B_3(t).
\end{cases}
\tag{20}
$$

According to Theorem 3, model (20) has a positive stable stochastic ecological equilibrium, provided that inequality (8) holds and $\lambda(x, h) > 0$. Moreover, the population densities of plankton and the concentration of phosphorus at the equilibrium are:

$$
\begin{aligned}
\langle P(x,h)\rangle &= \frac{c(x,h)\langle Z(x,h)\rangle + \eta(x,\rho_1)}{\alpha\mu(x)}, \\
\langle A(x,h)\rangle &= \frac{\kappa(h,\rho_2)}{\delta c(x,h)}, \\
\langle Z(x,h)\rangle &= \frac{\lambda(x,h)}{s_2(h)q(h) + ec(x,h)/\alpha\mu(x)}.
\end{aligned}
\tag{21}
$$

We next explore the evolution of algal cell size by applying the adaptive dynamics theory.

4.1 Monomorphic Evolutionary Dynamics

Similar to the derivation of (12), when rare mutant algal A_{mut} with a slightly different trait x_{mut} appears in the resident model (20) at a low density, the invasion fitness can be described as:

$$F_2(x, x_{\text{mut}}) = \alpha\mu(x_{\text{mut}})\langle P(x, h)\rangle - c(x_{\text{mut}}, h)\langle Z(x, h)\rangle - \eta(x_{\text{mut}}, \rho_1), \quad (22)$$

where $F_2(x, x) = 0$, the value of $\langle P(x, h)\rangle$ and $\langle Z(x, h)\rangle$ can be seen in (21). Intuitively, the effects of environmental stochasticity on mutant fitness are related to the sensitivity of zooplankton population and phosphorus concentration to environmental fluctuations as well as the noise caused algal loss rate.

The sign of $F_2(x, x_{\text{mut}})$ determines the fate of mutant algae, and the direction of evolution is determined by the sign of fitness gradient $D_2(x)$, by simple calculation,

$$D_2(x) = \left.\frac{\partial F_2(x, x_{\text{mut}})}{\partial x_{\text{mut}}}\right|_{x_{\text{mut}}=x} = \alpha\mu'(x)\langle P(x, h)\rangle - c'(x, h)\langle Z(x, h)\rangle - \eta'(x, \rho_1).$$

(23)

Since mutations are rare and sufficiently small, then similar to (14), the step-by-step evolution is approximately described as follows:

$$\frac{\mathrm{d}x}{\mathrm{d}\tau} = \frac{1}{2}\nu_x\xi_x^2\langle A(x, h)\rangle D_2(x), \quad (24)$$

where parameters in (24) have the same meaning as in (14). Model (20) together with (24) is called the stochastic evolutionary–phosphorus–algae–zooplankton (EPAZ) model.

If there exists a trait x^* satisfying

$$D_2(x^*) = \alpha\mu'(x^*)\langle P(x^*, h)\rangle - c'(x^*, h)\langle Z(x^*, h)\rangle - \eta'(x^*, \rho_1) = 0, \quad (25)$$

then x^* is called the evolutionary singular strategy and directional selection will cease there. Whether the directional evolution could approach x^* depends on the convergence stability of x^*, that is, attractor or repellor. If x^* is convergence stable, then whether the evolution will come to a halt or continue with branching is determined by the evolutionary stability of x^*. We next explore these two properties of x^* and define $h_1(x) = \frac{c'(x,h)}{c(x,h)} - \frac{\mu'(x)}{\mu(x)}, h_2(x) = \frac{\langle P(x,h)\rangle''}{\langle P(x,h)\rangle'} - \frac{\langle Z(x,h)\rangle''}{\langle Z(x,h)\rangle'}$; then, we obtain the main results in the following theorem, and the proof can be found in "Appendix C".

Theorem 5 *If $h_1(x^*) < h_2(x^*)$, then the evolutionary singularity x^* of model (24) is a repellor. Otherwise, x^* is either a CSS when $h_2(x^*) < \min\{h_1(x^*), 2h_1(x^*)\}$, or an evolutionary branching point when $0 > h_1(x^*) > h_2(x^*) > 2h_1(x^*)$. In this situation, x^* is convergence stable but lacks evolutionary stability, and the algal population will evolve to two species with different cell sizes.*

More details about Theorem 5 are listed in Table 2.

The evolution of a monomorphic algal population can also be analyzed graphically by means of PIPs, see Fig. 6.

When $\rho_1 = 0$, there only exists one evolutionary singularity and $x^* \approx 1.195$, see Fig. 6a. By calculation, $h_1(x^*) \approx -0.5658$ and $h_2(x^*) \approx -0.8285$, satisfying $h_1(x^*) > h_2(x^*) > 2h_1(x^*)$; this implies that B_1 is an evolutionary branching point. Similarly, when $\rho_1 = 0.47$, points B_2, B_3 in Fig. 6b, and when $\rho_1 = 0.68$, point B_4

Table 2 Evolutionary properties of x^*

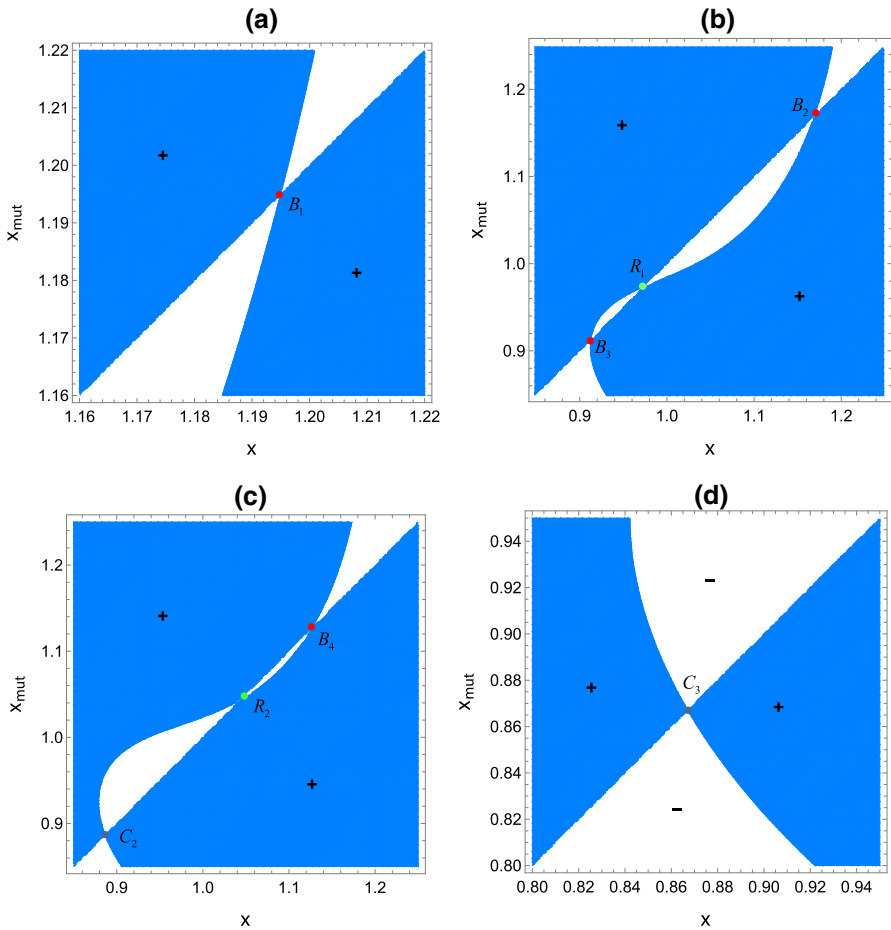|	$h_2(x^*) \geq 0$	$\begin{array}{l}|h_2(x^*)| < |h_1(x^*)| \\ (h_2(x^*) < 0)\end{array}$	$\begin{array}{l}|h_1(x^*)| < \\ |h_2(x^*)| < \\ 2|h_1(x^*)| \\ (h_2(x^*) < 0)\end{array}$	$\begin{array}{l}|h_2(x^*)| > 2|h_1(x^*)| \\ (h_2(x^*) < 0)\end{array}$
$h_1(x^*) > 0$	CSS or Repellor	CSS	CSS	CSS
$h_1(x^*) < 0$	Repellor	Repellor	Branching point	CSS

Fig. 6 **a** Pairwise invasibility plots when $\rho_1 = 0$; **b** pairwise invasibility plots when $\rho_1 = 0.47$; **c** pairwise invasibility plots when $\rho_1 = 0.68$; **d** pairwise invasibility plots when $\rho_1 = 0.9$. Here $P_{\text{in}} = 0.74$ and $h = 2.5$ in all panels. In the white regions, the fitness of the mutant is negative, while in the blue shaded regions, the fitness of the mutants is positive. Points K_7, C_3 are CSSs, points R_1, R_2 are repellors, points B_1, B_2, B_3 are evolutionary branching points. Other parameter values are listed in Table 1 (Colour figure online)
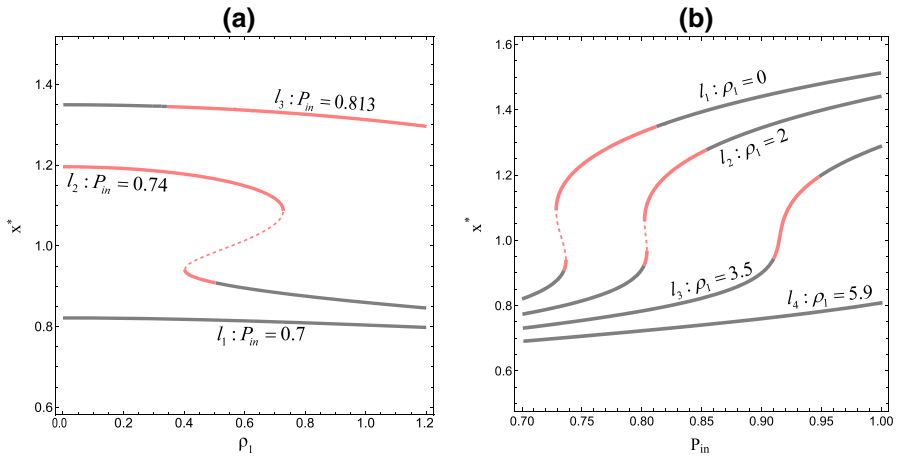
Fig. 7 **a** Bifurcation diagrams for stochastic fluctuation experienced by algae when $P_{in} = 0.7, 0.74, 0.813$, respectively; **b** bifurcation diagrams for phosphorus input level when $\rho_1 = 0, 2, 3.5, 5.9$, respectively. Here red solid lines indicate the evolutionary branching point, dashed red lines indicate the repellor, black solid lines indicate the CSS (Colour figure online)

in Fig. 6c is all evolutionary branching points. At these points, the algal population will evolve to two species with different cell sizes. Moreover, we can show that when $\rho_1 = 0.9$, point K_7 in Fig. 6c and point C_3 in Fig. 6d are both CSSs. In this situation, algal cell size will evolve to this evolutionary singularity and cease there, that is, they are the endpoints of the evolution process. Point R_2 in Fig. 6b and point R_2 in Fig. 6c are repellors.

We then investigate the effects of environmental fluctuation and phosphorus input level on algal cell size, in the presence of zooplankton. We obtain the theorem below.

Theorem 6 *The value of evolutionary singularity x^* at CSS or evolutionary branching point decreases with respect to ρ_1, i.e., environmental fluctuations drive algal evolution toward smaller cell sizes. Moreover, the value of x^* at CSS or evolutionary branching point increases with respect to the phosphorus input rate P_{in}, provided that $h_1(x^*) < 0$. While x^* is decreasing in P_{in} as long as $h_1(x^*) > 0$.*

The proof of Theorem 6 can be found in "Appendix C".

The dynamics of algal evolution as predicted by Theorem 6 are verified in Fig. 7. In panel (a), algal cell size shows an obvious decreasing trend with the increase of ρ_1 in different phosphorus levels. In panel (b), when $x^* \in (0.5, 1.6)$, $h_1(x^*) < 0$, and algal cell size increases significantly with the increase of P_{in}, under the influence of different environmental noise intensities. In what follows, we will provide a more detailed illustration about the effects of phosphorus input level as well as the environmental fluctuation on algal evolution. We elaborate our results mainly from the following aspects: the number of evolutionary singularities, the evolutionary trend, as well as the evolutionary outcomes of algal cell size.

For the effects of phosphorus inflows, we have the following conclusions:

(1) The increasing phosphorus inflow would drive algal evolution toward larger cell sizes with or without environmental fluctuation experienced by algae, provided that $h_1(x^*) < 0$, see Fig. 7b.

(2) In the absence of environmental fluctuation experienced by algae, a moderate phosphorus inflow, namely $P_{in} \in [0.734, 0.812]$, allows for the occurrence of evolutionary branching, i.e., the emergence of new algal species. We called the values of the endpoints of the interval as two phosphorus thresholds (left and right) at which the evolutionary stability of x^* will be altered. Oligotrophication ($P_{in} < 0.734$) or eutrophication ($P_{in} > 0.812$) will induce CSS, see l_1 in Fig. 7b.

(3) The increasing of environmental fluctuation experienced by algae will increase both the left and right phosphorus thresholds; meanwhile, the range of phosphorus inflow that allows for evolutionary branching narrows, see l_2 and l_3 in Fig. 7b. This implies that under the influence of environmental stochasticity ($\rho_1 < 5.9$), the emergence of new algal species requires the support of more phosphorus and is less likely to occur. If the environmental noise is extremely large ($\rho_1 \geq 5.9$), evolutionary branching will never occur, see l_4 in Fig. 7b.

For the environmental fluctuation experienced by algae, we have the following conclusions:

(1) Environmental fluctuation could drive algal evolution toward smaller cell sizes, and with a moderate phosphorus inflow, the decreasing trend is more significant, see Fig. 7a.

(2) From Fig. 7b we can see that, for a fixed P_{in} in the eutrophication environment, x^* is always a CSS in the absence of environmental fluctuation. While the existence of environmental fluctuation ($\rho_1 < 5.9$) could lead to the emergence of evolutionary branching, which is illustrated by the curve l_3 in Fig. 7a. Then, we conclude that small environmental fluctuation is conducive to the formation of new algal species in the eutrophication environment. Small environmental fluctuation also allows for the occurrence of evolutionary branching in a moderate phosphorus environment, see l_2 in Fig. 7a. From l_2, evolutionary branching will occur when $\rho_1 < \rho_1^* \approx 0.726$, and the evolutionary stability of x^* will be altered due to CSS, once environmental noise intensity goes beyond ρ_1^*, which is verified in Fig. 6. In an oligotrophic environment, evolutionary branching never occurs, see l_1 in Fig. 7a.

(3) From Fig. 6, we observe that, for a fixed moderate phosphorus inflow, a moderate environmental fluctuation could lead to multiple evolutionary singularities, which can be clearly seen from the curve l_2 in Fig. 7a. From l_2, when $\rho_1 \in (0.4, \rho_1^*)$, there will be three evolutionary singularities, namely two evolutionary branching points and one repellor when $\rho_1 \in (0.4, 0.5)$, one evolutionary branching point, one repellor and one CSS when $\rho_1 \in (0.5, \rho_1^*)$. When the noise intensity is large ($\rho_1 > \rho_1^*$), extremely small ($\rho_1 < 0.4$) or zero, x^* is unique. Moreover, in an oligotrophic environment, x^* is always unique, see l_1 in Fig. 7a.

As a summary, both the environmental fluctuation and the phosphorus input could significantly affect the adaptive dynamics of model (20). The existence of environmental fluctuation may increase the biodiversity of algae in relatively eutrophic environments and decrease it in relatively oligotrophic environments. Moreover, small

environmental fluctuation and moderate phosphorus inflow are beneficial to algal population diversity and consequently the sustainable development of lake ecosystem, while large noise and extreme phosphorus inflow have adverse effects.

Remark 3 Comparing the adaptive analysis of model (10) and model (20), we know that only in the presence of zooplankton population can environmental fluctuations and phosphorus input levels significantly affect the trends and outcomes of algal evolution. This implies that grazing pressure from zooplankton enhances algal biodiversity.

4.2 Dimorphic Evolutionary Analysis

By the analysis in Sect. 4.1, we can see that proper stochastic fluctuations and phosphorus inflow could lead to an evolutionary branching, which induces a dimorphic algal species with two different cell sizes, namely x_1 and x_2, respectively, from the initially monomorphic algal species with trait x. The stochastic PAZ model with two different algal species and fixed zooplankton body size can be described as follows:

$$
\begin{cases}
\begin{aligned}
\mathrm{d}P(t) = &\Big[e(P_{\mathrm{in}} - P) + \sum_{i=1}^{2} d_1 Q(x_i)A_i + \sum_{i=1}^{2}\big(Q(x_i) - \delta q(h)\big)c(x_i,h)A_i Z + d_2 q(h)Z \\
&- \sum_{i=1}^{2}\alpha\mu(x_i)PA_i Q(x_i)\Big]\mathrm{d}t + \sigma_1 P\mathrm{d}B_1(t),
\end{aligned} \\
\mathrm{d}A_1(t) = \big[\alpha\mu(x_1)PA_1 - c(x_1,h)A_1 Z - s_1(x_1)A_1 - d_1 A_1\big]\mathrm{d}t + \sigma_2(x_1,\rho_1)A_1\mathrm{d}B_2(t), \\
\mathrm{d}A_2(t) = \big[\alpha\mu(x_2)PA_2 - c(x_2,h)A_2 Z - s_1(x_2)A_2 - d_1 A_2\big]\mathrm{d}t + \sigma_2(x_1,\rho_1)A_2\mathrm{d}B_3(t), \\
\mathrm{d}Z(t) = \Big[\sum_{i=1}^{2}\delta c(x_i,h)A_i Z - s_2(h)Z - d_2 Z\Big]\mathrm{d}t + \sigma_3(h,\rho_2)Z\mathrm{d}B_4(t).
\end{cases}
\tag{26}
$$

For model (26), we provide the following assumptions and theorems.

Assumption 1 $\hat{\lambda}(x_i,h) > 0$, $i = 1, 2$.

Assumption 2 $\frac{1}{2}\max\{\sigma_1^2, \check{\sigma}_2^2, \sigma_3^2\} < \min\{e, \hat{s}_1, s_2\}$.

Assumption 3 $\min\{x_1, x_2\} < x < \max\{x_1, x_2\}$.

Here, the notations ˆ and ˇ stand for the minimum and maximum value, respectively, and the detailed expressions can be seen from Page 7.

Theorem 7 *For any given initial value* $(P(0), A_1(0), A_2(0), Z(0)) \in R_+^4$, *model* (26) *has a unique positive solution* $\Psi(t) = (P(t), A_1(t), A_2(t), Z(t))$ *for all* $t > 0$ *almost surely. Moreover, the solution satisfies*

$$
\limsup_{t\to\infty}\left[P(t) + \sum_{i=1}^{2}Q(x_i)A_i(t) + q(h)Z(t)\right] < \infty, \ a.s.
$$

Theorem 8 *For any given initial value* $\Psi(0) \in R_+^4$, *model* (26) *is stable in mean a.s., provided that Assumptions* 1–3 *hold. Moreover, the unique mean persistent level can be estimated in* (D.82).
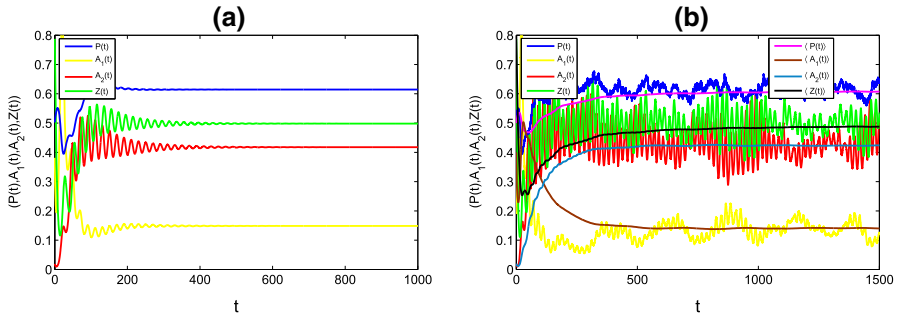
Fig. 8 **a** Time series for the stochastic model (26) when $\rho_1 = 0$; **b** time series for the stochastic model (26) when $\rho_1 = 0.1$; here $x_1 = 1.54$, $x_2 = 0.788$, $A_1(0) = 0.4$, $A_2(0) = 0.02$ in all panels, and other parameter values are same as in Fig. 3d

The proofs of Theorems 7 and 8 can be found in "Appendix D". Theorem 8 is verified by numerical simulations in Fig. 8.

Remark 4 From the proof of Theorem 8, we know that Assumptions 1–2 guarantee that at least one algal species could persist in model (26). If one of the algal species dies out, model (26) will ultimately degenerate to model (20). Assumption 3 ensures the stable coexistence of the two algal species. It reveals that if two algal species could coexist in model (26), the cell size x_1 of one algal species must larger than the original algal size x in model (20), while the other algal cell size is smaller than x. This implies that after the original algal species splits into two species at trait x, one of the new emerging algal species evolves in the direction of cell enlargement, while the other species evolves in the opposite direction. This can also be seen intuitively in the following simulated evolutionary tree, see Fig. 9 (c1)–(c3).

Next, we consider the existence of secondary branching on a much longer evolutionary time scale, i.e., whether evolution could lead to further evolutionary branching of an evolutionary tree or evolutionary stable coexistence for these two algal populations (Hui et al. 2018). We further assume the mutant either arises from algal species A_1 or from algal species A_2, but not both at a time. Similar to the above analysis, when rare mutant algae A_{mut} with trait x_{mut}, which is slightly different from x_1 and x_2, appears in the resident stochastic model (26) at a low density, the invasion fitness is given by

$$F_3(x_1, x_2, x_{mut}) = \alpha \mu(x_{mut})\langle P(x_1, x_2)\rangle - c(x_{mut}, h)\langle Z(x_1, x_2)\rangle - \eta(x_{mut}, \rho_1),$$
(27)

where $\langle P(x_1, x_2)\rangle$ and $\langle Z(x_1, x_2)\rangle$ are given in (D.82), which are, respectively, the phosphorus concentration and zooplankton population density at the stochastic ecological equilibrium of model (26). Obviously, $F_3(x_1, x_2, x_i) = 0$, $i = 1, 2$. The directions of evolution are governed by the fitness gradients, which are given by:

$$
\begin{cases}
D_{31}(x_1, x_2) = \dfrac{\partial F_3(x_1, x_2, x_{\text{mut}})}{\partial x_{\text{mut}}}\bigg|_{x_{\text{mut}}=x_1} = \alpha\mu'(x_1)\langle P(x_1, x_2)\rangle - c'(x_1, h)\langle Z(x_1, x_2)\rangle \\
\hphantom{D_{31}(x_1, x_2) = } - \eta'(x_1, \rho_1), \\
D_{32}(x_1, x_2) = \dfrac{\partial F_3(x_1, x_2, x_{\text{mut}})}{\partial x_{\text{mut}}}\bigg|_{x_{\text{mut}}=x_2} = \alpha\mu'(x_2)\langle P(x_1, x_2)\rangle \\
\hphantom{D_{32}(x_1, x_2) = } - c'(x_2, h)\langle Z(x_1, x_2)\rangle - \eta'(x_2, \rho_1).
\end{cases}
\tag{28}
$$

Since the mutations are rare and small, then based on the results in (Dieckmann and Law 1996), the step-by-step coevolutionary dynamics of traits x_1 and x_2 can be approximately described as follows:

$$
\begin{cases}
\dfrac{dx_1}{d\tau} = \dfrac{1}{2}\nu_{x_1}\xi_{x_1}^2\langle A_1(x_1, x_2)\rangle D_{31}(x_1, x_2) =: m_1(x_1, x_2)D_{31}(x_1, x_2), \\
\dfrac{dx_2}{d\tau} = \dfrac{1}{2}\nu_{x_2}\xi_{x_2}^2\langle A_2(x_1, x_2)\rangle D_{32}(x_1, x_2) =: m_2(x_1, x_2)D_{32}(x_1, x_2),
\end{cases}
\tag{29}
$$

where ν_{x_1} and ν_{x_2} are, respectively, the probabilities of individual mutation, which is born in resident algal species A_1 and A_2. $\xi_{x_1}^2$ and $\xi_{x_2}^2$ are, respectively, the variance of mutation distribution of phenotypic effect of algal species A_1 and A_2. $\langle A_1(x_1, x_2)\rangle$ and $\langle A_2(x_1, x_2)\rangle$ are, respectively, the population densities of algae species A_1 and A_2 at the stochastic ecological equilibrium, and the estimated values are given in (D.82). $D_{31}(x_1, x_2)$ and $D_{32}(x_1, x_2)$ are fitness gradients described as in (28). If there exists a pair of traits (x_1^*, x_2^*) at which fitness gradients vanish, i.e.,

$$
\begin{cases}
\alpha\mu'(x_1^*)\langle P(x_1^*, x_2^*)\rangle - c'(x_1^*, h)\langle Z(x_1^*, x_2^*)\rangle - \eta'(x_1^*, \rho_1) = 0, \\
\alpha\mu'(x_2^*)\langle P(x_1^*, x_2^*)\rangle - c'(x_2^*, h)\langle Z(x_1^*, x_2^*)\rangle - \eta'(x_2^*, \rho_1) = 0,
\end{cases}
\tag{30}
$$

then (x_1^*, x_2^*) is called an "evolutionary singular dimorphism". By investigating the convergence stability and the evolutionary stability of (x_1^*, x_2^*), we have the following theorem with the detailed proof presented in "Appendix E".

Theorem 9 *The two algal species with different cell sizes will reach an evolutionary stable coexistence after first evolutionary branching, i.e., the evolutionary singular dimorphism (x_1^*, x_2^*) is a CSS, provided that $h_{2i}(x_1^*, x_2^*) > 0$ hold for both $i \in \{1, 2\}$. While (x_1^*, x_2^*) is a repellor if there exists at least one $i \in \{1, 2\}$, such that $h_{2i}(x_1^*, x_2^*) < 0$. Here, $h_{2i}(x_1, x_2) = \alpha\mu(x_i)\langle P(x_1, x_2)\rangle''_{x_i} - c(x_i, h)\langle Z(x_1, x_2)\rangle''_{x_i}$, $i = 1, 2$.*

Remark 5 From the proof Theorem 9, we know that with the existence of zooplankton, after the first evolutionary branching, once there exists an evolutionary singular dimorphism (x_1^*, x_2^*) which is convergence stable, it must also be evolutionarily stable, i.e., CSS. This suggests a final endpoint of the evolution, and two algal species with different cell sizes will reach an evolutionary stable coexistence under proper environmental fluctuations.

The expected courses of evolution in Theorem 9 are illustrated in Fig. 9. Figure 9 characterizes the coevolution process of two algal species with moderate phosphorus
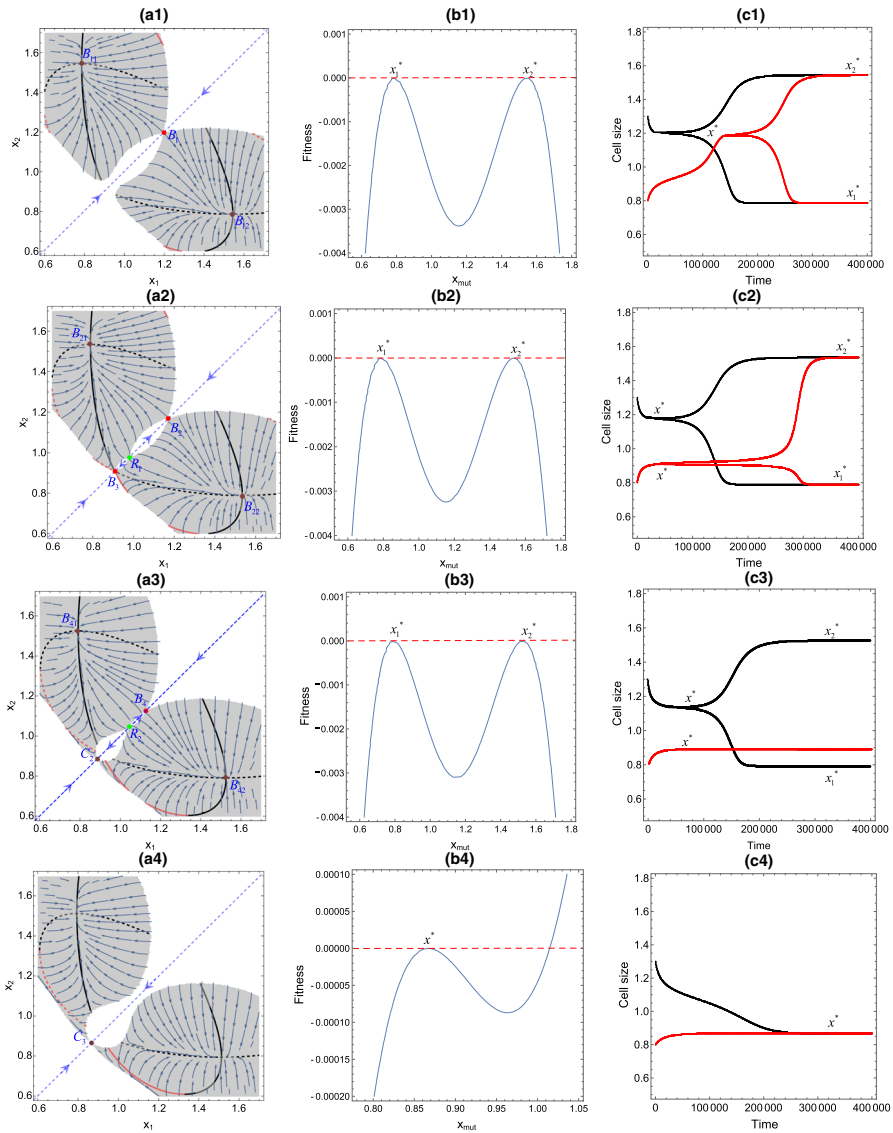
Fig. 9 **a1**–**a4** The trait coevolution of two algal species when $\rho = 0, 0.47, 0.68, 0.9$, respectively; **b1**–**b4** are fitness landscapes when $\rho = 0, 0.47, 0.68, 0.9$, respectively; **c1**–**c4** are the long-term evolutionary dynamics from $x(0) = 0.8$ and $x(0) = 1.3$ when $\rho = 0, 0.47, 0.68, 0.9$, respectively. Other parameters are same as in Fig. 6. In **a1**–**a4**, the shaded areas indicate protected dimorphism, which are separated by stable (black) and unstable (red) isoclines at which selection gradient vanishes in either x_1-direction (solid) or x_2-direction (dashed). Arrows on the main diagonal show the evolutionary directions of x in a monomorphic environment. The vector fields denote the directions of evolutionary change of traits x_1 and x_2 in a dimorphic environment. Points $B_{11}, B_{12}, B_{21}, B_{22}, B_{41}, B_{42}$ denote evolutionary stable singular coalitions from the initial branching points B_1, B_2 (B_3) and B_4, respectively, which are shown in Fig. 6. Repellors R_1, R_2, CSSs K_7, C_3 can also be seen in Fig. 6 (Colour figure online)

inflow ($P_{\text{in}} = 0.74$), following the evolution process of a single algal population illustrated in Fig. 6.

And the illustration is divided into four cases.

(1) When $\rho_1 = 0$, according to Fig. 6a, the evolutionary singularity $x^* \approx 1.195$ is a unique evolutionary branching point (B_1). In this situation, algal population with any initial cell size will first evolve to this point and evolutionary branching will occur here. Consequently, the original algal population becomes two algal species with different cell sizes, and then, the evolution continues to proceed towards $x_1^* \approx 0.7881$, $x_2^* \approx 1.544$, respectively, see Fig. 9a1. By calculation, $h_{21}(x_1^*, x_2^*) \approx 0.1972 > 0$, $h_{22}(x_1^*, x_2^*) \approx 0.1627 > 0$, according to Theorem 9, the evolutionary singular dimorphism (x_1^*, x_2^*) is a CSS, which implies that no further evolutionary branching will occur and a final evolutionary endpoint has been reached. Visually from Fig. 9a1, both B_{11} and B_{12} are convergence stable and are the intersection points of black solid line and the black dashed line. This is verified in Fig. 9b1, which plots the fitness landscape and the red dashed straight line represents $F_3(x_1, x_2, x_{\text{mut}}) = 0$. From Fig. 9b1, mutant traits near both x_1^* and x_2^* are below the red line, which implies that any mutant x_{mut} near x_1^* or x_2^* always satisfies $F_3(x_1, x_2, x_{\text{mut}}) < 0$, so they cannot invade successfully. They are both CSSs. The above evolution process can be clearly seen by the simulative evolutionary tree in Fig. 9c1. From Fig. 9c1, a monomorphic algal species with trait 1.3 or 0.8 will first converge to $x^* \approx 1.195$ where it undergoes evolutionary branching, and the monomorphic algal population then splits into two different species. The two algal species continue to evolve until their cell sizes reach x_1^*, x_2^*, respectively, and then, the two algal populations will stably coexist in a much longer evolutionary timescale.

(2) When $\rho_1 = 0.47$, from Fig. 6b we can see that there are three evolutionary singularities, two evolutionary branching points B_2, B_3 and one repellor R_1 at which the trait is approximately 0.974. Then, the initial algal population with a trait that is larger than 0.974 will first converge to $x^* \approx 1.171$ (B_2); otherwise, it will converge to $x^* \approx 0.912$ (B_3). After the occurrence of evolutionary branching at B_2 or B_3, the monomorphic algal population then splits into two different species. The two species continue to evolve until they reach the evolutionary stable coalition with $x_1^* \approx 0.7899$, $x_2^* \approx 1.535$, see Fig. 9a2–c2.

(3) When $\rho_1 = 0.68$, there also exists three evolutionary singularities, see Fig. 6c. Unlike the second case, the three evolutionary singularities are, respectively, one evolutionary branching point B_4, one CSS K_7 and one repellor R_2 at which the trait is approximately 1.045. Then, the initial algal population with a trait that is smaller than 1.045 will converge to $x^* \approx 0.8887$ (K_7), and the evolution will cease there. Otherwise it first converges to $x^* \approx 1.126$ (B_4), at which the monomorphic algal population will split into two different species. The two species continue to evolve until they reach the evolutionary stable coalition with $x_1^* \approx 0.7916$, $x_2^* \approx 1.527$, see Fig. 9a3–c3.

(4) When $\rho_1 = 0.9$, as illustrated in Fig. 6d, there only exists a unique CSS. At this situation, algal population with any initial cell size will all converge to $x^* \approx 0.8667$ (C_3) and the evolution will come to a halt, see Fig. 9a4–c4.

Moreover, noticing from Fig. 9, when evolutionary branching could occur for the algal population with initial cell size 1.3, the difference between the cell sizes of the two emerging algal species (the branching width, i.e., the value of $|x_2^* - x_1^*|$) shrinks as ρ_1 increases, and the branching will disappear once the noise intensity goes beyond the threshold ρ_1^*. From the above analysis, we know that environmental fluctuation could not only drive algal evolution toward smaller cell sizes, but also determine the eventual outcomes of algal evolution. With a moderate phosphorus inflow, small environmental fluctuations tend to increase the diversity of algal species and meanwhile reduce the difference between different algal species, while large environmental fluctuations have an adverse effect on algal diversity.

5 Coevolution of Algae and Zooplankton

5.1 Coevolutionary Dynamics

We then investigate the coevolutionary dynamics of model (2). In model (2), algae and zooplankton can both evolve with their phenotypic traits, namely algal cell size and zooplankton body size, respectively. We assume there is either a mutant algae or a mutant zooplankton, but not both simultaneously. Then, when a mutant algae with a slightly different trait x_{mut} enters into the resident community at a low density, the invasion fitness is given by:

$$F_4(x, y, x_{\text{mut}}) = \alpha \mu(x_{\text{mut}}) \langle P(x, y) \rangle - c(x_{\text{mut}}, y) \langle Z(x, y) \rangle - \eta(x_{\text{mut}}, \rho_1), \quad (31)$$

where $\langle P(x, y) \rangle$ and $\langle Z(x, y) \rangle$ are the concentration of phosphorus and the population of zooplankton species at the stochastic ecological equilibrium, which are estimated in equalities (9). It is obvious that if $F_4(x, y, x_{\text{mut}}) > 0$, then the population density of mutant algae will initially increase, that is to say, the mutant algae can invade. Similarly, the invasion fitness for a mutant zooplankton with trait y_{mut} is given by:

$$F_5(x, y, y_{\text{mut}}) = \delta c(x, y_{\text{mut}}) \langle A(x, y) \rangle - \kappa(y_{\text{mut}}, \rho_2), \quad (32)$$

where $\langle A(x, y) \rangle$ is the stochastic ecological equilibrium population density of algal species estimated in (9). If $F_5(x, y, y_{\text{mut}}) > 0$, then the mutant zooplankton can invade.

Through continuing invasion and substitution, algae and zooplankton will keep evolving. The directions of their coevolution are determined by the fitness gradients $D_4(x, y)$ and $D_5(x, y)$, which are given by:

$$\begin{cases} D_4(x, y) := \dfrac{\partial F_4(x, y, x_{\text{mut}})}{\partial x_{\text{mut}}} \bigg|_{x_{\text{mut}} = x} = \alpha \mu'(x) \langle P(x, y) \rangle - c_x'(x, y) \langle Z(x, y) \rangle - \eta'(x, \rho_1), \\[2mm] D_5(x, y) := \dfrac{\partial F_5(x, y, y_{\text{mut}})}{\partial y_{\text{mut}}} \bigg|_{y_{\text{mut}} = y} = \delta c_y'(x, y) \langle A(x, y) \rangle - \kappa'(y, \rho_2), \end{cases} \quad (33)$$

where $c'_x(x, y) = \frac{\partial c(x,y)}{\partial x}$, $c'_y(x, y) = \frac{\partial c(x,y)}{\partial y}$, $\kappa'(y, \rho_2) = \frac{\partial \kappa(y, \rho_2)}{\partial y}$. Because the mutations are rare and small, the step-by-step coevolution dynamics of algal cell size x and zooplankton body size y can be approximated as Dieckmann and Law (1996):

$$\begin{cases} \dfrac{dx}{d\tau} = \dfrac{1}{2}\nu_x\xi_x^2\langle A(x, y)\rangle D_4(x, y) := m_3(x, y)D_4(x, y), \\ \dfrac{dy}{d\tau} = \dfrac{1}{2}\nu_y\xi_y^2\langle Z(x, y)\rangle D_5(x, y) := m_4(x, y)D_5(x, y), \end{cases} \tag{34}$$

where ν_y is the probability of individual mutation which is born in resident zooplankton population, and ξ_y^2 is the variance of phenotypic effect of zooplankton mutations. The quantities $\langle A(x, y)\rangle$ and $\langle Z(x, y)\rangle$ are, respectively, the population densities of algae and zooplankton at the stochastic ecological equilibrium. The quantities $D_4(x, y)$ and $D_5(x, y)$ are, respectively, fitness gradients as shown in expressions (33). Other parameters are same as in model (14). Model (34) together with (2) is called the coevolutionary phosphorus–algae–zooplankton (CEPAZ) model.

If there exists a pair of traits (x^*, y^*) at which the directional coevolution ceases, i.e.,

$$\begin{cases} D_4(x^*, y^*) = \alpha\mu'(x^*)\langle P(x^*, y^*)\rangle - c'_x(x^*, y^*)\langle Z(x^*, y^*)\rangle - \eta'(x^*, \rho_1) = 0, \\ D_5(x^*, y^*) = \delta c'_y(x^*, y^*)\langle A(x^*, y^*)\rangle - \kappa'(y^*, \rho_2) = 0, \end{cases} \tag{35}$$

then (x^*, y^*) is called the "coevolutionary singular coalition". Whether (x^*, y^*) is convergence stable or not is determined by the Jacobian matrix of evolutionary dynamics (34) at this point. And the Jacobian matrix $\mathcal{J}$ of (34) at (x^*, y^*) is given by

$$\mathcal{J} = \begin{pmatrix} m_3(x^*, y^*)\dfrac{\partial D_4(x, y)}{\partial x} & m_3(x^*, y^*)\dfrac{\partial D_4(x, y)}{\partial y} \\ m_4(x^*, y^*)\dfrac{\partial D_5(x, y)}{\partial x} & m_4(x^*, y^*)\dfrac{\partial D_5(x, y)}{\partial y} \end{pmatrix}_{x=x^*, y=y^*}. \tag{36}$$

The coevolutionary singular coalition is locally convergence stable, provided that the Jacobian matrix satisfies $\det(\mathcal{J}) > 0$ and $\text{tr}(\mathcal{J}) < 0$. Moreover, (x^*, y^*) is evolutionary stable, provided that the following two conditions both hold:

$$\left.\frac{\partial^2 F_4(x, y, x_{\text{mut}})}{\partial x_{\text{mut}}^2}\right|_{\substack{y=y^* \\ x_{\text{mut}}=x=x^*}} = \alpha\mu''(x^*)\langle P(x^*, y^*)\rangle - c''_x(x^*, y^*)\langle Z(x^*, y^*)\rangle$$
$$- \eta''(x^*, \rho_1) < 0, \tag{37}$$

$$\left.\frac{\partial^2 F_5(x, y, y_{\text{mut}})}{\partial y_{\text{mut}}^2}\right|_{\substack{x=x^* \\ y_{\text{mut}}=y=y^*}} = \delta c''_y(x^*, y^*)\langle A(x^*, y^*)\rangle - \kappa''(y^*, \rho_2) < 0. \tag{38}$$

If (x^*, y^*) is evolutionary stable, then it cannot be invaded by nearby traits. If (x^*, y^*) is both evolutionary stable and convergence stable, then it is a CSS. At this situation, both algae and zooplankton can stably coexist on a long-term timescale of evolution.

Furthermore, if (x^*, y^*) is convergence stable, but at least one trait lacks evolutionary stability and allows for mutual invasibility nearby, then evolutionary branching in the corresponding species could occur. From (38), we know that whether evolutionary branching will occur in zooplankton species depends on the shape and relative intensity of the asymmetric capture rate and zooplankton total loss rate; this is consistent with the analysis in Landi et al. (2013). The stochastic ecological equilibrium population density of algae also plays an important role in the occurrence of evolutionary branching. There are three scenarios at (x^*, y^*) that allow the occurrence of evolutionary branching in zooplankton species. Scenario one is that the capture rate is concave with respect to y, and the total loss rate of zooplankton is convex or a first-order linear function. Scenario two is that the capture rate is strongly concave, and the total loss rate of zooplankton is relatively weakly concave. Scenario three is that the capture rate is weakly convex and the total loss rate of zooplankton is relatively strongly convex. Correspondingly, there are also three scenarios at (x^*, y^*) that evolutionary branching will not occur in zooplankton species. By analyzing the convergence stability and evolutionary stability of (x^*, y^*), we have the following theorem.

Theorem 10 *Under the conditions of* $\det(\mathcal{J}) > 0$ *and* $\mathrm{tr}(\mathcal{J}) < 0$, *then at the evolutionary singular coalition* (x^*, y^*) *of model* (34)*, the following conclusions hold. If inequalities* (37) *and* (38) *are also satisfied, then* (x^*, y^*) *is a CSS; otherwise, evolutionary branching in algal species will occur if* (37) *is not satisfied, and evolutionary branching in zooplankton species will occur if* (38) *is not satisfied.*

Remark 6 From (38), we can see that the shapes of sinking rate and environmental fluctuation of zooplankton could determine the diversity of zooplankton. By calculation, we can prove that the functions we choose in Table 1 are satisfying the scenarios that y^* is always an ESS, more details can be found in "Appendix F".

Remark 7 The effects of environmental stochasticity on the coevolution process are mainly reflected in the sensitivity of plankton populations and phosphorus concentration to environmental fluctuations as well as the plankton loss caused by environmental fluctuations.

Remark 8 From Theorem 10, evolutionary branching in the algal or zooplankton species may occur if one of the traits lacks evolutionary stability. If both x^* and y^* lack evolutionary stability and they evolve with different speeds, then which species can undergo evolutionary branching depend on their speed of evolution: the faster one can undergo branching. Since evolutionary branching in one species generally changes the frequency-dependent fitness function, the slower evolving trait may no longer be near a branching point, i.e., they may have missed the opportunity for branching. Also, the speed of evolution of a species is limited by the trait values and the number of mutants, which is proportional to the number of residents (Kisdi 1999).

5.2 Evolutionary Stable Coexistence of One Zooplankton and Two Algal Species

From the above analysis, we know that under suitable conditions algal population will split into two species with different cell sizes x_1 and x_2, respectively. In the following,

we will investigate whether the dimorphic algal species can evolutionary stably coexist with a monomorphic zooplankton species. The population dynamics of two algal and one zooplankton species is given by:

$$
\begin{cases}
\begin{aligned}
\mathrm{d}P(t) ={}& \Big[e(P_{\mathrm{in}} - P) + \sum_{i=1}^{2} d_1 Q(x_i) A_i + \sum_{i=1}^{2} \big(Q(x_i) - \delta q(y) \big) c(x_i, y) A_i Z \\
& + d_2 q(y) Z - \sum_{i=1}^{2} \alpha \mu(x_i) P A_i Q(x_i) \Big] \mathrm{d}t + \sigma_1 P \mathrm{d}B_1(t), \\
\mathrm{d}A_1(t) ={}& \big[\alpha \mu(x_1) P A_1 - c(x_1, y) A_1 Z - s_1(x_1) A_1 - d_1 A_1 \big] \mathrm{d}t + \sigma_2(x_1, \rho_1) A_1 \mathrm{d}B_2(t), \\
\mathrm{d}A_2(t) ={}& \big[\alpha \mu(x_2) P A_2 - c(x_2, y) A_2 Z - s_1(x_2) A_2 - d_1 A_2 \big] \mathrm{d}t + \sigma_2(x_2, \rho_1) A_2 \mathrm{d}B_3(t), \\
\mathrm{d}Z(t) ={}& \Big[\sum_{i=1}^{2} \delta c(x_i, y) A_i Z - s_2(y) Z - d_2 Z \Big] \mathrm{d}t + \sigma_3(y, \rho_2) Z \mathrm{d}B_4(t).
\end{aligned}
\end{cases}
\tag{39}
$$

From the proof in "Appendix D", we know that, when $\check{\lambda}(x_i, y) > 0$, $i = 1, 2$, model (39) has a stable stochastic ecological equilibrium $(\langle P(x_1, x_2, y) \rangle, \langle A_1(x_1, x_2, y) \rangle, \langle A_2(x_1, x_2, y) \rangle, \langle Z(x_1, x_2, y) \rangle)$, which is estimated in (D.83).

When rare mutant algae A_{mut} with trait x_{mut}, which is slightly different from x_1 and x_2, appears in the resident stochastic model (39) at a low density, the invasion fitness is given by:

$$
F_6(x_1, x_2, y, x_{\mathrm{mut}}) = \alpha \mu(x_{\mathrm{mut}}) \langle P(x_1, x_2, y) \rangle - c(x_{\mathrm{mut}}, y) \langle Z(x_1, x_2, y) \rangle - \eta(x_{\mathrm{mut}}, \rho_1).
\tag{40}
$$

Similarly, when rare mutant algae Z_{mut} with trait y_{mut}, which is slightly different from y, appears in the resident stochastic model (39) at a low density, the invasion fitness is given by:

$$
F_7(x_1, x_2, y, x_{\mathrm{mut}}) = \sum_{i=1}^{2} \delta c(x_i, y_{\mathrm{mut}}) \langle A_i(x_1, x_2, y) \rangle - \kappa(y_{\mathrm{mut}}, \rho_2).
\tag{41}
$$

By calculation, the fitness gradients $D_{61}(x_1, x_2, y)$, $D_{62}(x_1, x_2, y)$ and $D_7(x_1, x_2, y)$ are given by

$$
\begin{cases}
\begin{aligned}
D_{61}(x_1, x_2, y) :={}& \left. \frac{\partial F_6(x_1, x_2, y, x_{\mathrm{mut}})}{\partial x_{\mathrm{mut}}} \right|_{x_{\mathrm{mut}} = x_1} = \alpha \mu'(x_1) \langle P(x_1, x_2, y) \rangle \\
& - c'_{x_1}(x_1, y) \langle Z(x_1, x_2, y) \rangle - \eta'(x_1, \rho_1), \\
D_{62}(x_1, x_2, y) :={}& \left. \frac{\partial F_6(x_1, x_2, y, x_{\mathrm{mut}})}{\partial x_{\mathrm{mut}}} \right|_{x_{\mathrm{mut}} = x_2} = \alpha \mu'(x_2) \langle P(x_1, x_2, y) \rangle \\
& - c'_{x_2}(x_1, y) \langle Z(x_1, x_2, y) \rangle - \eta'(x_2, \rho_1), \\
D_7(x_1, x_2, y) :={}& \left. \frac{\partial F_7(x_1, x_2, y, y_{\mathrm{mut}})}{\partial y_{\mathrm{mut}}} \right|_{y_{\mathrm{mut}} = y} = \sum_{i=1}^{2} \delta c'_y(x_i, y) \langle A_i(x_1, x_2, y) \rangle \\
& - \kappa'(y, \rho_2).
\end{aligned}
\end{cases}
\tag{42}
$$

Because the mutations are rare and small, the step-by-step coevolution dynamics of traits x_1, x_2 and y can be approximated as Dieckmann and Law (1996):

$$
\begin{cases}
\dfrac{dx_1}{d\tau} = \dfrac{1}{2}\nu_{x1}\xi_{x1}^2\langle A_1(x_1,x_2,y)\rangle D_{61}(x_1,x_2,y) := m_{31}(x_1,x_2,y)D_{61}(x_1,x_2,y), \\
\dfrac{dx_2}{d\tau} = \dfrac{1}{2}\nu_{x2}\xi_{x2}^2\langle A_2(x_1,x_2,y)\rangle D_{62}(x_1,x_2,y) := m_{32}(x_1,x_2,y)D_{62}(x_1,x_2,y), \quad (43)\\
\dfrac{dy}{d\tau} = \dfrac{1}{2}\nu_y\xi_y^2\langle Z(x_1,x_2,y)\rangle D_7(x_1,x_2,y) := m_4(x_1,x_2,y)D_7(x_1,x_2,y).
\end{cases}
$$

The evolutionary singularity $X^* = (x_1^*, x_2^*, \tilde{y}^*)$ of model (43) can be achieved by letting the right side of (42) to 0. X^* is evolutionary stable, provided that the following three conditions all hold:

$$
\left.\frac{\partial^2 F_6(x_1,x_2,y,x_{\text{mut}})}{\partial x_{\text{mut}}^2}\right|_{\substack{y=y^* \\ x_2=x_2^* \\ x_{\text{mut}}=x_1=x_1^*}} = \alpha\mu''(x_1^*)\langle P(x_1^*,x_2^*,y^*)\rangle
$$

$$
- c_{x_1}''(x_1^*,y^*)\langle Z(x_1^*,x_2^*,y^*)\rangle - \eta''(x_1^*,\rho_1) < 0, \tag{44}
$$

$$
\left.\frac{\partial^2 F_6(x_1,x_2,y,x_{\text{mut}})}{\partial x_{\text{mut}}^2}\right|_{\substack{y=y^* \\ x_1=x_1^* \\ x_{\text{mut}}=x_2=x_2^*}} = \alpha\mu''(x_2^*)\langle P(x_1^*,x_2^*,y^*)\rangle
$$

$$
- c_{x_2}''(x_2^*,y^*)\langle Z(x_1^*,x_2^*,y^*)\rangle - \eta''(x_2^*,\rho_1) < 0, \tag{45}
$$

$$
\left.\frac{\partial^2 F_7(x_1,x_2,y,y_{\text{mut}})}{\partial y_{\text{mut}}^2}\right|_{\substack{x_1=x_1^* \\ x_2=x_2^* \\ y_{\text{mut}}=y=y^*}} = \sum_{i=1}^{2}\delta c_y''(x_i^*,y^*)\langle A_i(x_1^*,x_2^*,y^*)\rangle - \kappa''(y^*,\rho_2) < 0. \tag{46}
$$

For the convergence stability of X^*, we analyze it by numerical simulation in the next subsection. The simulations suggest the following Theorem holds.

Theorem 11 *The one zooplankton and two algal species with different cell sizes will reach an evolutionary stable coexistence after first evolutionary branching, i.e., X^* is a CSS, provided that X^* is convergence stable and (44), (45) and (46) are all satisfied.*

Remark 9 If X^* is a CSS, it represents an eventual outcome of the process of algal–zooplankton coevolution, and one zooplankton and two algal species could stably coexist on a much longer evolutionary timescale. While if X^* is convergence stable but one of the algal species lacks evolutionary stability, then a further evolutionary branching in the algal species might occur, we could use the same methods to investigate the possibilities of high levels of polymorphism in algal species and find out the eventual outcome of the algal–zooplankton coevolutionary process, but a full exploration is beyond the scope of this paper, and the readers can refer to Landi et al. (2013).
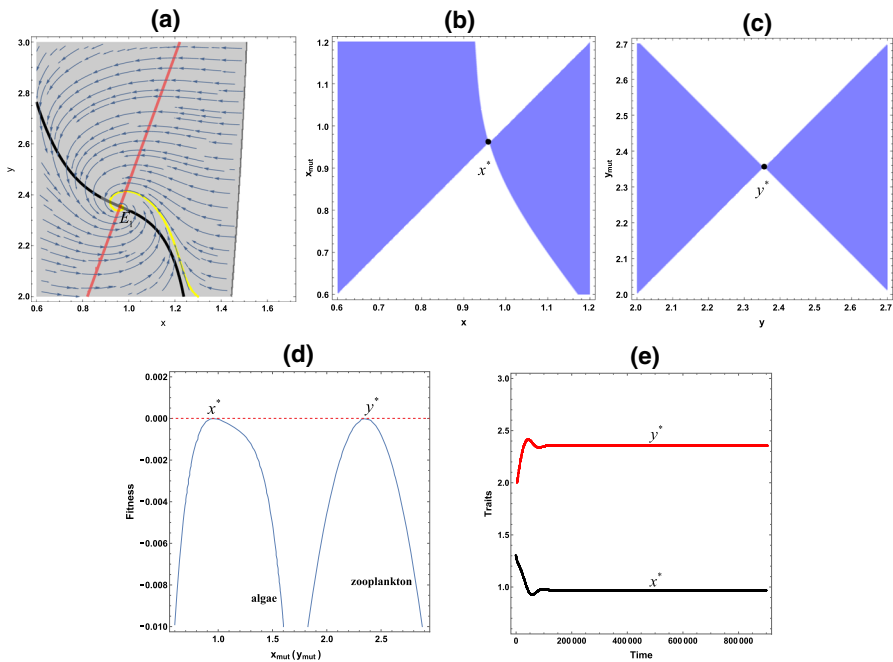
Fig. 10 **a** Coevolution of traits in oligotrophication; **b** PIP for fixed zooplankton trait $y = y^* = 2.355$; **c** PIP for fixed algal trait $x = x^* = 0.9626$; **d** Fitness landscape plots when $(x^*, y^*) = (0.9626, 2.355)$; **e** Simulated evolutionary tree in oligotrophication. Here $P_{in} = 0.6$, $\rho = 0.1$ in all panels. Other parameters are same as in Fig. 6. In **a**, the grey region is the feasible region for plankton sizes, in which model (2) is persistent in mean, the arrows indicate directions of co-evolution of algal and zooplankton traits, and the black and red curves indicate, respectively, isoclines of x and y. The solid curves indicate, evolutionary, singularities which are evolutionary stable and the solid yellow curve represents the projected orbit on the (x, y)-plane, starting from the initial traits $(1.3, 2)$. In **b** or **c**, the blue shaded regions indicate that the fitness of the mutant algae or zooplankton is positive. In **e**, the black and red curves represent algal cell size and zooplankton body size, respectively (Colour figure online)

5.3 Numerical Simulation

We perform some numerical simulations with three different phosphorus input levels, namely oligotrophication ($P_{in} \leq 0.643$), moderate ($0.643 < P_{in} \leq 0.765$) and eutrophication ($P_{in} > 0.765$), respectively, aiming to investigate the influence of environmental fluctuations on the coevolution process of plankton. For convenience, we always choose $\rho_1 = \rho_2 = \rho$ for numerical simulations in this section. In an oligotrophic environment ($P_{in} = 0.6$), we find that once the evolutionary singular coalition (x^*, y^*) is convergence stable, it would be a CSS, no matter how strong the intensities of environmental noise are, see Fig. 10.

In Fig. 10a, point $E_1 = (x^*, y^*) \approx (0.9626, 2.355)$ is both convergence stable and evolutionary stable; therefore, the evolutionary singular coalition (the intersection of the black curve and the red curve) represents an eventual outcome of the coevolutionary process, algae and zooplankton will evolve towards E_1 and cease there. In an oligotrophic environment, the finally evolutionary outcome always contains a

monomorphic algal and a monomorphic zooplankton species, independent of the noise intensities, see Fig. 10b–e. This implies that when phosphorus is extremely scarce, environmental fluctuations have no significant influence on the outcomes of plankton evolution, i.e., oligotrophication inhibits plankton diversity.

With a moderate phosphorus inflow ($P_{in} = 0.74$), when $\rho = 0$, the evolutionary singular coalition $E_2 = (x^*, y^*) \approx (1.025, 2.508)$ is convergence stable, and it is the intersection of the black dashed curve and the red solid curve, which implies that at point E_2, zooplankton species is also evolutionary stable, but algal species is not; then, the algal species admits an evolutionary branching at this point, see Fig. 11a1.

The monomorphic algal population then splits into two different species; then, two algal and one zooplankton species continue to evolve on a much longer evolutionary time scale until their traits reach $(x_1^*, x_2^*, \tilde{y}^*) \approx (1.492, 0.8161, 2.471)$. Moreover, for the fixed $y = \tilde{y}^* \approx 2.471$, x_1^* and x_2^* are both CSSs (the intersection of the black dashed curve and the black solid curve), see Fig. 11a2. This implies that the two algal species with diverging traits and one zooplankton could stably coexist after the first evolutionary branching of algal species, and the finally evolutionary outcome contains a dimorphic algal and a monomorphic zooplankton species, see Fig. 11a3. As the increasing of noise intensities, the evolutionary singular coalition moves roughly to the left along the black curve, and the range of algal cell size that allows for evolutionary branching will shrink, see the black dashed curve in Fig. 11b1. From Fig. 11b1, when $\rho = 1.7$, plankton traits will first converge to $E_3 = (x^*, y^*) \approx (1.004, 2.46)$, at which evolutionary branching occurs in algal species, and then, two algal and one zooplankton species continue to evolve until their traits reach $(x_1^*, x_2^*, \tilde{y}^*) \approx (1.339, 0.886, 2.447)$ and stably coexist, see Fig. 11b2, b3. As the increase of ρ continues, the evolutionary singular coalition becomes a CSS and the coevolution will cease there, once it goes beyond the threshold value $\rho_m^* \approx 2.17$, see Fig. 11c1. In this situation, no evolutionary branching will occur in both algal and zooplankton populations, see Fig. 11c2–c3. Moreover, we observe from Fig. 11a3–c3 that the difference between the cell sizes of two new emerging algal species decreases significantly as ρ increases, and there would be no new algal species at all once the noise intensity goes beyond ρ_m^*. As a summary, in a moderate phosphorus environment, small noises facilitate algal biodiversity, and the existence of environmental fluctuations minimizes the cell size differences between the new emerging algal species. Large noises decrease algal biodiversity due to CSS.

In an eutrophic environment ($P_{in} = 0.93$), the Red Queen dynamics could occur, corresponding to the phenomenon that algal cell size and zooplankton body size infinitely coevolve to a stable limit cycle, see Fig. 12a–d.

When $\rho = 0$, the evolutionary singular coalition E_5 lacks convergence stability, i.e., it is a repellor, and model (34) admits a Hopf bifurcation, see Fig. 12a. In this situation, the directional coevolution cannot approach E_5, instead the traits of algae and zooplankton will evolve to a stable limit cycle, which is also illustrated in Fig. 12b. The limit cycle shrinks dramatically when ρ increases to 2.2, see Fig. 12c, d. When ρ approaches the critical value $\rho_{e1}^* \approx 2.75$, the limit cycle will ultimately disappear. For example, when $\rho = 3$, the evolutionary singular coalition $E_7 \approx (1.037, 2.542)$ becomes convergence stable. Meanwhile, zooplankton species is evolutionary stable, but algal species is not in this case. Then, E_7 is a branching point and algal population will split into two different species. Moreover, the traits
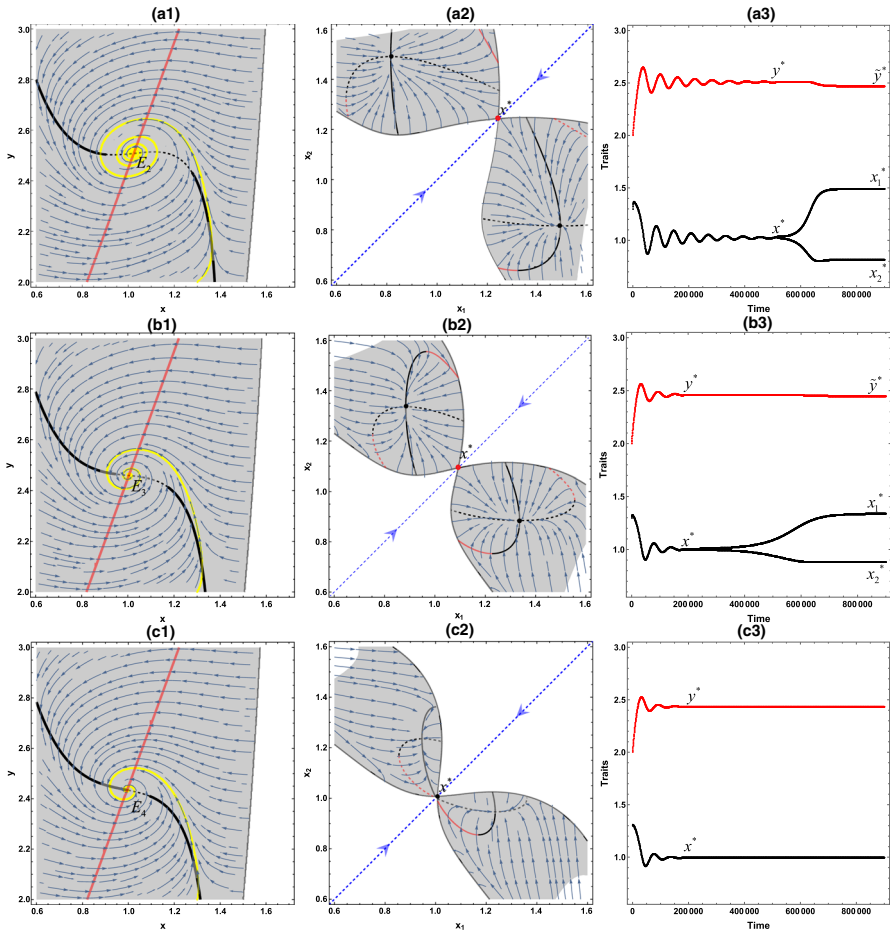
Fig. 11 **a1–c1** Coevolution of traits with moderate phosphorus inflow when $\rho = 0, 1.7, 2.17$, respectively; **a2–c2**: trait coevolution of two algal species for fixed zooplankton trait $y = \tilde{y}^*$ with moderate phosphorus inflow when $\rho = 0, 1.7, 2.17$, respectively; **a3–c3** simulated evolutionary tree with moderate nutrient input when $\rho = 0, 1.7, 2.17$, respectively; here $P_{\text{in}} = 0.74$ in all panels, other parameters are same as in Fig. 10. In **a1–c1**, the dashed curves indicate evolutionary singularities which are not evolutionary stable; other curves, arrows and grey regions have the same meaning as in Fig. 10a. In **a2–c2**, the curves, arrows, shaded areas and points have the same meaning as in Fig. 9. In **a3–c3**, the black and red curves represent algal cell size and zooplankton body size, respectively (Colour figure online)

of two algal and one zooplankton species will continue to evolve until they reach $(x_1^*, x_2^*, \tilde{y}^*) \approx (1.395, 0.8173, 2.523)$ and stably coexist in there, see Fig. 12e, f. When $\rho = \rho_{e2}^* \approx 4.12$, $E_8 \approx (1.01, 2.473)$ becomes a CSS and no evolutionary branching will occur, the coevolution will cease there, see Fig. 12g, h.

As a summary, the algal–zooplankton coevolution could have different evolutionary outcomes due to the varieties of phosphorus inflow and noise intensities. In what follows, we will numerically investigate how phosphorus inflow and environmental fluctuations affect the trends of such a coevolution process. For a fixed phosphorus
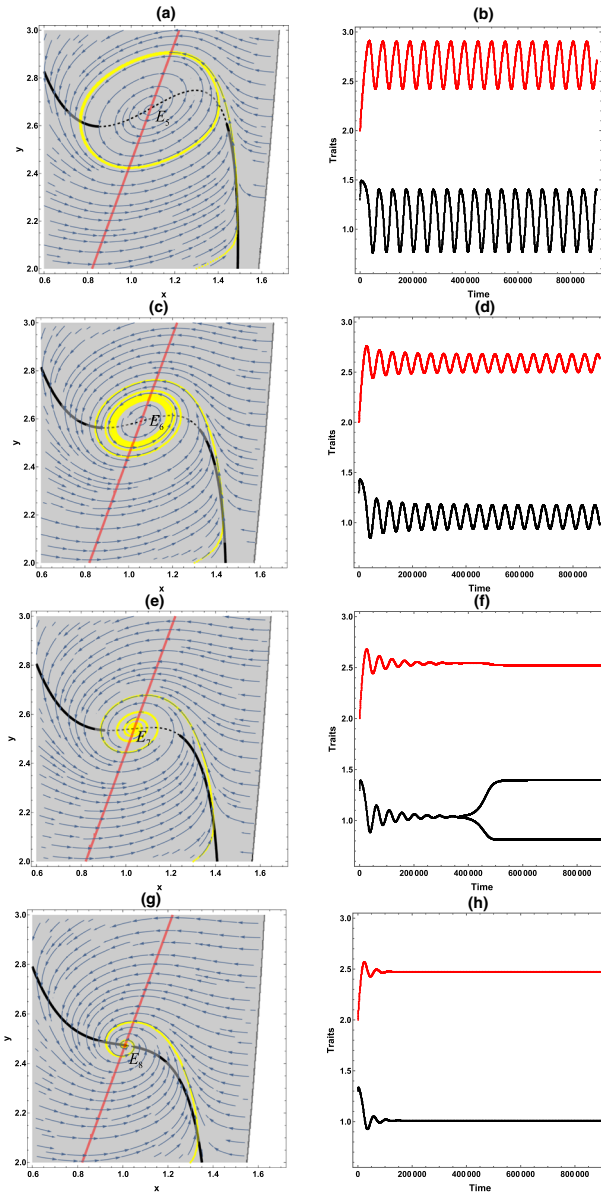
Fig. 12 The first column represents coevolution of traits in eutrophic environment when $\rho = 0, 2.2, 3, 4.12$, respectively; the second column is simulated evolutionary trees with moderate phosphorus inflow when $\rho = 0, 2.2, 3, 4.12$. Here $P_{in} = 0.93$ in all panels. In the first column, the curves, arrows and grey regions have the same meaning as in Fig. 11a1. In the right line, the black and red curves represent algal cell size x and zooplankton body size y, respectively
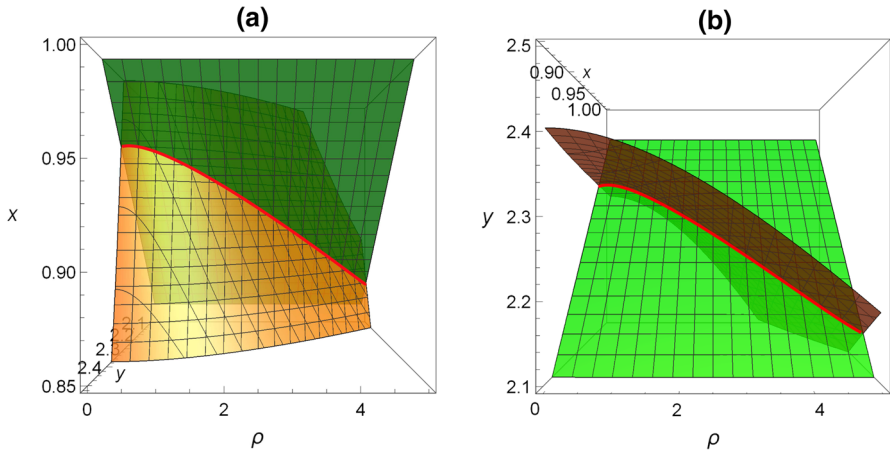
Fig. 13 **a** The top view of the three-dimensional bifurcation diagram for x versus ρ; **b** the front view of the three-dimensional bifurcation diagram for y versus ρ. Here $P_{\mathrm{in}} = 0.74$ in all panels. The orange and green surfaces indicate zero fitness gradients for algae and zooplankton, and the red solid curve is the intersection of these two surfaces, illustrating how the value of evolutionary singular coalition changes with respect to the noise intensity (Colour figure online)
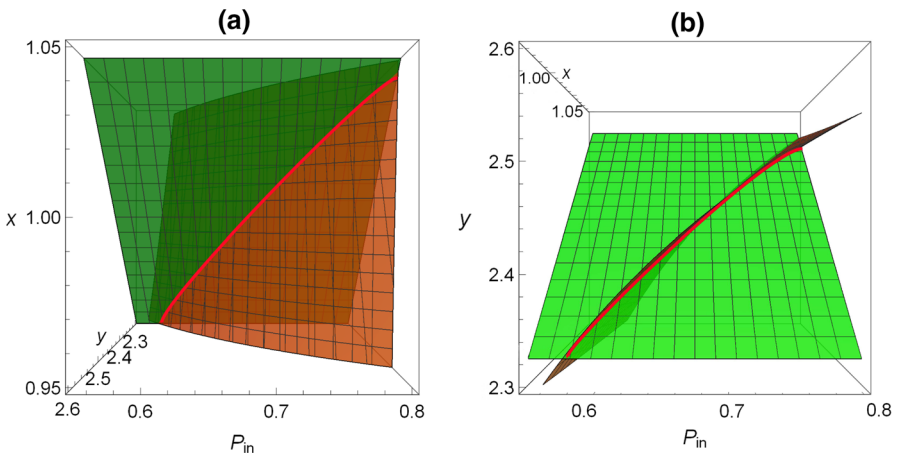

Fig. 14 **a** The top view of the three-dimensional bifurcation diagram for x versus P_{in}; **b** the front view of the three-dimensional bifurcation diagram for y versus P_{in}. Here $\rho = 0.1$ in all panels. The two surfaces have the same meaning as in Fig. 13, and the red solid curves are illustrating how the value of evolutionary singular coalition changes with respect to phosphorus inflow (Colour figure online)

inflow level, the increase of noise intensities could drive both algal and zooplankton evolution toward smaller traits, see Fig. 13. Fixing the noise intensities, we also find that the both algal cell size and zooplankton body size will increase with the phosphorus inflow level, see Fig. 14.

According to remark 6 and the above numerical simulations, when we choose zooplankton sinking rate as in Table 1, no evolutionary branching will occur in zooplankton
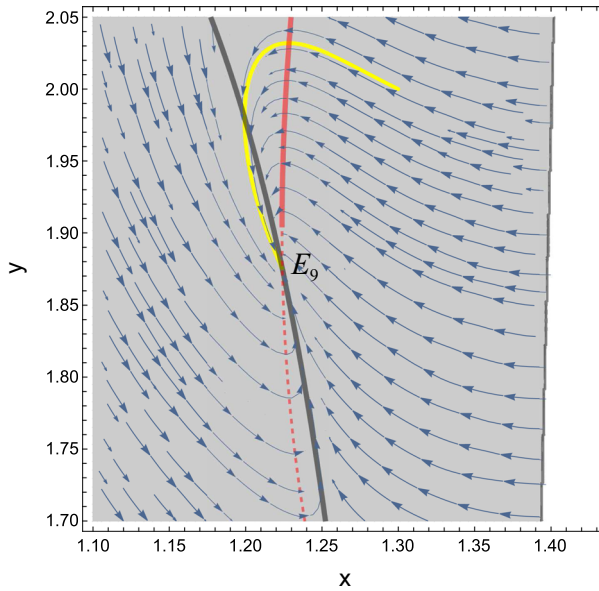
Fig. 15 The coevolution of algal cell size and zooplankton body size. Here $s_2(y) = \frac{1}{6} \ln y$, $P_{in} = 0.6$, $c_m = 0.68$, $\rho = 0.01$, other parameters are same as in Fig. 11. The curves, arrows and grey regions have the same meaning as in Fig. 11a1

species. We then give another example to illustrate the possibility of zooplankton species undergoing evolutionary branching, see Fig. 15.

From Fig. 15, the evolutionary singular coalition $E_9 = (x^*, y^*) \approx (1.225, 1.875)$ is convergence stable, and it is also the intersection of black solid and red dashed lines; then, x^* is evolutionary stable but y^* is not. At this situation, plankton traits will first converge to E_9; then, the monomorphic zooplankton population will split into two different species at this point, and for the further coevolution of one algal and two zooplankton species on a much longer evolutionary time scale, the readers can refer to Landi et al. (2013). As a summary, zooplankton sinking rate with different forms could lead to different evolutionary outcomes of zooplankton species. Moreover, from the proof in "Appendix F", we can see that without zooplankton sinking and environmental fluctuation experienced by zooplankton, y^* is always an ESS, and this conclusion is consistent with the studies in Jiang et al. (2005), Landi et al. (2013)).

6 Discussion

In this paper, we constructed a stochastic EPAZ model by incorporating adaptive changes of algal cell size, zooplankton body size and environmental fluctuations into a deterministic nonevolutionary PAZ model. For the stochastic model, we analyzed the asymptotic behaviors of plankton dynamics. Moreover, we obtain several important predictions about the evolutionary patterns and outcomes of algal cell size under the influence of environmental stochasticity.

Our major findings can be summarized as follows. First, we obtain the threshold $\lambda(x, y)$ that determines the persistence and extinction of zooplankton population in model (2). Model (2) could achieve a positive stable stochastic ecological equilibrium, provided that environmental fluctuations are weak enough such that $\lambda(x, y) > 0$. Otherwise, zooplankton population will go to extinction. It is worth mentioning that when there exist two algal species, the conditions that ensure the persistence of the four-dimensional model (39) become harder to derive. In addition to the traditional methods in analyzing the asymptotic behaviors of stochastic model, the relations between the traits of new emerging algal species and the original species also need to be considered. Second, environmental fluctuations could drive algal evolution toward smaller size, in the scenarios with or without zooplankton, algae evolves only or plankton coevolve (Jiang et al. 2005). This result is also consistent with the secular changes in algal size structure on geological time scales (Finkel et al. 2005). When only algal evolves, zooplankton could amplify the impact of environmental fluctuations on the declining trend of algal cell size with a moderate phosphorus input level. In the coevolutionary dynamics, environmental fluctuations could also lead to smaller zooplankton. More interestingly, in an eutrophic environment, weak fluctuations can keep plankton traits evolving infinitely to a stable limit cycle, which could explain the cyclic changes in the size of *Foraminifera* that feed on diatoms during the Cenozoic Era (Schmidt et al. 2004). Third, better phosphorus level could lead to larger zooplankton and larger algal cell size in the scenarios algae evolves only ($h_1(x^*) < 0$) and plankton coevolve. This is in accordance with the general ecological phenomenon that small phytoplankton species tend to settle in an oligotrophication environment, such as the oceanic gyres, and larger phytoplankton species are more likely to dominate in nutrient abundant areas, such as continental margins and upwelling zones (Agawin and Duarte 2000; Irigoien et al. 2004; Li 2002), while algal cell size will not respond to the changing phosphorus inflow in the absence of zooplankton. Fourth, no evolutionary branching will occur without zooplankton, which verifies the competitive exclusion principle (Hardin and G. 1960) from the perspective of adaptive dynamics. With the existence of zooplankton, environmental stochasticity could lead to multiple evolutionary singularities and different evolutionary outcomes. In a moderate phosphorus environment, small environmental fluctuations could cause the emergence of evolutionary branching and consequently algal diversity will increase, and the existence of environmental fluctuation could narrow the cell size difference between the new emerging algal species, while large fluctuations will lead to CSS. The existence of environmental fluctuations could benefit algal diversity in an eutrophic environment and have an adverse effect in an oligotrophic environment. Moreover, the diversity of zooplankton could be increased by choosing a suitable function for zooplankton sinking and environmental fluctuation experienced by zooplankton, which differs with the scenario without zooplankton sinking and environmental stochasticity (Jiang et al. 2005).

As a summary, environmental stochasticity as well as phosphorus inflow could significantly affect plankton traits as well as their biological diversity in the presence of zooplankton, and the developed methodologies could potentially be used to investigate the adaptive dynamics of any ecological model in a fluctuate environment. However, there are still some questions remain unsolved. In the coevolutionary dynamics, evolutionary branching in zooplankton species could occur with suitable zooplankton

sinking rate and environmental fluctuations; then, zooplankton will split into two different species. Whether the one algal and two zooplankton species could continue to coexist on a much longer timescale of evolution or evolutionary suicide phenomenon (Parvinen 2005) would occur is beyond the scope of this paper. The possibilities for the occurrence of secondary or further evolutionary branching of an evolutionary tree on plankton species, and whether the branching in algal species can induce the branching in zooplankton species (Jian et al. 2016) also deserve to be analyzed. Moreover, the consideration of predation pressure on zooplankton (e.g., planktivorous fish prefer to feed upon zooplankton in larger body sizes) is necessary in some situations, and this selective predation pressure may lead to the increase in algal cell size (Brooks and Dodson 1965). Furthermore, there are other types of environmental perturbations in nature such as the recently happened flooding in Henan, China, the severe heat in the USA, Canada, earthquake, tsunami and so on, which cannot be described by the white noises introduced in our stochastic models. These natural disasters could also significantly affect the aquatic ecosystem; therefore, it is necessary to further consider the influence of other noise types, for example, $L\acute{e}vy$ noise (Bao and Yuan 2012). Furthermore, instead of a single phenotypic trait, considering the coevolution of multiple traits, such as the ability of nutrient composition and light absorption of algae, is an intriguing but challenging direction.

Availability of Data and Materials Data sharing was not applicable to this article as no datasets were generated or analyzed during the current study.

Declarations

Conflict of interest The author declares that he has no competing interests.

Appendix A: Proof of Theorem 2

Proof Applying the Itô's formula to the second and third equations of A and Z in model (2), integrating both sides from 0 to t and then dividing t on both sides yield

$$\frac{1}{t} \ln \frac{A(t)}{A(0)} = \alpha\mu(x)\frac{1}{t}\int_0^t P(s)\mathrm{d}s - c(x,y)\frac{1}{t}\int_0^t Z(s)\mathrm{d}s - \eta(x,\rho_1) + \sigma_2(x,\rho_1)\frac{M_2(t)}{t}, \tag{A.47}$$

$$\frac{1}{t} \ln \frac{Z(t)}{Z(0)} = \delta c(x,y)\frac{1}{t}\int_0^t A(s)\mathrm{d}s - \kappa(y,\rho_2) + \sigma_3(y,\rho_2)\frac{M_3(t)}{t}, \tag{A.48}$$

where $M_i(t) = \int_0^t \mathrm{d}B_i(t)$, $i = 1, 2, 3$. Let $V_1 = P + Q(x)A + q(y)Z$, then

$$dV_1 = [eP_{in} - eP - s_1(x)Q(x)A - s_2(y)q(y)Z]\,dt + \sigma_1 P dB_1(t)$$
$$+ \sigma_2(x, \rho_1)Q(x)A dB_2(t) + \sigma_3(y, \rho_2)q(y)Z dB_3(t) \tag{A.49}$$
$$\leq \big(eP_{in} - h_1 V_1\big)dt + \sigma_1 P dB_1(t) + \sigma_2(x, \rho_1)Q(x)A dB_2(t) + \sigma_3(y, \rho_2)q(y)Z dB_3(t),$$

where $h_1 = \min\{e, s_1(x), s_2(y)\}$. Integrating both sides of Eq. (A.49) from 0 to t and dividing t on both sides lead to

$$\frac{\psi_1}{t} = eP_{in} - e\frac{1}{t}\int_0^t P(s)ds - s_1(x)Q(x)\frac{1}{t}\int_0^t A(s)ds - s_2(y)q(y)\frac{1}{t}\int_0^t Z(s)ds,$$
$$\tag{A.50}$$

where $\psi(t) = V_1(t) - V_1(0) - \sigma_1 N_1(t) - \sigma_2(x, \rho_1)Q(x)N_2(t) - \sigma_3(y, \rho_2)q(y)N_3(t)$, $N_j(t) = \int_0^t \Phi_j(s)dB_j(t)$, $j = 1, 2, 3$. According to Theorem 1 and the strong law of large numbers for local martingales (Mao 2006), we have

$$\lim_{t\to\infty} \frac{M_i(t)}{t} = 0, \quad \lim_{t\to\infty} \frac{N_j(t)}{t} = 0, \quad \lim_{t\to\infty} \frac{\psi_1(t)}{t} = 0, \quad i, j = 1, 2, 3, \quad a.s.$$
$$\tag{A.51}$$

We next are going to prove Theorem 2 step by step based on Eqs. (A.47)–(A.51).

(1) We first prove the first conclusion of Theorem 3. From (A.50),

$$\frac{1}{t}\int_0^t P(s)ds \leq P_{in} - \frac{\psi_1}{et}, \tag{A.52}$$

Substituting (A.52) into (A.47) yields

$$\frac{1}{t}\ln\frac{A(t)}{A(0)} \leq \alpha\mu(x)P_{in} - \eta(x, \rho_1) - \frac{\alpha\mu(x)}{e}\frac{\psi_1}{t} + \sigma_2(x, \rho_1)\frac{M_2(t)}{t},$$

then when $P_{in} < \frac{\eta(x, \rho_1)}{\alpha\mu(x)}$, together with (A.51) we have $\limsup_{t\to\infty}\frac{\ln A(t)}{t} < 0$, that is

$$\lim_{t\to\infty} A(t) = 0, \quad a.s.$$

Consequently from (A.48), $\lim_{t\to\infty} Z(t) = 0$, $a.s.$ Moreover, according to (A.50) and (A.51), $\langle P \rangle = P_{in}$. The first conclusion of Theorem 2 is proved.

(2) We now proceed to the proof of the second conclusion. From (A.50),

$$\frac{1}{t}\int_0^t P(s)ds = P_{in} - \frac{s_1(x)Q(x)}{e}\frac{1}{t}\int_0^t A(s)ds$$
$$- \frac{s_2(y)q(y)}{e}\frac{1}{t}\int_0^t Z(s)ds - \frac{\psi_1}{et}, \tag{A.53}$$

Substituting (A.53) into (A.47) yields

$$
\frac{1}{t} \ln \frac{A(t)}{A(0)} = \alpha\mu(x)P_{\text{in}} - \eta(x, \rho_1) - \frac{\alpha\mu(x)s_1(x)Q(x)}{e} \frac{1}{t} \int_0^t A(s)\mathrm{d}s + \sigma_2(x, \rho_1)\frac{M_2(t)}{t}
$$
$$
- \frac{\alpha\mu(x)}{e} \frac{\psi_1}{t} - \left(\frac{\alpha\mu(x)s_2(y)q(y)}{e} + c(x, y) \right) \frac{1}{t} \int_0^t Z(s)\mathrm{d}s. \qquad (A.54)
$$

Obviously,

$$
\frac{1}{t} \ln \frac{A(t)}{A(0)} \leq \alpha\mu(x)P_{\text{in}} - \eta(x, \rho_1) - \frac{\alpha\mu(x)s_1(x)Q(x)}{e} \frac{1}{t} \int_0^t A(s)\mathrm{d}s
$$
$$
- \frac{\alpha\mu(x)}{e} \frac{\psi_1}{t} + \sigma_2(x, \rho_1)\frac{M_2(t)}{t}.
$$

When $P_{\text{in}} > \frac{\eta(x,\rho_1)}{\alpha\mu(x)}$, it then follows from Lemma 4 in Liu and Bai (2016) that

$$
\overline{\langle A(x, y) \rangle} \leq \frac{(\alpha\mu(x)P_{\text{in}} - \eta(x, \rho_1))e}{\alpha\mu(x)s_1(x)Q(x)} = \frac{1}{s_1(x)Q(x)} \left(eP_{\text{in}} - \frac{e\eta(x, \rho_1)}{\alpha\mu(x)} \right), \quad a.s.
$$
$$
(A.55)
$$

Substituting (A.55) into (A.48) leads to

$$
\limsup_{t \to \infty} \frac{\ln Z(t)}{t} \leq \delta c(x, y)\overline{\langle A(x, y) \rangle} - \kappa(y, \rho_2)
$$
$$
= \frac{\delta c(x, y)}{s_1(x)Q(x)}\lambda(x, y),
$$

thus when $\lambda(x, y) < 0$, $\limsup_{t\to\infty} \frac{\ln Z(t)}{t} < 0$, i.e., $\lim_{t\to\infty} Z(t) = 0$, a.s. Thus, for any $\varepsilon_1 > 0$, there exists $T_1 > 0$ and a set Ω_{ε_1} with $\mathcal{P}(\Omega_{\varepsilon_1}) > 1 - \varepsilon_1$, such that for any $t > T_1$ and $\omega \in \Omega_{\varepsilon_1}$, $\left(\frac{\alpha\mu(x)s_2(y)q(y)}{e} + c(x, y) \right) \frac{1}{t} \int_0^t Z(s)\mathrm{d}s < \varepsilon_1$ holds. It then follows from (A.54) that

$$
\frac{1}{t} \ln \frac{A(t)}{A(0)} \geq \alpha\mu(x)P_{\text{in}} - \eta(x, \rho_1) - \varepsilon_1 - \frac{\alpha\mu(x)s_1(x)Q(x)}{e} \frac{1}{t} \int_0^t A(s)\mathrm{d}s
$$
$$
- \frac{\alpha\mu(x)}{e} \frac{\psi_1}{t} + \sigma_2(x, \rho_1)\frac{M_2(t)}{t}.
$$

Again, according to Lemma 4 in Liu and Bai (2016) and the arbitrariness of ε_1,

$$
\underline{\langle A(x, y) \rangle} \geq \frac{1}{s_1(x)Q(x)} \left(eP_{\text{in}} - \frac{e\eta(x, \rho_1)}{\alpha\mu(x)} \right), \quad a.s. \qquad (A.56)
$$

Combining (A.56) with (A.55), we have $\langle A(x) \rangle = \frac{1}{s_1(x)Q(x)} \left(eP_{\text{in}} - \frac{e\eta(x,\rho_1)}{\alpha\mu(x)} \right)$, a.s. Consequently, it is easy to obtain from (A.50) that $\langle P(x) \rangle = \frac{\eta(x,\rho_1)}{\alpha\mu(x)}$, a.s. The second conclusion is thus proved.

(3) We now are going to prove the last conclusion of Theorem 2. From (A.48) and together with Lemma 1,

$$\overline{\langle A(x, y)\rangle} \leq \frac{\kappa(y, \rho_2)}{\delta c(x, y)}, \quad a.s. \tag{A.57}$$

Moreover, according to (A.54) we have

$$\left(\frac{\alpha\mu(x)s_2(y)q(y)}{e} + c(x, y) \right) \underline{\langle Z(x, y)\rangle}$$

$$\geq \alpha\mu(x)P_{\text{in}} - \eta(x, \rho_1) - \frac{\alpha\mu(x)s_1(x)Q(x)}{e}\overline{\langle A(x, y)\rangle}. \tag{A.58}$$

Together with (A.57), we can conclude that when $\lambda(x, y) > 0$,

$$\underline{\langle Z(x, y)\rangle} \geq \frac{\lambda(x, y)}{s_2(y)q(y) + ec(x, y)/\alpha\mu(x)} > 0, \quad a.s.$$

Then, we have $\limsup_{t\to\infty} \frac{\ln A(t)}{t} = 0$, a.s., otherwise, $\lim_{t\to\infty} A(t) = 0$, and consequently $\lim_{t\to\infty} Z(t) = 0$, a.s. According to (A.47),

$$\frac{1}{t}\ln\frac{A(t)}{A(0)} \leq \alpha\mu(x)\frac{1}{t}\int_0^t P(s)\mathrm{d}s - c(x, y)\frac{1}{t}\int_0^t Z(s)\mathrm{d}s + \sigma_2(x, \rho_1)\frac{M_2(t)}{t},$$

consequently,

$$\underline{\langle P(x, y)\rangle} \geq \frac{c(x, y)}{\alpha\mu(x)}\overline{\langle Z(x, y)\rangle} > 0, \quad a.s.$$

Applying the same method to (A.48), we have $\underline{\langle A(x, y)\rangle} > 0, \quad a.s.$ The proof is thus completed.

□

Appendix B: Proof of Theorem 3

Before the proof of Theorem 3, we need the following lemma from Khasminskii (2012). Suppose that $X(t)$ is a homogeneous Markov process in n-dimension Euclidean space R^n, satisfying the following stochastic differential equation:

$$\mathrm{d}X(t) = b(X)\mathrm{d}t + \sum_{r=1}^k \sigma_r(X)\mathrm{d}B_r(t), \tag{B.59}$$

where $\sigma_r(X) = (\sigma_r^1(X), \sigma_r^2(X)\dots, \sigma_r^n(X))^T$, $B(X) = (a_{ij}(X))_{n\times n}$ is the diffusion matrix of $X(t)$ with $a_{ij}(X) = \sum_{r=1}^k \sigma_r^i(X)\sigma_r^j(X)$.

Lemma 2 (Khasminskii 2012). *If there exists a bounded open domain $U \subset R^n$ with regular boundary, satisfying the following properties:*

(H1) The diffusion matrix $B(x)$ is strictly positive definite for all $x \in U$;
(H2) There exists a nonnegative C^2-function $V(X)$ such that $\mathscr{L}V(X)$ is negative on $X \in R^n \setminus U$.

Then, the Markov process $X(t)$ of the stochastic model (B.59) admits a unique stationary distribution $\pi(\cdot)$, and for any integrable function $f(\cdot)$ with regard to the measure π, the following equation holds,

$$P\left(\lim_{t\to\infty} \frac{1}{t}\int_0^t f(X(t))\mathrm{d}t = \int_{R^n} f(x)\pi(\mathrm{d}x)\right) = 1.$$

In what follows, we are going to apply Lemma 2 to prove the existence of a unique ergodic stationary distribution for model (2).

Proof Define a nonnegative C^2-Lyapunov function

$$V_2 = M_2 V_{21} + V_{22} + V_{23} - V_2^*,$$

V_2^* is the minimum value of $V_2(P, A, Z)$ and

$$V_{21} = -m_3 \ln Z - m_4 \ln A + m_5 Z - V_1, \quad V_{22} = \frac{1}{\theta_1 + 2} V_1^{\theta_1 + 2}, \quad V_{23} = -\ln P,$$

where $m_3 = \frac{s_1(x)Q(x)}{\delta c(x,y)}$, $m_4 = \frac{e}{\alpha\mu(x)}$, $m_5 = (m_4 c(x, y) + s_2(y)q(y))/(s_2(y) + d_2)$, $0 < \theta_1 < 1$ is a constant which is small enough such that

$$h_1(x, y) := \min\{e, s_1(x), s_2(y)\} - \frac{\theta_1 + 1}{2} \max\{\sigma_1^2, \sigma_2^2(x, \rho_1), \sigma_3^2(y, \rho_2)\} > 0,$$

and the positive constant M_2 satisfying

$$-M_2\lambda(x, y) + f_1^u \leq -2,$$

where $f^u = \sup_{t \in (0,\infty)} f(t)$ and the function f_1 will be determined later.

By using the Itô formula, we have

$$\mathscr{L}V_{21}$$
$$= -s_1(x)Q(x)A + m_3\kappa(y, \rho_2) - eP + m_4c(x, y)Z + m_4\eta(x, \rho_1)$$
$$+ m_5\delta c(x, y)AZ - m_5(s_2(y) + d_2)Z - eP_{\text{in}} + eP + s_1(x)Q(x)A + s_2(y)q(y)Z$$
$$= m_3\kappa(y, \rho_2) + m_4\eta(x, \rho_1)$$
$$+ m_5\delta c(x, y)AZ - eP_{\text{in}}$$
$$= -\lambda(x, y) + m_5\delta c(x, y)AZ.$$

$$\mathscr{L}V_{22}$$
$$= eP_{\text{in}}(P + Q(x)A + q(y)Z)^{\theta_1+1}$$
$$- (P + Q(x)A + q(y)Z)^{\theta_1+1}(eP + s_1(x)Q(x)A + s_2(y)q(y)Z)$$
$$+ \frac{\theta_1 + 1}{2}(P + Q(x)A + q(y)Z)^{\theta_1}(\sigma_1^2 P^2$$
$$+ \sigma_2^2(x, \rho_1)Q^2(x)A^2 + \sigma_3^2(y, \rho_2)q^2(y)Z^2)$$
$$\leq eP_{\text{in}}(P + Q(x)A + q(y)Z)^{\theta_1+1}$$
$$- \min\{e, s_1(x), s_2(y)\}(P + Q(x)A + q(y)Z)^{\theta_1+2}$$
$$+ \frac{(\theta + 1)\max\{\sigma_1^2, \sigma_2^2(x, \rho_1), \sigma_3^2(y, \rho_2)\}}{2}$$
$$(P + Q(x)A + q(y)Z)^{\theta_1+2}$$
$$= -h_1(x, y)(P + Q(x)A + q(y)Z)^{\theta_1+2}$$
$$+ eP_{\text{in}}(P + Q(x)A + q(y)Z)^{\theta_1+1}.$$

$$\mathscr{L}V_{23}$$
$$= -\frac{eP_{\text{in}}}{P} + e - \frac{d_1 Q(x)A + (Q(x) - \delta q(y))c(x, y)AZ + d_2 q(y)Z}{P}$$
$$+ \alpha\mu(x)Q(x)A + \frac{\sigma_1^2}{2}$$
$$\leq -\frac{eP_{\text{in}}}{P} + \alpha\mu(x)Q(x)A + e + \frac{\sigma_1^2}{2}.$$

Then,

$$\mathcal{L}V_2$$
$$\leq -M_2\lambda(x, y) + M_2 m_5\delta c(x, y)AZ - h_1(x, y)(P + Q(x)A + q(y)Z)^{\theta_1+2}$$
$$+ eP_{\text{in}}(P + Q(x)A + q(y)Z)^{\theta_1+1}$$
$$- \frac{eP_{\text{in}}}{P} + \alpha\mu(x)Q(x)A + e + \frac{\sigma_1^2}{2}$$
$$:= -M_2\lambda(x, y) + M_2 m_5\delta c(x, y)AZ - \frac{eP_{\text{in}}}{P} + f_1(P, A, Z),$$

where

$$
\begin{aligned}
f_1(P, A, Z) = & -h_1(x, y)(P + Q(x)A + q(y)Z)^{\theta_1+2} \\
& + eP_{\text{in}}(P + Q(x)A + q(y)Z)^{\theta_1+1} + \alpha\mu(x)Q(x)A + e + \frac{\sigma_1^2}{2}.
\end{aligned}
$$

Denote

$$
\Upsilon(N, \tilde{P}, Z) = -M_2\lambda(x, y) + M_2 m_5 \delta c(x, y)AZ - \frac{eP_{\text{in}}}{P} + f_1(P, A, Z),
$$

then

$$
\Upsilon(P, A, Z) \leq
\begin{cases}
\Upsilon(0, A, Z) \to -\infty, & \text{as } P \to 0^+, \\
\Upsilon(\infty, \tilde{P}, Z) \to -\infty, & \text{as } P \to \infty, \\
-M_2\lambda(x, y) + f_1^u \leq -1, & \text{as } A \to 0^+, \\
\Upsilon(P, \infty, Z) \to -\infty, & \text{as } A \to \infty, \\
-M_2\lambda(x, y) + f_1^u \leq -1, & \text{as } Z \to 0^+, \\
\Upsilon(P, A, \infty) \to -\infty, & \text{as } Z \to \infty.
\end{cases}
$$

Thus, we can take $0 < \varepsilon_2 < 1$ sufficiently small such that

$$
\mathcal{L}V_2(t, P, A, Z) \leq -1, \quad \text{for any } (P, A, Z) \in R_+^3 \setminus U_1,
$$

where $U_1 = [\varepsilon_2, \frac{1}{\varepsilon_2}] \times [\varepsilon_2, \frac{1}{\varepsilon_2}] \times [\varepsilon_2, \frac{1}{\varepsilon_2}]$. Moreover, there exists a positive constant $M_3 = \min\{\sigma_1^2 P^2, \sigma_2^2(x, \rho_1)A^2, \sigma_3^2(y, \rho_2)Z^2\}$, such that

$$
\sigma_1^2 P^2 \zeta_1^2 + \sigma_2^2(x, \rho_1)A^2\zeta_2^2 + \sigma_3^2(y, \rho_2)Z^2\zeta_3^2 \geq M_3\|\zeta\|^2,
$$

for all $(P, A, Z) \in U_1$, $\zeta = (\zeta_1, \zeta_2, \zeta_3) \in R^3$. Then, based on Lemma 2, model (2) has a unique ergodic stationary distribution $\pi(.)$. Moreover, according to the ergodic property, the solution of model (2) $\Phi(t) = (P(t), A(t), Z(t))$ satisfying

$$
\mathcal{P}\left\{\langle\Phi_i(x, y)\rangle = \int_{R_+^3} \phi_i\pi(\mathrm{d}\phi_1, \mathrm{d}\phi_2, \mathrm{d}\phi_3)\right\} = 1, \quad i = 1, 2, 3. \tag{B.60}
$$

We then show that $\lim_{t\to\infty} \frac{\ln A(t)}{t} = 0$, from (A.47), (B.60) and the strong law of large numbers for martingales, the limits of $\frac{1}{t}\ln A(t)$ exist. If $\lim_{t\to\infty} \frac{\ln A(t)}{t} \neq 0$, then together with Lemma 1, $\limsup_{t\to\infty} \frac{\ln A(t)}{t} < 0$, consequently, $\lim_{t\to\infty} A(t) = 0$, which contradicts with (B.60). Similarly, we have $\lim_{t\to\infty} \frac{\ln Z(t)}{t} = 0$. Then, according to the Itô formula we have

$$
\begin{cases}
0 = \lim_{t\to\infty} \dfrac{\ln A(t) - \ln A(0)}{t} = \alpha\mu(x)\langle P(x,y)\rangle - c(x,y)\langle Z(x,y)\rangle - \eta(x,\rho_1) \\
\qquad\qquad\qquad\qquad\qquad\qquad\qquad + \sigma_2(x,\rho_1)\lim_{t\to\infty}\dfrac{M_2(t)}{t}, \\
0 = \lim_{t\to\infty} \dfrac{\ln Z(t) - \ln Z(0)}{t} = \delta c(x,y)\langle A(x,y)\rangle - \kappa(y,\rho_2) + \sigma_3(y,\rho_2)\lim_{t\to\infty}\dfrac{M_3(t)}{t}, \quad \text{(B.61)}\\
0 = \lim_{t\to\infty} \dfrac{V_{11}(t) - V_{11}(0)}{t} = eP_{\mathrm{in}} - e\langle P(x,y)\rangle - s_1(x)Q(x)\langle A(x,y)\rangle - s_2(y)q(y)\langle Z(x,y)\rangle \\
\quad + \sigma_1\lim_{t\to\infty}\dfrac{N_1(t)}{t} + \sigma_2(x,\rho_1)Q(x)\lim_{t\to\infty}\dfrac{N_2(t)}{t} + \sigma_3(y,\rho_2)q(y)\lim_{t\to\infty}\dfrac{N_3(t)}{t}.
\end{cases}
$$

By using and the strong law of large numbers for martingales, $\lim_{t\to\infty}\frac{M_i(t)}{t} = \lim_{t\to\infty}\frac{N_j(t)}{t} = 0$, $i = 2, 3$, $j = 1, 2, 3$, then obviously (B.61) has a unique positive solution, provided that $\lambda(x, y) > 0$, and

$$
\begin{cases}
\langle P(x,y)\rangle = \dfrac{c(x,y)\langle Z(x,y)\rangle + \eta(x,\rho_1)}{\alpha\mu(x)}, \\
\langle A(x,y)\rangle = \dfrac{\kappa(y,\rho_2)}{\delta c(x,y)}, \\
\langle Z(x,y)\rangle = \dfrac{\lambda(x,y)}{s_2(y)q(y) + \frac{ec(x,y)}{\alpha\mu(x)}}.
\end{cases}
\qquad\text{(B.62)}
$$

This completes the proof of Theorem 3. $\qquad\qquad\qquad\qquad\qquad\qquad\qquad\square$

Appendix C: Proofs of Theorems 5 and 6

Proof of Theorem 5

Our main aim in this part is to derive the conditions under which x^* is evolutionary stable and convergence stable. To achieve that, we first need the following results. From the first equation of (B.61), when $y = h$ is a constant we have

$$
\alpha\mu(x)\langle P(x,h)\rangle - c(x)\langle Z(x,h)\rangle = \eta(x,\rho_1). \qquad\text{(C.63)}
$$

Taking the partial derivative of both sides of (C.63) with respect to x leads to

$$
\alpha\mu'(x)\langle P(x,h)\rangle + \alpha\mu(x)\langle P(x,h)\rangle' - c'(x,h)\langle Z(x,h)\rangle - c(x,h)\langle Z(x,h)\rangle' = \eta'(x,\rho_1).
$$
$$\text{(C.64)}$$

Combining with Eq. (25), we have

$$
c(x^*,h)\langle Z(x^*,h)\rangle' - \alpha\mu(x^*)\langle P(x^*,h)\rangle' = 0. \qquad\text{(C.65)}
$$

We know that x^* is an ESS, i.e., the fitness will achieve its maximum at x^*, provided that

$$\left.\frac{\partial^2 F_2(x, x_{\text{mut}})}{\partial x_{\text{mut}}^2}\right|_{x_{\text{mut}}=x=x^*} = \alpha\mu''(x^*)\langle P(x^*, h)\rangle - c''(x^*, h)\langle Z(x^*, h)\rangle - \eta''(x^*, \rho_1) < 0.$$

$$(C.66)$$

Taking the second partial derivative of both sides of (C.63) with respect to x leads to

$$\begin{aligned}
&\alpha\mu''(x^*)\langle P(x^*, h)\rangle - c''(x^*, h)\langle Z(x^*, h)\rangle - \eta''(x^*, \rho_1) \\
&= 2c'(x^*, h)\langle Z(x^*, h)\rangle' - 2\alpha\mu'(x^*)\langle P(x^*, h)\rangle' + c(x, h)\langle Z(x^*, h)\rangle'' \\
&\quad - \alpha\mu(x)\langle P(x^*, h)\rangle''.
\end{aligned}$$

$$(C.67)$$

Substituting (C.65) into (C.67), we have

$$\begin{aligned}
&\left.\frac{\partial^2 F_2(x, x_{\text{mut}})}{\partial x_{\text{mut}}^2}\right|_{x_{\text{mut}}=x=x^*} \\
&= 2c(x^*, h)\langle Z(x^*, h)\rangle' \left(\frac{c'(x^*, h)}{c(x^*, h)} - \frac{\mu'(x^*)}{\mu(x^*)}\right) - c(x^*, h)\langle Z(x^*, h)\rangle' \\
&\quad \left(\frac{\langle P(x^*, h)\rangle''}{\langle P(x^*, h)\rangle'} - \frac{\langle Z(x^*, h)\rangle''}{\langle Z(x^*, h)\rangle'}\right) \\
&= c(x^*, h)\langle Z(x^*, h)\rangle'(2h_1(x^*) - h_2(x^*)),
\end{aligned}$$

$$(C.68)$$

where

$$h_1(x) = \frac{c'(x, h)}{c(x, h)} - \frac{\mu'(x)}{\mu(x)}, \qquad h_2(x) = \frac{\langle P(x, h)\rangle''}{\langle P(x, h)\rangle'} - \frac{\langle Z(x, h)\rangle''}{\langle Z(x, h)\rangle'}. \quad (C.69)$$

Obviously, if $\langle Z(x^*, h)\rangle'(2h_1(x^*) - h_2(x^*)) < 0$ holds, then x^* is an ESS. Once x^* is an ESS, there is no possibility of further evolution changes by small mutation. Moreover, the singular strategy x^* is convergence stable, provided that

$$\begin{aligned}
&\left.\frac{\partial D_2(x)}{\partial x}\right|_{x=x^*} \\
&= \alpha\mu''(x^*)\langle P(x^*, h)\rangle - c''(x^*, h)\langle Z(x^*, h)\rangle \\
&\quad - \eta''(x^*, \rho_1) + \alpha\mu'(x^*)\langle P(x^*, h)\rangle' - c'(x^*, h)\langle Z(x^*, h)\rangle' \\
&= c'(x^*, h)\langle Z(x^*, h)\rangle' - \alpha\mu'(x^*)\langle P(x^*, h)\rangle' + c(x^*, h)\langle Z(x^*, h)\rangle'' - \alpha\mu(x^*)\langle P(x^*, h)\rangle'' \\
&= c(x^*, h)\langle Z(x^*, h)\rangle'(h_1(x^*) - h_2(x^*)) \\
&< 0.
\end{aligned}$$

$$(C.70)$$

We then determine the sign of $\langle Z(x^*, h)\rangle'$. From the third equation of (B.61) and the second equation of (B.62),

$$eP_{\text{in}} - e\langle P(x, h)\rangle - s_2(h)q(h)\langle Z(x, h)\rangle = \frac{s_1(x)Q(x)\kappa(h, \rho_2)}{\delta c(x, h)},$$

then taking the partial derivative of both sides with respect to x, we have

$$-e\langle P(x,h)\rangle' - s_2(h)q(h)\langle Z(x,h)\rangle' = \frac{\kappa(h,\rho_2)}{\delta}g'(x),$$

where $g(x) = \frac{s_1(x)}{c(x,h)}Q(x)$. Since $\left(\frac{s_1(x)}{c(x,h)}\right)' = \frac{2k_1 x \exp(v(x-\theta h)^2)}{c_m}(vx^2 - v\theta hx + 1) > 0$ and $Q'(x) > 0$, then $g'(x) > 0$. This together with (C.65) we can conclude that $\langle Z(x^*,h)\rangle' < 0$ and $\langle P(x^*,h)\rangle' < 0$. Then, from (C.68) and (C.70) we know that when $h_1(x^*) < h_2(x^*)$, x^* is a repellor. When $h_1(x^*) > h_2(x^*)$, x^* is convergence stable; meanwhile, it is an ESS as long as $2h_1(x^*) > h_2(x^*)$ or an evolutionary branching point if $2h_1(x^*) < h_2(x^*)$. Theorem 5 is thus proved.

We then give some analysis about Table 2. Combining with Eqs. (C.63), (25) and (B.60) leads to

$$\left(\frac{\mu'(x^*)}{\mu(x^*)} - \frac{c'(x^*,h)}{c(x^*,h)}\right)\left(\frac{\eta'(x^*,\rho_1)}{\eta(x^*,\rho_1)} - \frac{\mu'(x^*)}{\mu(x^*)}\right) > 0,$$

and

$$\left(\frac{\mu'(x^*)}{\mu(x^*)} - \frac{c'(x^*,h)}{c(x^*,h)}\right)\left(\frac{\eta'(x^*,\rho_1)}{\eta(x^*,\rho_1)} - \frac{c'(x^*,h)}{c(x^*,h)}\right) > 0,$$

which implies that

$$\frac{\eta'(x^*,\rho_1)}{\eta(x^*,\rho_1)} > \frac{\mu'(x^*)}{\mu(x^*)} > \frac{c'(x^*,h)}{c(x^*,h)} \quad \text{or} \quad \frac{c'(x^*,h)}{c(x^*,h)} > \frac{\mu'(x^*)}{\mu(x^*)} > \frac{\eta'(x^*,\rho_1)}{\eta(x^*,\rho_1)} > 0.$$
$$\text{(C.71)}$$

It easy to see that $h_1(x^*) \neq 0$, $x^* \in \left(0, \min\left\{\theta h, \sqrt{\frac{a_3}{a_1}}\right\}\right)$ or $x^* \in (\theta h, \infty)$.

From (C.69), the sign of $h_1(x^*)$ is only determined by the sign of $\frac{c'(x^*,h)}{c(x^*,h)} - \frac{\mu'(x^*)}{\mu(x^*)}$. When $\frac{c'(x^*,h)}{c(x^*,h)} > \frac{\mu'(x^*)}{\mu(x^*)} > 0$, $h_1(x^*) > 0$, satisfying $2h_1(x^*) > h_1(x^*)$. Then once x^* is convergence stable, i.e., $h_1(x^*) > h_2(x^*)$, the inequality $2h_1(x^*) > h_2(x^*)$ is also holds, i.e., x^* is also an ESS. At this situation, x^* is either a CSS or a repellor, and $x^* \in (0, \min\{\theta h, \sqrt{a_3/a_1}\})$. When $\frac{\mu'(x^*)}{\mu(x^*)} > \frac{c'(x^*,h)}{c(x^*,h)}$, $h_1(x^*) < 0$, and when $h_2(x^*) \geq 0$, $h_1(x^*) < h_2(x^*)$ always holds, thus x^* is a repellor. When $h_2(x^*) < 0$, it can be divided into three scenarios: (1) $h_1(x^*) < h_2(x^*) < 0$, at this situation, x^* is a repellor; (2) $h_2(x^*) < 2h_1(x^*) < 0$, at this point, x^* is a CSS; (3) $h_1(x^*) > h_2(x^*) > 2h_1(x^*)$, then x^* is an evolutionary branching point, which implies the algal population will split up into two species with different cell size. This confirms Table 2.

Proof of Theorem 6

In this part, we mainly investigate how environmental fluctuation and phosphorus content affect the trend of algal evolution in the presence of zooplankton. According to (25),

$$\frac{\partial D_2(x^*)}{\partial \rho_1}$$

$$= \alpha\mu'(x^*)\frac{\partial\langle P(x^*,h)\rangle}{\partial\rho_1} - c'(x^*,h)\frac{\partial\langle Z(x^*,h)\rangle}{\partial\rho_1} - \frac{\partial^2\eta(x,\rho_1)}{\partial x\partial\rho_1}\Big|_{x=x^*} \quad\quad\text{(C.72)}$$

$$= \alpha\frac{\mu'(x^*)}{\mu(x^*)}\mu(x^*)\frac{\partial\langle P(x^*,h)\rangle}{\partial\rho_1} - \frac{c'(x^*,h)}{c(x^*,h)}c(x^*,h)\frac{\partial\langle Z(x^*,h)\rangle}{\partial\rho_1} - \frac{\partial^2\eta(x,\rho_1)}{\partial x\partial\rho_1}\Big|_{x=x^*}.$$

From (21),

$$\frac{@\langle Z(x,h)\rangle}{@\rho_1} = -\frac{\frac{e}{\alpha\mu(x)}\sigma_2(x,\rho_1)\frac{\partial\sigma_2(x,\rho_1)}{\partial\rho_1}}{s_2(h)q(h) + \frac{ec(x,h)}{\alpha\mu(x)}} < 0,$$

and

$$\frac{@\langle P(x,h)\rangle}{@\rho_1} = \frac{\sigma_2(x,\rho_1)\frac{\partial\sigma_2(x,\rho_1)}{\partial\rho_1}}{\alpha\mu(x)}\left(-\frac{\frac{ec(x,h)}{\alpha\mu(x)}}{s_2(h)q(h) + \frac{ec(x,h)}{\alpha\mu(x)}} + 1\right) > 0.$$

Moreover, from the first equation of (B.61),

$$\alpha\mu(x)\langle P(x,h)\rangle - c(x,h)\langle Z(x,h)\rangle = \eta(x,\rho_1),$$

then

$$\alpha\mu(x)\frac{\partial\langle P(x,h)\rangle}{\partial\rho_1} - c(x,h)\frac{\partial\langle Z(x,h)\rangle}{\partial\rho_1} = \frac{\partial\eta(x,\rho_1)}{\partial\rho_1}.$$

It then follows from (C.72), when $\frac{\mu'(x^*)}{\mu(x^*)} > \frac{c'(x^*,h)}{c(x^*,h)}$,

$$\frac{\partial D_2(x^*)}{\partial\rho_1} < \frac{\mu'(x^*)}{\mu(x^*)}\left[\alpha\mu(x^*)\frac{\partial\langle P(x^*,h)\rangle}{\partial\rho_1} - c(x^*,h)\frac{\partial\langle Z(x^*,h)\rangle}{\partial\rho_1}\right] - \frac{\partial^2\eta(x,\rho_1)}{\partial x\partial\rho_1}\Big|_{x=x^*}$$

$$= \frac{\mu'(x^*)}{\mu(x^*)}\frac{\partial\eta(x^*,\rho_1)}{\partial\rho_1} - \frac{\partial^2\eta(x,\rho_1)}{\partial x\partial\rho_1}\Big|_{x=x^*}$$

$$= \frac{a_3 - a_1 x^{*2}}{(a_1 x^{*2} + a_2 x^* + a_3)x^*}\frac{x^{*4}k_3^2 k_4\rho_1}{(k_4 + \rho_1)^3} - \frac{4x^{*3}k_3^2 k_4\rho_1}{(k_4 + \rho_1)^3}$$

$$= \left(\frac{-5a_1 x^{*2} - 4a_2 x^* - 3a_3}{a_1 x^{*2} + a_2 x^* + a_3}\right)\frac{x^{*3}k_3^2 k_4\rho_1}{(k_4 + \rho_1)^3}$$

$$< 0.$$

Otherwise, $\frac{c'(x^*,h)}{c(x^*,h)} > \frac{\mu'(x^*)}{\mu(x^*)} > 0$, since $v < \frac{4}{\theta^2 h^2}$, then

$$
\frac{\partial D_2(x^*)}{\partial \rho_1} < \frac{c'(x^*,h)}{c(x^*,h)} \frac{\partial \eta(x^*,\rho_1)}{\partial \rho_1} - \frac{\partial^2 \eta(x,\rho_1)}{\partial x \partial \rho_1}\bigg|_{x=x^*}
$$

$$
= 2v(\theta h - x^*)\frac{x^{*4}k_3^2 k_4 \rho_1}{(k_4+\rho_1)^3} - \frac{4x^{*3}k_3^2 k_4 \rho_1}{(k_4+\rho_1)^3}
$$

$$
= \left(-2vx^{*2} + 2v\theta h x^* - 4\right)\frac{x^{*3}k_3^2 k_4 \rho_1}{(k_4+\rho_1)^3}
$$

$$
< 0.
$$

Since our concern is the CSS or evolutionary branching point, then $-\frac{\partial D_1(x^*)}{\partial x^*} > 0$. By the implicit function theorem, we have

$$
\frac{dx^*}{d\rho_1} = \frac{\frac{\partial D_2(x^*)}{\partial \rho_2}}{-\frac{\partial D_2(x^*)}{\partial x^*}} < 0.
$$

Moreover, from Eq. (21), we have $\frac{\partial \langle P(x,h)\rangle}{\partial P_{\text{in}}} = \frac{c(x,h)}{\alpha\mu(x)}\frac{\partial \langle Z(x,h)\rangle}{\partial P_{\text{in}}}$ and $\frac{\partial \langle Z(x,h)\rangle}{\partial P_{\text{in}}} = \frac{e}{s_2(h)q(h)+ec(x,h)/\alpha\mu(x)} > 0$. Then,

$$
\frac{\partial D_2(x^*)}{\partial P_{\text{in}}} = \alpha\mu'(x)\frac{\partial \langle P(x^*,h)\rangle}{\partial P_{\text{in}}} - c'(x^*,h)\frac{\partial \langle Z(x^*,h)\rangle}{\partial P_{\text{in}}}
$$

$$
= c(x^*,h)\frac{\partial \langle Z(x^*,h)\rangle}{\partial P_{\text{in}}}\left(\frac{\mu'(x^*)}{\mu(x^*)} - \frac{c'(x^*,h)}{c(x^*,h)}\right)
$$

$$
= -c(x^*,h)h_1(x^*)\frac{\partial \langle Z(x^*,h)\rangle}{\partial P_{\text{in}}}.
$$

Then if $h_1(x^*) < 0$,

$$
\frac{dx^*}{dP_{\text{in}}} = \frac{\frac{\partial D_2(x^*)}{\partial P_{\text{in}}}}{-\frac{\partial D_2(x^*)}{\partial x^*}} > 0,
$$

otherwise $h_1(x^*) > 0$, and $\frac{dx^*}{dP_{\text{in}}} < 0$. This completes the proof. $\square$

Appendix D: Proofs of Theorems 7 and 8

Proof of Theorem 7

Proof Since the coefficients of model (26) are locally Lipschitz in R_+^4, then there exists a unique local solution $(P(t), A_1(t), A_2(t), Z(t))$ of model (26) on the interval $(0, \tau_e)$, where τ_e denotes the explosion time. In order to prove $\tau_e = \infty$, we only need to

construct a nonnegative C^2-function V_3 satisfying $\mathcal{L}V_3 \leq M_3$, where M_3 is a positive constant (Mao et al. 2002). Define the nonnegativity function $V_3 : R_+^4 \to R_+$ by

$$V_3 = m_6 V_{31} - V_{32} - V_3^*,$$

where $V_{31} = P + \sum_{i=1}^{2} Q(x_i)A_i + qZ$, $V_{32} = m_7 \ln P + \sum_{i=1}^{2} \ln A_i + \ln Z$, V_3^* is the minimum value point of $V_3(P, A_1, A_2, Z)$ and $m_6 = \frac{2\check{c}}{s_2 q}$, $m_7 = \frac{\delta \hat{c}}{\alpha \check{u} \check{Q}}$. Then by using the Itô formula, we have

$$\mathcal{L}V_3 \leq m_6 e P_{\text{in}} + \sum_{i=1}^{2} \eta(x_i, \rho_1) + m_7 e + \kappa(h, \rho_2) := M_3.$$

Arguing similarly as in Mao et al. (2002), we can obtain the first part of Theorem 7. Moreover, by using the Itô formula to model (26) again, we have

$$
\begin{aligned}
\mathrm{d}V_{31} \\
= &\left[e P_{\text{in}} - e P - \sum_{i=1}^{2} s_1(x_i) Q(x_i) A_i - s_2(h) q(h) Z \right] \mathrm{d}t \\
&+ \sigma_1 P \mathrm{d}B_1(t) + \sigma_3(h, \rho_2) q(h) Z \mathrm{d}B_4(t) \\
&+ \sum_{i=1}^{2} \sigma_2(x_i, \rho_1) Q(x_i) A_i \mathrm{d}B_{i+1}(t) \\
\leq &\left(e P_{\text{in}} - h_2 V_{31} \right) \mathrm{d}t + \sigma_1 P \mathrm{d}B_1(t) \\
&+ \quad \sum_{i=1}^{2} \sigma_2(x_i, \rho_1) Q(x_i) A_i \mathrm{d}B_{i+1}(t) + \sigma_3(h, \rho_2) q(h) Z \mathrm{d}B_4(t),
\end{aligned}
$$

where $h_2 = \min\{e, \hat{s}_1, s_2(h)\}$. Considering the following model

$$
\begin{cases}
\mathrm{d}Y = \left(e P_{\text{in}} - h_2 V_{31} \right) \mathrm{d}t + \sigma_1 P \mathrm{d}B_1(t) + \sum_{i=1}^{2} \sigma_2(x_i, \rho_1) Q(x_i) A_i \mathrm{d}B_{i+1}(t) \\
\qquad\qquad\quad + \sigma_3(h, \rho_2) q(h) Z \mathrm{d}B_4(t), \\
Y(0) = V_{31}(0).
\end{cases}
\tag{D.73}
$$

Then, the solution of Eq. (D.73) has the following form

$$Y(t) = \frac{e P_{\text{in}}}{h_2} + Y(0) - \left(\frac{e P_{\text{in}}}{h_2} \right) \exp(-h_2 t) + M(t),$$

where

$$M(t) = \sigma_1 \int_0^t \exp[-h_2(t-s)] P(s) \mathrm{d}B_1(s) + \sum_{i=1}^{2} \sigma_2(x_i, \rho_1) Q(x_i)$$

$$\int_0^t \exp[-h_2(t-s)]A_i(s)\mathrm{d}B_{i+1}(s)$$

$$+ \sigma_3(h, \rho_2)q(h)\int_0^t \exp[-h_2(t-s)]Z(s)\mathrm{d}B_4(s)$$

is a local martingale satisfying $M(0) = 0$, a.s. The stochastic comparison theorem implies $V_{31}(t) \leq Y(t)$, a.s.

Define $Y(t) = Y(0) + B(t) - U(t) + M(t)$, where $B(t) = \frac{eP_{\text{in}}}{h_2}[1 - \exp(-h_2 t)]$, $U(t) = Y(0)[1 - \exp(-h_2 t)]$, $B(0) = U(0) = 0$. Obviously, $B(t)$ and $U(t)$ are continuous adapted increasing processes. With the aid of the nonnegative semimartingale convergence theorem (Mao 2006), we have $\lim_{t\to\infty} Y(t) < \infty$, a.s. Thus, $\lim_{t\to\infty} V_{31}(t) < \infty$, a.s. This completes the proof.   □

Proof of Theorem 8

Let

$$\tilde{A} = \sum_{i=1}^2 Q(x_i)A_i,$$

then model (26) becomes a three-dimensional model. We first prove that when $\hat{\lambda}(x_i, h) > 0$, $i = 1, 2$, the new three-dimensional model admits a unique stationary distribution. The proof is similar to the proof of Theorem 3 in "Appendix B". Define a nonnegative $\mathcal{C}^2-$Lyapunov function

$$V_4 = M_3 V_{41} + V_{42} + V_{43} - V_4^*,$$

V_4^* is the minimum value of $V_4(P, \tilde{A}, Z)$ and

$$V_{41} = m_8 Z - m_9 \ln Z - m_{10} \ln \tilde{A} - (P + \tilde{A} + q(h)Z),$$
$$V_{32} = \frac{1}{\theta_2 + 2}(P + \tilde{A} + q(h)Z)^{\theta_2 + 2}, \quad V_{43} = -\ln P,$$

where $m_8 = (m_{10}\check{c}(x_i, h) + s_2(h)q(h))/(s_2(h) + d_2)$, $m_9 = \frac{\check{s}_1 \check{Q}}{\delta\hat{c}(x_i,h)}$, $m_{10} = \frac{e}{\alpha\hat{\mu}}$, $0 < \theta_2 < 1$ is a constant which is small enough such that

$$h_3(x_1, x_2) := \min\{e, \hat{s}_1, s_2\} - \frac{\theta_2 + 1}{2}\max\{\sigma_1^2, \check{\sigma}_2^2, \sigma_3^2\} > 0,$$

and the positive constant M_3 satisfying

$$-M_3\hat{\lambda}(x_i, h) + f_2^u \leq -2,$$

where $f_2 = -h_3(x_1, x_2)(P + \tilde{A} + q(h)Z)^{\theta_1 + 2} + e P_{\text{in}}(P + \tilde{A} + q(h)Z)^{\theta_1 + 1} + \alpha \check{\mu} \tilde{A} + e + \frac{\sigma_1^2}{2}$. By using the Itô formula, we can compute that

$$
\begin{aligned}
\mathcal{L}V_4 \leq & -M_3 \left[\hat{\lambda}(x_i, h) - \frac{m_8 \delta \check{c}(x_i, h)}{\hat{Q}} \tilde{A}Z \right] \\
& - h_3(x_1, x_2)(P + \tilde{A} + q(h)Z)^{\theta_1 + 2} + e P_{\text{in}}(P + \tilde{A} + q(h)Z)^{\theta_1 + 1} \\
& - \frac{e P_{\text{in}}}{P} + \alpha \check{\mu} \tilde{P} + e + \frac{\sigma_1^2}{2} \\
= & -M_3 \left[\hat{\lambda}(x_i, h) - \frac{m_8 \delta \check{c}(x_i, h)}{\hat{Q}} \tilde{A}Z \right] - \frac{e P_{\text{in}}}{P} + f_2(P, \tilde{A}, Z).
\end{aligned}
$$

Then following the same logic as the proof in "Appendix B", we can obtain that, when $\hat{\lambda}(x_i, h) > 0$, $i = 1, 2$, the new three-dimensional model has a unique stationary distribution $\nu(.)$ and it is ergodic. According to the ergodic property, the solution of the new three-dimensional model $\Psi(t) = (P(t), \tilde{A}(t), Z(t))$ satisfying

$$
\mathcal{P} \left\{ \langle \Psi_j(x_1, x_2) \rangle = \int_{R_+^3} \psi_j \nu(\mathrm{d}\psi_1, \mathrm{d}\psi_2, \mathrm{d}\psi_3) \right\} = 1, \quad j = 1, 2, 3. \quad \text{(D.74)}
$$

This suggests that the new three-dimensional model could achieve a relative stable state, i.e., the long-time mean persistent level of the concentration of dissolved inorganic phosphorus, the amount of organophosphorus in the entire algal species and the zooplankton carbon density remain unchanged a.s., no matter how many algal species exists in the model. If one of the algal species goes to extinction, then the dimorphic model (26) will ultimately degenerate to the original monomorphic model (20), and the following equations hold,

$$
\langle P(x_1, x_2) \rangle = \langle P(x, h) \rangle, \quad \langle \tilde{A}(x_1, x_2) \rangle = Q(x) \langle A(x, h) \rangle, \quad \langle Z(x_1, x_2) \rangle = \langle Z(x, h) \rangle, \quad a.s.
$$
$$
\text{(D.75)}
$$

We next prove that when $\min\{x_1, x_2\} < x < \max\{x_1, x_2\}$ holds, model (26) is stable in mean. To achieve that, we only need to prove $\langle A_1(x_1, x_2) \rangle > 0$ and $\langle A_2(x_1, x_2) \rangle > 0$. It is easy to compute that

$$
\begin{aligned}
& \mathrm{d}(P + \tilde{A} + q(h)Z) \\
& = \left[e P_{\text{in}} - eP - s_2(h)q(h)Z - s_1(x_1)Q(x_1)A_1 - s_1(x_2)Q(x_2)A_2 \right] \mathrm{d}t + \sigma_1 N \mathrm{d}B_1(t) \\
& \quad + \sigma_2(x_1, \rho_1)Q(x_1)P_1 \mathrm{d}B_2(t) + \sigma_2(x_2, \rho_1)Q(x_2)P_3 \mathrm{d}B_2(t) + \sigma_3(h, \rho_2)q(h)Z \mathrm{d}B_4(t).
\end{aligned}
$$

Integrating the above equation from 0 to t and dividing by t on both sides lead to

$$
e P_{\text{in}} - \frac{e}{t} \int_0^t P(s)\mathrm{d}s - \frac{s_2(h)q(h)}{t} \int_0^t Z(s)\mathrm{d}s - \sum_{i=1}^2 \frac{s_1(x_i)Q(x_i)}{t} \int_0^t A_i(s)\mathrm{d}s = \frac{\psi_2(t)}{t},
$$
$$
\text{(D.76)}
$$

where $\psi_2(t) = R(t) - R(0) - H(t)$, $H(t) = \sigma_1 \int_0^t N(s) \mathrm{d}B_1(s) + \sum_{i=1}^2 \sigma_2(x_i, \rho) Q(x_i)$ $\int_0^t P_i(s) \mathrm{d}B_{1+i}(s) + \sigma_3(h, \rho_2) q(h) \int_0^t Z(s) \mathrm{d}B_4(s)$, $R(t) = P(t) + \sum_{i=1}^2 Q(x_i) A_i(t) + q(h) Z(t)$. According to Theorem 1 and the strong law of large numbers for local martingales (Mao 2006):

$$\lim_{t\to\infty} \frac{\psi_2(t)}{t} = 0,$$

then together with (D.75), (B.62) and the third equation of (B.61), we have

$$
\begin{aligned}
&\frac{s_1(x) Q(x) \kappa(h, \rho_2)}{\delta c(x, h)} \\
&= e P_{\text{in}} - e\langle P(x, h)\rangle - s_2 q(h)\langle Z(x, h)\rangle = e P_{\text{in}} - e\langle P(x_1, x_2)\rangle - s_2(h) q(h)\langle Z(x_1, x_2)\rangle \\
&= \lim_{t\to\infty} \sum_{i=1}^2 \frac{s_1(x_i) Q(x_i)}{t} \int_0^t A_i(s) \mathrm{d}s.
\end{aligned}
\tag{D.77}
$$

Moreover, from (D.75) and (B.62),

$$\frac{\kappa(h, \rho_2) Q(x)}{\delta c(x, h)} = Q(x)\langle A(x, h)\rangle = \lim_{t\to\infty} \sum_{i=1}^2 \frac{Q(x_i)}{t} \int_0^t A_i(s) \mathrm{d}s. \tag{D.78}$$

Noticing the fact that, for any $f(t), g(t) < \infty$,

$$\liminf_{t\to\infty}[f(t) + g(t)] \le \liminf_{t\to\infty} f(t) + \limsup_{t\to\infty} g(t) \le \limsup_{t\to\infty}[f(t) + g(t)],$$

and if $\lim_{t\to\infty}[f(t) + g(t)]$ exists, $\liminf_{t\to\infty} f(t) + \limsup_{t\to\infty} g(t) = \lim_{t\to\infty}[f(t) + g(t)]$. Then, together with (D.78) and (D.77),

$$
\begin{cases}
Q(x_1)\overline{\langle A_1(x_1, x_2)\rangle} + Q(x_2)\underline{\langle A_2(x_1, x_2)\rangle} = \frac{\kappa(h, \rho_2) Q(x)}{\delta c(x, h)}, \\
s_1(x_1) Q(x_1)\overline{\langle A_1(x_1, x_2)\rangle} + s_1(x_2) Q(x_2)\underline{\langle A_2(x_1, x_2)\rangle} = \frac{s_1(x) Q(x) \kappa(h, \rho_2)}{\delta c(x, h)},
\end{cases}
\tag{D.79}
$$

and

$$
\begin{cases}
Q(x_1)\underline{\langle A_1(x_1, x_2)\rangle} + Q(x_2)\overline{\langle A_2(x_1, x_2)\rangle} = \frac{\kappa(h, \rho_2) Q(x)}{\delta c(x, h)}, \\
s_1(x_1) Q(x_1)\underline{\langle A_1(x_1, x_2)\rangle} + s_1(x_2) Q(x_2)\overline{\langle A_2(x_1, x_2)\rangle} = \frac{s_1(x) Q(x) \kappa(h, \rho_2)}{\delta c(x, h)}.
\end{cases}
\tag{D.80}
$$

When $\min\{x_1, x_2\} < x < \max\{x_1, x_2\}$, by solving (D.79) and (D.80) we can obtain that:

$$\overline{\langle A_1(x_1, x_2)\rangle} = \underline{\langle A_1(x_1, x_2)\rangle} = \frac{\kappa(h, \rho_2) Q(x)}{\delta c(x, h) Q(x_1)} \frac{s(x_2) - s(x)}{s(x_2) - s(x_1)},$$

$$\overline{\langle A_2(x_1, x_2)\rangle} = \underline{\langle A_2(x_1, x_2)\rangle} = \frac{\kappa(h, \rho_2) Q(x)}{\delta c(x, h) Q(x_2)} \frac{s(x_1) - s(x)}{s(x_1) - s(x_2)}.$$

According to the description of x-functions in Table 1, $s'(x) > 0$, then $\min\{s(x_1),$ $s(x_2)\} < s(x) < \max\{s(x_1), s(x_2)\}$. Consequently, we can conclude that $\langle A_1(x_1, x_2)\rangle$ > 0 and $\langle A_2(x_1, x_2)\rangle > 0$.

Our next step is to explicitly express the persistence level of model (26) in terms of x_1 and x_2 only. Following similar methods as in the derivation of (B.62), the solution of model (26) satisfying $\lim_{t\to\infty} \frac{\ln A_i(t)}{t} = 0$, $\lim_{t\to\infty} \frac{\ln Z(t)}{t} = 0$, $i = 1, 2$. Together with (D.77) leads to:

$$
\begin{cases}
\alpha\mu(x_1)\langle P(x_1, x_2)\rangle - c(x_1, h)\langle Z(x_1, x_2)\rangle = \eta(x_1, \rho_1), \\
\alpha\mu(x_2)\langle P(x_1, x_2)\rangle - c(x_2, h)\langle Z(x_1, x_2)\rangle = \eta(x_2, \rho_1), \\
\delta c(x_1, h)\langle A_1(x_1, x_2)\rangle + \delta c(x_2, h)\langle A_2(x_1, x_2)\rangle = \kappa(h, \rho_2), \\
e\langle P(x_1, x_2)\rangle + s_1(x_1)Q(x_1)\langle A_1(x_1, x_2)\rangle + s_1(x_2)Q(x_2)\langle A_2(x_1, x_2)\rangle + \\
s_2(y)q(y)\langle Z(x_1, x_2)\rangle = e P_{\text{in}}.
\end{cases}
\tag{D.81}
$$

Through simple calculation, (D.81) has a unique positive solution as follows:

$$
\begin{aligned}
\langle P(x_1, x_2)\rangle &= \frac{c(x_2, h)\eta(x_1, \rho_1) - c(x_1, h)\eta(x_2, \rho_1)}{\alpha c(x_2, h)\mu(x_1) - \alpha c(x_1, h)\mu(x_2)}, \\
\langle A_1(x_1, x_2)\rangle &= \frac{s_1(x_2)Q(x_2)\kappa(h, \rho_2) - \delta c(x_2, h)f_3}{\delta c(x_1, h)s_1(x_2)Q(x_2) - \delta c(x_2, h)s_1(x_1)Q(x_1)}, \\
\langle A_2(x_1, x_2)\rangle &= \frac{\delta c(x_1, h)f_3 - s_1(x_1)Q(x_1)\kappa(h, \rho_2)}{\delta c(x_1, h)s_1(x_2)Q(x_2) - \delta c(x_2, h)s_1(x_1)Q(x_1)}, \\
\langle Z(x_1, x_2)\rangle &= \frac{\mu(x_2)\eta(x_1, \rho_1) - \mu(x_1)\eta(x_2, \rho_1)}{c(x_2)\mu(x_1) - c(x_1)\mu(x_2)},
\end{aligned}
\tag{D.82}
$$

where $f_3 = e P_{\text{in}} - e\langle P(x_1, x_2)\rangle - s_2(h)q(h)\langle Z(x_1, x_2)\rangle$. The proof is completed.

Remark 10 Note that when zooplankton species also evolves, Theorem 7 and 8 also hold, and the long-time mean persistent level becomes:

$$
\begin{aligned}
\langle P(x_1, x_2, y)\rangle &= \frac{c(x_2, y)\eta(x_1, \rho_1) - c(x_1, y)\eta(x_2, \rho_1)}{\alpha c(x_2, y)\mu(x_1) - \alpha c(x_1, y)\mu(x_2)}, \\
\langle A_1(x_1, x_2, y)\rangle &= \frac{s_1(x_2)Q(x_2)\kappa(y, \rho_2) - \delta c(x_2, y)f_4}{\delta c(x_1, y)s_1(x_2)Q(x_2) - \delta c(x_2, y)s_1(x_1)Q(x_1)}, \\
\langle A_2(x_1, x_2, y)\rangle &= \frac{\delta c(x_1, y)f_4 - s_1(x_1)Q(x_1)\kappa(y, \rho_2)}{\delta c(x_1, y)s_1(x_2)Q(x_2) - \delta c(x_2, y)s_1(x_1)Q(x_1)}, \\
\langle Z(x_1, x_2, y)\rangle &= \frac{\mu(x_2)\eta(x_1, \rho_1) - \mu(x_1)\eta(x_2, \rho_1)}{c(x_2, y)\mu(x_1) - c(x_1, y)\mu(x_2)},
\end{aligned}
\tag{D.83}
$$

where $f_4 = e P_{\text{in}} - e\langle P(x_1, x_2, y)\rangle - s_2(y)q(y)\langle Z(x_1, x_2, y)\rangle$.

Appendix E: Proof of Theorem 9

In this part, we mainly investigate the convergence stability and the evolutionary stability of (x_1^*, x_2^*). Taking the partial derivatives of the first and second equations of (D.81), with respect to x_1, x_2, respectively, leads to

$$\alpha\mu'(x_1)\langle P(x_1, x_2)\rangle + \alpha\mu(x_1)\frac{\partial\langle P(x_1, x_2)\rangle}{\partial x_1}$$

$$-c'(x_1, h)\langle Z(x_1, x_2)\rangle - c(x_1, h)\frac{\partial\langle Z(x_1, x_2)\rangle}{\partial x_1} = \eta'(x_1, \rho_1),$$

$$\alpha\mu'(x_2)\langle P(x_1, x_2)\rangle + \alpha\mu(x_2)\frac{\partial\langle P(x_1, x_2)\rangle}{\partial x_2}$$

$$-c'(x_2, h)\langle Z(x_1, x_2)\rangle - c(x_2, h)\frac{\partial\langle Z(x_1, x_2)\rangle}{\partial x_2} = \eta'(x_2, \rho_1).$$

Together with (30) leads to

$$c(x_i^*, h)\frac{\partial\langle Z(x_1, x_2)\rangle}{\partial x_i}\bigg|_{x_i=x_i^*} = \alpha\mu(x_i^*)\frac{\partial\langle P(x_1, x_2)\rangle}{\partial x_i}\bigg|_{x_i=x_i^*}, \quad i = 1, 2. \quad \text{(E.84)}$$

Also from the first and second equations of (D.81), we can compute that

$$c(x_i, h)\frac{\partial\langle Z(x_1, x_2)\rangle}{\partial x_j} = \alpha\mu(x_i)\frac{\partial\langle P(x_1, x_2)\rangle}{\partial x_j}, \quad i, j = 1, 2, \; i \neq j. \quad \text{(E.85)}$$

Combining Eq. (E.85) with (E.84) leads to,

$$c(x_i^*, h)\left(\frac{\mu(x_j^*)}{\mu(x_i^*)} - \frac{c(x_j^*, h)}{c(x_i^*, h)}\right)\frac{\partial\langle Z(x_1, x_2)\rangle}{\partial x_i}\bigg|_{x_i=x_i^*} = 0, \quad \text{(E.86)}$$

where $i, j = 1, 2$ and $i \neq j$. Moreover, from the expression of $\langle Z(x_1, x_2)\rangle$ in (D.82), we know that

$$[c(x_i, h)\mu(x_j) - c(x_j, h)\mu(x_i)][\eta(x_j, \rho_1)\mu(x_i) - \eta(x_i, \rho_1)\mu(x_j)] > 0,$$

otherwise, it will contradict with (D.74). Then, from (E.86), we have

$$\frac{\partial\langle Z(x_1, x_2)\rangle}{\partial x_i}\bigg|_{x_i=x_i^*} = \frac{\partial\langle P(x_1, x_2)\rangle}{\partial x_i}\bigg|_{x_i=x_i^*} = 0, \quad i = 1, 2. \quad \text{(E.87)}$$

Let

$$h_{1i}(x_1, x_2) = c'(x_i, h)\frac{\partial\langle Z(x_1, x_2)\rangle}{\partial x_i} - \alpha\mu'(x_i)\frac{\partial\langle P(x_1, x_2)\rangle}{\partial x_i},$$

$$h_{2i}(x_1, x_2) = \alpha\mu(x_i)\frac{\partial^2\langle P(x_1, x_2)\rangle}{\partial x_i^2} - c(x_i, h)\frac{\partial^2\langle Z(x_1, x_2)\rangle}{\partial x_i^2}.$$

Obviously, $h_{1i}(x_1, x_2) = 0$, $i = 1, 2$. The evolutionary singular dimorphism (x_1^*, x_2^*) is evolutionary stable if for both $i \in \{1, 2\}$, the following inequality holds,

$$
\begin{aligned}
\left.\frac{\partial F_3^2(x_1, x_2, x_{\text{mut}})}{\partial x_{\text{mut}}^2}\right|_{y=x=x_i^*} &= \alpha\mu''(x_i^*)\langle P(x_1^*, x_2^*)\rangle - c''(x_i^*, h)\langle Z(x_1^*, x_2^*)\rangle - \left.\frac{\partial^2\eta(x_i, \rho_1)}{\partial x_i^2}\right|_{x_i=x_i^*} \\
&= 2h_{1i}(x_1^*, x_2^*) - h_{2i}(x_1^*, x_2^*) \\
&= -h_{2i}(x_1^*, x_2^*) \\
&< 0.
\end{aligned}
\tag{E.88}
$$

Furthermore, the local convergence stability at the evolutionary singular dimorphism (x_1^*, x_2^*) is determined by the Jacobian matrix of evolutionary dynamics (29) at this point. The Jacobian matrix $\mathcal{J}$ of (29) at (x_1^*, x_2^*) is given by:

$$
\begin{aligned}
\mathcal{J} &= \left.\begin{bmatrix} m_1(x_1^*, x_2^*)\dfrac{\partial D_{31}(x_1, x_2)}{\partial x_1} & m_1(x_1^*, x_2^*)\dfrac{\partial D_{31}(x_1, x_2)}{\partial x_2} \\[2mm] m_2(x_1^*, x_2^*)\dfrac{\partial D_{32}(x_1^*, x_2^*)}{\partial x_1} & m_2(x_1^*, x_2^*)\dfrac{\partial D_{32}(x_1, x_2)}{\partial x_2} \end{bmatrix}\right|_{x_1=x_1^*,\ x_2=x_2^*} \\[4mm]
&= \begin{bmatrix} m_1(x_1^*, x_2^*)\dfrac{\partial D_{31}(x_1, x_2)}{\partial x_1}\bigg|_{\substack{x_1=x_1^* \\ x_2=x_2^*}} & 0 \\[4mm] 0 & m_2(x_1^*, x_2^*)\dfrac{\partial D_{32}(x_1, x_2)}{\partial x_2}\bigg|_{\substack{x_1=x_1^* \\ x_2=x_2^*}} \end{bmatrix} \\[4mm]
&= \begin{bmatrix} -m_1(x_1^*, x_2^*)h_{21}(x_1^*, x_2^*) & 0 \\[2mm] 0 & -m_2(x_1^*, x_2^*)h_{22}(x_1^*, x_2^*) \end{bmatrix},
\end{aligned}
\tag{E.89}
$$

then if the Jacobian matrix satisfies $\det(\mathcal{J}) > 0$ and $\text{tr}(\mathcal{J}) < 0$, i.e., $h_{2i}(x_1^*, x_2^*) > 0$ hold for both $i \in \{1, 2\}$, the evolutionary singular dimorphism is locally convergence stable. From the above analysis, it is obvious that once the evolutionary singular dimorphism (x_1^*, x_2^*) is convergence stable, it must also be evolutionary stable, i.e., it is a CSS. Otherwise, i.e., there at least exists one $i \in \{1, 2\}$, such that $h_{2i}(x_1^*, x_2^*) < 0$, the evolutionary singular dimorphism is a repellor. This completes the proof.

Appendix F: Proof of Remark 6

Proof When $s_2(y) = \frac{1}{\beta_3}\exp(k_2 y)$, in order to prove y^* is always an ESS, we only need to prove that inequality (38) is always holds. Combing the second equation of (35) and the expression of $\langle A(x, y)\rangle$ in (9) leads to

$$
\langle A(x^*, y^*)\rangle_y' = 0,
\tag{F.90}
$$

and

$$\frac{\kappa'(y^*, \rho_2)}{\delta c_y'(x^*, y^*)} = \frac{\kappa(y^*, \rho_2)}{\delta c(x^*, y^*)} = \langle A(x^*, y^*) \rangle, \tag{F.91}$$

where

$$c(x, y) = c_m \exp(-v(x - \theta y)^2), \quad \kappa(y) = \frac{1}{\beta_3} \exp(k_2 y) + d_2 + \frac{\tilde{m}}{2} \exp(-2k_7 y),$$

$$\tilde{m} = \left(\frac{k_5 \rho_2}{k_6 + \rho_2}\right)^2.$$

By calculation,

$$c_y'(x^*, y^*) = 2c_m \theta v(x^* - \theta y^*) \exp(-v(x^* - \theta y^*)^2), \tag{F.92}$$

$$c_y''(x^*, y^*) = 2v\theta^2 c_m (2v(x^* - \theta y^*)^2 - 1) \exp(-v(x^* - \theta y^*)^2), \tag{F.93}$$

$$\kappa'(y^*) = \frac{k_2}{\beta_3} \exp(k_2 y^*) - \tilde{m} k_7 \exp(-2k_7 y^*), \tag{F.94}$$

$$\kappa''(y^*) = \frac{k_2^2}{\beta_3} \exp(k_2 y^*) + 2\tilde{m} k_7^2 \exp(-2k_7 y^*) > 0. \tag{F.95}$$

If $0 < 2v(x^* - \theta y^*)^2 \leq 1$, $c_y''(x^*, y^*) \leq 0$, then according to (38) and (F.95), we have,

$$\left.\frac{\partial^2 F_5(x, y, y_{\text{mut}})}{\partial y_{\text{mut}}^2}\right|_{x=x^*} < 0.$$

We then prove if $2v(x^* - \theta y^*)^2 > 1$, $\left.\frac{\partial^2 F_5(x, y, y_{\text{mut}})}{\partial y_{\text{mut}}^2}\right|_{x=x^*} < 0$ also holds.

When $2v(x^* - \theta y^*)^2 > 1$, substituting (F.91)-(F.95) into (38) leads to

$$\left.\frac{\partial^2 F_5(x, y, y_{\text{mut}})}{\partial y_{\text{mut}}^2}\right|_{\substack{x=x^* \\ y_{\text{mut}}=y=y^*}}$$

$$= \delta c_y''(x^*, y^*)\langle A(x^*, y^*)\rangle - \kappa''(y^*, \rho_2)$$

$$= c_y''(x^*, y^*)\frac{\kappa'(y^*, \rho_2)}{c_y'(x^*, y^*)} - \kappa''(y^*, \rho_2) \tag{F.96}$$

$$= \theta(2v(x^* - \theta y^*)^2 - 1)\frac{\frac{k_2}{\beta_3} \exp(k_2 y^*) - \tilde{m} k_7 \exp(-2k_7 y^*)}{x^* - \theta y^*} - \kappa''(y^*, \rho_2)$$

$$< 2\theta v(x^* - \theta y^*)^2 \frac{\frac{k_2}{\beta_3} \exp(k_2 y^*) - \tilde{m} k_7 \exp(-2k_7 y^*)}{x^* - \theta y^*} - \kappa''(y^*, \rho_2).$$

We then divide our proof into two cases.

(1). $x^* > \theta y^*$, then $\frac{k_2}{\beta_3} \exp(k_2 y^*) - \tilde{m} k_7 \exp(-2k_7 y^*) > 0$ and from (F.91),

$$k_2 > \frac{\frac{k_2}{\beta_3} \exp(k_2 y^*) - \tilde{m} k_7 \exp(-2k_7 y^*)}{\frac{1}{\beta_3} \exp(k_2 y^*) + d_2 + \frac{\tilde{m}}{2} \exp(-2k_7 y^*)} = 2\theta v(x^* - \theta y^*) > 0. \quad \text{(F.97)}$$

Substitute (F.97) into (F.96), we have

$$\begin{aligned}
\left. \frac{\partial^2 F_5(x, y, y_{\text{mut}})}{\partial y_{\text{mut}}^2} \right|_{\substack{x=x^* \\ y_{\text{mut}}=y=y^*}} &< 2\theta v(x^* - \theta y^*) \frac{k_2}{\beta_3} \exp(k_2 y^*) - \frac{k_2^2}{\beta_3} \exp(k_2 y^*) \\
&< \frac{k_2^2}{\beta_3} \exp(k_2 y^*) - \frac{k_2^2}{\beta_3} \exp(k_2 y^*) \\
&= 0.
\end{aligned} \quad \text{(F.98)}$$

(2). $x^* < \theta y^*$, then $\frac{k_2}{\beta_3} \exp(k_2 y^*) - \tilde{m} k_7 \exp(-k_7 y^*) < 0$ and from (F.91),

$$2k_7 > \frac{\tilde{m} k_7 \exp(-2k_7 y^*) - \frac{k_2}{\beta_3} \exp(k_2 y^*)}{\frac{1}{\beta_3} \exp(k_2 y^*) + d_2 + \frac{\tilde{m}}{2} \exp(-2k_7 y^*)} = 2\theta v(\theta y^* - x^*) > 0. \quad \text{(F.99)}$$

then

$$\begin{aligned}
\left. \frac{\partial^2 F_5(x, y, y_{\text{mut}})}{\partial y_{\text{mut}}^2} \right|_{\substack{x=x^* \\ y_{\text{mut}}=y=y^*}} &< 2v\theta(\theta y^* - x^*)\tilde{m} k_7 \exp(-2k_7 y^*) - 2\tilde{m} k_7^2 \exp(-2k_7 y^*) \\
&< 2\tilde{m} k_7^2 \exp(-2k_7 y^*) - 2\tilde{m} k_7^2 \exp(-2k_7 y^*) \\
&= 0.
\end{aligned} \quad \text{(F.100)}$$

Then, $\left. \frac{\partial^2 F_5(x, y, y_{\text{mut}})}{\partial y_{\text{mut}}^2} \right|_{\substack{x=x^* \\ y_{\text{mut}}=y=y^*}} < 0$ always holds. The proof is thus completed. $\qquad \square$

References

Agawin, N.S.R., Duarte, C.M.: Nutrient and temperature control of the contribution of picoplankton to phytoplankton biomass and production. Limnol. Oceanogr. **45** 591–600 (2000)

Bandyopadhyay, M., Saha, T., Pal, R.: Deterministic and stochastic analysis of a delayed allelopathic phytoplankton model within fluctuating environment. Nonlinear Anal. Hybrid **2**, 958–970 (2008)

Bao, J., Yuan, C.: Stochastic population dynamics driven by Lévy noise. J. Math. Anal. Appl. **391**, 363–375 (2012)

Brooks, J.L., Dodson, S.I.: Predation, body Size, and composition of plankton. Science **150**, 28–35 (1965)

Butterfield, N.J.: Plankton ecology and the proterozoic–phanerozoic transition. Paleobiology **23**, 247–262 (1997)

Carpenter, S.R., Cole, J.J., Pace, M.L., Batt, R.D., Brock, W.A., Cline, T.J., Coloso, J., Hodgson, J.R., Kitchell, J.F., Seekell, D.A., et al.: Early warnings of regime shifts: a whole-ecosystem experiment. Science **332**, 1079–1082 (2011)

Christiansen, F.B.: On conditions for evolutionary stability for a continuously varying character. Am. Nat. **138**, 37–50 (1991)

Cohen, J.E., Jonsson, T., Carpenter, S.R.: Ecological community description using the food web, species abundance, and body size. Proc. Natl. Acad. Sci. U.S.A. **100**, 1781–1786 (2003)

Dercole, F., Geritz, S.: Unfolding the resident-invader dynamics of similar strategies. J. Theor. Biol. **394**, 231–254 (2015)

Dercole, F., Rossa, F.D., Landi, P.: The transition from evolutionary stability to branching: a catastrophic evolutionary shift. Sci. Rep. **6**, 26310 (2016)

Dercole, F., Rinaldi, S.: Analysis of Evolutionary Processes: The Adaptive Dynamics Approach and Its Applications. Princeton University Press, Princeton (2008)

Dieckmann, U., Law, R.: The dynamical theory of coevolution: a derivation from stochastic ecological processes. J. Math. Biol. **34**, 579–612 (1996)

Dieckmann, U., Marrow, P., Law, R.: Evolutionary cycling in predator-prey interactions: population dynamics and the red queen. J. Theor. Biol. **176**, 91–102 (1995)

Diekmann, O., Jabin, P.S., Perthame, B.: The dynamics of adaptation: an illuminating example and a Hamilton–Jacobi approach. Theor. Popul. Biol. **67**, 257–271 (2005)

Edwards, A.M., Andrew, Y.: The role of higher predation in plankton population models. J. Plankton Res. **22** 1085–1112 (2000)

Eshel, I.: Evolutionary and continuous stability. J. Theor. Biol. **103**, 99–111 (1983)

Falkowski, P.G., Barber, R.T., Smetacek, V.: Biogeochemical controls and feedbacks on ocean primary production. Science **281**, 200–206 (1998)

Falkowski, P.G., Katz, M.E., Knoll, A.H., Quigg, A., Raven, J.A., Schofield, O., Taylor, F.J.R.: The evolution of modern eukaryotic phytoplankton. Science **305**, 354–360 (2004)

Figueiredo, G., Schwamborn, R., Bertrand, A., Munaron, J.M., Loc'H, F.L.: Body size and stable isotope composition of zooplankton in the western tropical Atlantic. J. Mar. Syst. **212**, 103449 (2020)

Finkel, Z.V., Katz, M.E., Wright, J.D., Schofield, O., Falkowski, P.G.: Climatically driven macroevolutionary patterns in the size of marine diatoms over the Cenozoic. Proc. Natl. Acad. Sci. U.S.A. **102**, 8927–8932 (2005)

Geritz, S.A.H.: Resident-invader dynamics and the coexistence of similar strategies. J. Math. Biol. **50**, 67–82 (2005)

Geritz, S.A.H., Kisdi, E., Meszena, G., Metz, J.A.J.: Evolutionarily singular strategies and the adaptive growth and branching of the evolutionary tree. Evol. Ecol. **12**, 35–57 (1998)

Hanazato, T.: Response of a zooplankton community to insecticide application in experimental ponds: a review and the implications of the effects of chemicals on the structure and functioning of freshwater communities. Environ. Pollut. **101**, 361–373 (1998)

Hardin, G.: The competitive exclusion principle. Science **131**, 1292–1297 (1960)

Hui, C., Hui, C., Minoarivelo, O.H., Minoarivelo, O.H., Landi, P.: Modelling coevolution in ecological networks with adaptive dynamics. Math. Methods Appl. Sci. **41**, 8407–8422 (2018)

Ichimi, K., Kawamura, T., Yamamoto, A., Tada, K., Harrison, P.J.: Extremely high growth rate of the small diatom chaetoceros salsugineum isolated from an estuary in the eastern seto inland sea, Japan 1. J. Phycol. **48**, 1284–1288 (2012)

Irigoien, X., Huisman, J., Harris, R.P.: Global biodiversity patterns of marine phytoplankton and zooplankton. Nature **429**, 863–867 (2004)

JaGer, C., Diehl, S., Emans, M.: Physical determinants of phytoplankton production, algal stoichiometry, and vertical nutrient fluxes. Am. Nat. **175**, E91 (2010)

Jian, Z., Wang, J., Huang, G.: Evolutionary diversification of prey and predator species facilitated by asymmetric interactions. PLOS ONE **11**, e0163753 (2016)

Jiang, L., Schofield, O.M., Falkowski, P.G.: Adaptive evolution of phytoplankton cell size. Am. Nat. **166**, 496–505 (2005)

Khasminskii, R.: Stochastic Stability of Differential Equations, 2nd edn. Springer, Berlin (2012)

Kisdi, E.: Evolutionary branching under asymmetric competition. J. Theor. Biol. **197**, 149–162 (1999)

Landi, P., Dercole, F., Rinaldi, S.: Branching scenarios in eco-evolutionary prey-predator models. SIAM J. Appl. Math. **73**, 1634–1658 (2013)

Li, W.K.W.: Macroecological patterns of phytoplankton in the northwestern North Atlantic Ocean. Nature **419**, 154–157 (2002)

Litchman, E., Klausmeier, A.C., Yoshiyama, K.: Contrasting size evolution in marine and freshwater diatoms. Proc. Natl. Acad. Sci. U.S.A. **106** 2665–2670 (2009)

Litchman, E., Pinto, d.T.P., Klausmeier, A.C., Thomas, K.M., Yoshiyama, K.: Linking traits to species diversity and community structure in phytoplankton. Hydrobiologia **653** 15–28 (2010)

Liu, M., Bai, C.: Analysis of a stochastic tri-trophic food-chain model with harvesting. J. Math. Biol. **73**, 597–625 (2016)

Loladze, I., Kuang, Y., Elser, J.J.: Stoichiometry in producer-grazer systems: linking energy flow with element cycling. Bullet. Math. Biol. **62**, 1137–1162 (2000)

Mao, X. Stochastic Differential Equations and Applications. 2nd Edn, Horwood, Chichester (2007)

Mao, X., Marion, G., Renshaw, E.: Environmental Brownian noise suppresses explosions in population dynamics. Stoch. Proc. Appl. **97**, 95–110 (2002)

Mclaughlin, B.R.B.: Size changes in the marine diatom coscinodiscus nodulifer A. Schmidt in the equatorial pacific. Micropaleontology **23**, 216–222 (1977)

Melbourne, B.A., Hastings, A.: Extinction risk depends strongly on factors contributing to stochasticity. Nature **454**, 100 (2008)

Meng, X., Liu, R., Liu, L., Zhang, T.: Evolutionary analysis of a predator–prey community under natural and artificial selections. Appl. Math. Model. **39**, 574–585 (2015)

Mitchell, F.S.: Some effects of agricultural development and fluctuations in water level on the phytoplankton productivity and zooplankton of a New Zealand reservoir. Freshwater Biol. **5** 547–562 (1975)

Moczydłowska, M.: Early Cambrian phytoplankton diversification and appearance of trilobites in the Swedish Caledonides with implications for coupled evolutionary events between primary producers and consumers. Lethaia **35**, 191–214 (2010)

Murphy, C.R., Hart, J.T.: Phytoplankton periodicity in Antarctic surface waters. Geogr. Rev. **35**, 344–345, (1945)

Parvinen, K.: Evolutionary suicide. Acta Biotheor. **53**, 241–264 (2005)

Peace, A., Wang, H., Kuang, Y.: Dynamics of a producer-grazer model incorporating the effects of excess food nutrient content on grazer's growth. Bullet. Math. Biol. **76**, 2175–2197 (2014)

Peters, R.H.: The ecological implications of body size. Cambridge University Press (1983)

Polovina, J.J., Woodworth, P.A.: Declines in phytoplankton cell size in the subtropical oceans estimated from satellite remotely-sensed temperature and chlorophyll, 1998–2007. Deep sea Res. Part **II**(77), 82–88 (2012)

Pu, Z., Cortez, M.H., Jiang, L.: Predator-prey coevolution drives productivity–richness relationships in planktonic systems. Am. Nat. **189**, 28–42 (2017)

Raven, J.A.: The twelfth Tansley Lecture, small is beautiful: the picophytoplankton. Funct. Ecol. **12**, 503–513 (1998)

Ripa, J., Dieckmann, U.: Mutant invasions and adaptive dynamics in variable environments. Evolution **67**, 1279–1290 (2013)

Rossa, F.D., Dercole, F., Landi, P.: The branching bifurcation of adaptive dynamics. Int. J. Bifurc. Chaos **25**, 1540001 (2015)

Schmidt, D.N., Thierstein, H.R., Bollmann, J., Schiebel, R.: Abiotic forcing of plankton evolution in the Cenozoic. Science **303**, 207–210 (2004)

Servais, T., Lehnert, O., Li, J., Mullins, G.L., Vecoli, M.: The Ordovician Biodiversification: revolution in the oceanic trophic chain. Lethaia **41**, 99–109 (2010)

Sheldon, R.W., Prakash, A., Sutcliffe, W.H.: The size distribution of particles in the ocean. Limnol. Oceanogr. **17**, 327–340 (1972)

Sterner, R.W., Elser, J.J.: Ecological stoichiometry: The biology of elements from molecules to the biosphere. In: Ecological Stoichiometry: The Biology of Elements from Molecules to the Biosphere (2002)

Stomp, M., Huisman, J., De Jongh, F., Veraart, A.J., Gerla, D., Rijkeboer, M., Ibelings, B.W., Wollenzien, U., Stal, L.J.: Adaptive divergence in pigment composition promotes phytoplankton biodiversity. Nature **432**, 104–107 (2004)

Tang, E.P.Y., Peters, R.H.: The allometry of algal respiration. J. Plankton Res. **17**, 303–315 (1995)

Wang, H., Dunning, K., Elser, J.J., Kuang, Y.: Daphnia species invasion, competitive exclusion, and chaotic coexistence. Discrete Cont. Dyn B **12**, 481–493 (2009)

Wang, H., Kuang, Y., Loladze, I.: Dynamics of a mechanistically derived stoichiometric producer-grazer model. J. Biol. Dyn. **2**, 286–296 (2008)

Wang, H., Smith, H.L., Kuang, Y., Elser, J.J.: Dynamics of stoichiometric bacteria-algae interactions in the epilimnion. Siam J. Appl. Math. **68**, 503–522 (2007)

White, J.W., Botsford, L.W., Hastings, A., Holland, M.D.: Stochastic models reveal conditions for cyclic dominance in sockeye salmon populations. Ecol. Monogr. **84**, 69–90 (2014)

Yu, X., Yuan, S., Zhang, T.: The effects of toxin-producing phytoplankton and environmental fluctuations on the planktonic blooms. Nonlinear Dyn. **91**, 1653–1668 (2018)

Zhang, W., Zhao, S., Meng, X., Zhang, T.: Evolutionary analysis of adaptive dynamics model under variation of noise environment. Appl. Math. Model. **84**, 222–239 (2020)

Zhao, Q., Liu, S., Niu, X.: Stationary distribution and extinction of a stochastic nutrient-phytoplankton-zooplankton model with cell size. Math. Methods Appl. Sci. **43**, 3886–3902 (2020)

Zhao, Y., Yuan, S., Zhang, T.: The stationary distribution and ergodicity of a stochastic phytoplankton allelopathy model under regime switching. Commun. Nonlinear Sci. **37**, 131–142 (2016)

Zhao, Y., Yuan, S., Zhang, T.: Stochastic periodic solution of a non-autonomous toxic-producing phytoplankton allelopathy model with environmental fluctuation. Commun. Nonlinear Sci. **44**, 266–276 (2017)